Thermally induced diffusion phenomena and compound interlayer structural changes in EUV multilayers

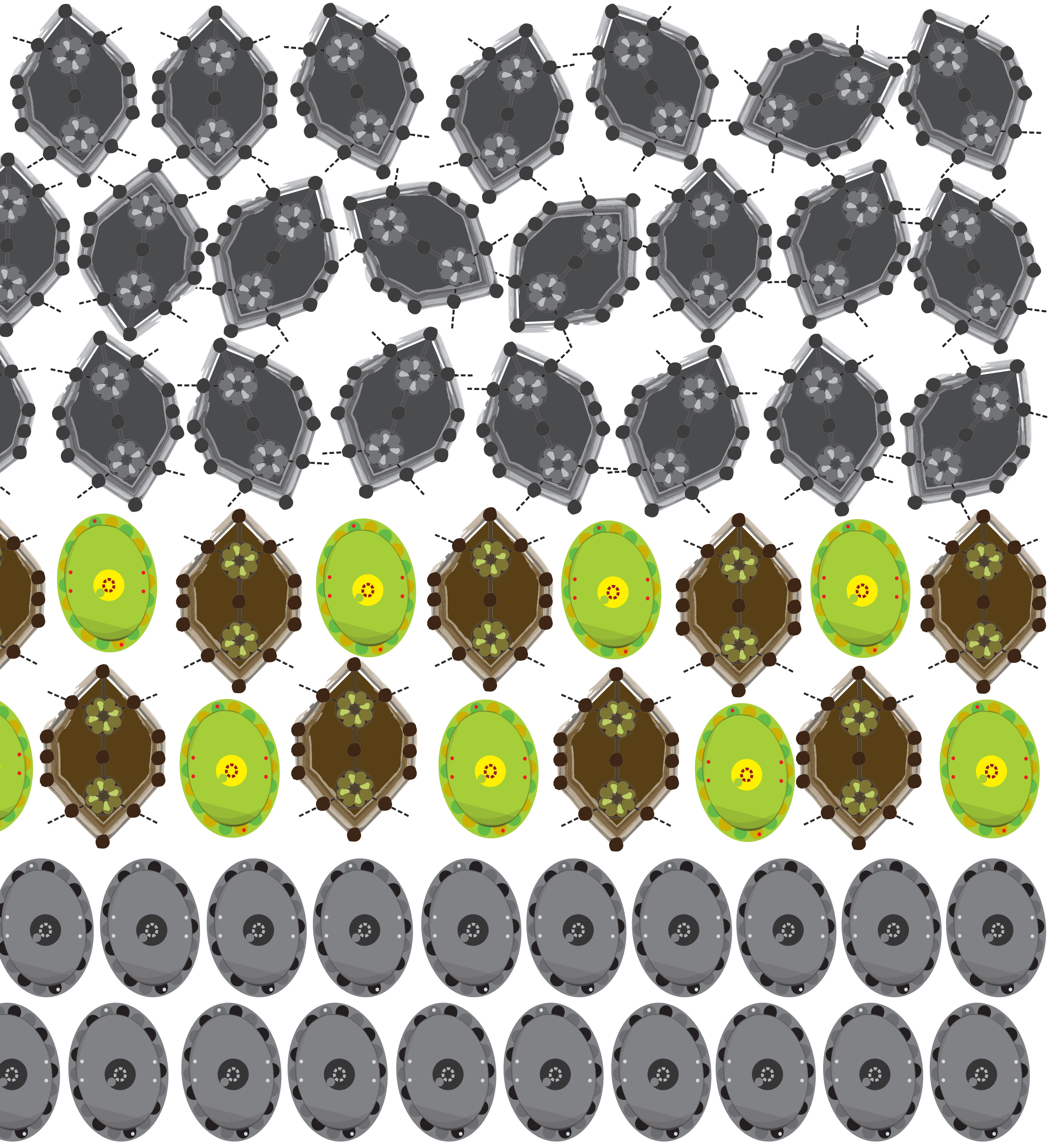

Steven Lawrence Nyabero

Thermally induced diffusion phenomena and compound interlayer structural changes in EUV multilayers

Steven Lawrence Nyabero

Ph.D. committee

Chairman:

Prof. dr. G. van der Steenhoven	University of Twente

Secretary:

Prof. dr. G. van der Steenhoven	University of Twente

Promoter:

Prof. dr. F. Bijkerk	University of Twente FOM Institute DIFFER

Assistant Promoter:

Dr. ir. R. W. E. van de Kruijs	FOM Institute DIFFER

Members:

Prof. dr. J. W. M. Frenken	Leiden University Advanced Research Center for Nanolithography
Prof. dr. ir. J. W. M. Hilgenkamp	University of Twente
Prof. dr. A. P. Mosk	University of Twente
Prof. dr. H. H. Brongersma	Eindhoven University of Technology Imperial College London
Dr. D. K. G. de Boer	Philips Research

Cover: A Tinga Tinga artististic impression of a multilayered structure which consists of amorphous aggregrates, a compound interlayer and a crystalline layer. Designed and created by Mugisha A. Basasingohe.

THERMALLY INDUCED DIFFUSION PHENOMENA AND COMPOUND INTERLAYER STRUCTURAL CHANGES IN EUV MULTILAYERS

PROEFSCHRIFT

ter verkrijging van de
graad van doctor aan de Universiteit Twente,
op gezag van de rector magnificus,
prof. dr. H. Brinksma,
volgens besluit van het College voor Promoties
in het openbaar te verdedigen op
vrijdag 7 februari 2014 om 12:45 uur

door

Steven Lawrence Nyabero

geboren op 29 juli 1983
te Dar es Salaam, Tanzania

Dit proefschrift is goedgekeurd door de promotor

Prof. dr. F. Bijkerk

en assistent promotor

Dr. ir. R. W. E. van de Kruijs

ISBN: 978-94-6259-070-0

For my mom.

> “Every man gotta right to decide his own destiny.”
> ~ Bob Marley

This work is part of the research programme ‘Controlling photon and plasma induced processes at EUV optical surfaces (CP3E)’ of the ‘Stichting voor Fundamenteel Onderzoek der Materie (FOM)’, which is financially supported by the ‘Nederlandse Organisatie voor Wetenschappelijk Onderzoek (NWO)’. The CP3E programme is co-financed by Carl Zeiss SMT and ASML. We also acknowledge financial support from Agentschap NL (EXEPT project).

This thesis is based on the following publications:

Chapter 3:

S. L. Nyabero, R. W. E. van de Kruijs, A. E. Yakshin, E. Zoethout, F. Bijkerk, "Thermally induced interface chemistry in Mo/B_4C/Si/B_4C multilayered films," *Journal of Applied Physics* **112**, 054317 (2012).

Chapter 4:

S. L. Nyabero, R. W. E. van de Kruijs, A. E. Yakshin, E. Zoethout, G. van Blanckenhagen, J. Bosgra, R. A. Loch, F. Bijkerk, "Interlayer growth in Mo/B_4C multilayered structures upon thermal annealing," *Journal of Applied Physics* **113**, 144310 (2013).

Chapter 5:

S. L. Nyabero, R. W. E. van de Kruijs, A. E. Yakshin, F. Bijkerk, "Enhanced thermal stability of extreme ultraviolet multilayers by balancing diffusion-induced structural changes," *Applied Physics Letters* **103**, 093105 (2013).

Chapter 6:

S. L. Nyabero, R. W. E. van de Kruijs, A. E. Yakshin, J. Bosgra, E. Zoethout, I. A. Makhotkin, F. Bijkerk, "Thermally induced interlayer structural changes in La/B multilayers," submitted.

Chapter 7:

S. L. Nyabero, R. W. E. van de Kruijs, A. E. Yakshin, I. A. Makhotkin, J. Bosgra, F. Bijkerk, "Diffusion induced structural changes in La/B-based multilayers for 6.7 nm radiation," accepted for publication in the *Journal of Micro/Nanolithography, MEMS, and MOEMS (JM3)*.

CONTENT

1. Introduction

1.1. Motivation

The lecture given at an American Physical Society meeting by renowned physicist Richard Feynman more than half a century ago [1], strongly influenced the development of nanoscience. In the lecture, Feynman discussed the possibilities of manipulating matter at the atomic scale. Amongst many examples, he discussed possible consequences of miniaturization of electronic devices and making microscopes that could image much smaller features compared to what was possible at the time. The lecture inspired the scientific community to pursue a lot of fascinating studies that have led to advances in science and technology.

Materials tailored in nanoscale can exhibit interesting properties that are different from what they show in macroscale, providing tools to make a wide range of unique applications a reality. The increase of surface area to volume ratio alters properties of materials as the effects of interfaces and surfaces become prominent. Au is a prime example. At the macroscale, Au particles are known to be inert [2]. Au nanoparticles are actually found to be highly reactive and can be employed as catalysts in chemical reactions [2]. Interesting novel properties can also be exhibited by nanoscale layered structures of different materials. For example, multilayered perovskite-like materials which have basically the same crystallographic structure are known to show different interface electronic properties, ranging from dielectric insulators and ferroelectrics to metals, ferromagnets, and superconductors [3]. Another good example of nanoscale multilayered structures can be found in the field of spintronics, where the electron (spin) transport properties are tailored by combining nanoscale layers/domains of ferromagnetic and anti-ferromagnetic materials [4]. These examples give us a glimpse of how fascinating the novel properties of nanoscale materials can be. Understanding the mechanisms of phenomena exhibited by nanoscale materials can be of paramount importance for applications, as it enables the appropriate manipulation of the properties – by mitigating the undesired effects and enhancing the desired ones.

Optics is another branch of physics that has been impacted by the application of nanoscale materials. For instance, in nanophotonics, controlling light by using nanoscale crystals and plasmonics is now a reality [5]. This thesis will focus on one specific case of a one-dimensional photonic crystal, namely that of an artificial Bragg crystal, where the optical properties of multilayered nanoscale structures are used to develop normal-incidence reflecting optics for the extreme ultraviolet (EUV) wavelength range.

Before the emergence of nanoscience, the EUV region (λ = 5 nm – 100 nm) of the electromagnetic spectrum had not been explored since there were no right tools. This is due to the fact that the region has a large number of atomic resonances [6]. Moreover, both imaging and manufacturing of electronic circuits with sub-100 nm features was not feasible using conventional refractive optics for guiding light. Consider a refractive index of a certain element, given by:

$$\tilde{n} = 1 - \delta + i\beta = n + ik \ , \tag{1.1}$$

with

$$\delta = \frac{2\pi\rho_a r_o}{k_o^{\ 2}}\left(f^{0}(0) + f\,'\right), \tag{1.2}$$

$$\beta = \frac{2\pi\rho_a r_o}{k_o^{\ 2}}\left(f\,''\right), \tag{1.3}$$

where, ρ_a is the atomic density, r_o is the classical electron radius, $k_o = 2\pi/\lambda$ with λ being the wavelength, $f^o(0)$ is the number of electrons in the atom, and f' and f'' are anomalous scattering factors (related to electronic excitation and absorption), which can be found in ref. [7]. In the EUV wavelength region, the contrast in $n = 1\text{-}\delta$ for materials is very small, while the absorption, related to β, cannot be ignored. In this region, the absorption is high, making it impossible to use refractive optics.

Multilayer reflective optics is the only viable option which can be used to guide EUV light at angles larger than the critical angle* [6]. Due to low normal incidence reflectance of single-film coatings, multilayer coatings have to be designed, consisting of stacked layers of typically sub-nanometer to tens of nanometer thickness, depending on the operational wavelength. The operation principle mimics crystal Bragg reflectors and is based on constructive interference of reflections from the layer interfaces in the stack.

Since the emergence of multilayered optical coatings, there have been opportunities for advances in both science and technology. EUV photoelectron spectroscopy [6] – used to reveal information about elemental composition and chemical bonds on material surfaces – makes use of multilayer mirrors in the Schwarzschild objective [6]. Multilayers are also used in diagnostics of hot plasmas which radiate at wavelengths in the EUV range [6]. Similarly, in astronomy and development of EUV lasers, multilayers are ideal for isolating certain spectral lines [6]. The application of multilayer coatings in EUV lithography (EUVL) would enable the semiconductor industry to continue miniaturizing electronic components [6]. It should be noted that, the understanding of the principles for the EUV region can also be used in the soft X-ray region ($\lambda = 0.2$ nm – 5 nm), and vice-versa.

The performance of multilayers is intrinsically linked to the properties of the layer materials as well as the interaction between the various nanoscale layers. Usually, the properties of nanoscale layers are different from those of macroscale materials. For instance, the density and the crystallinity of layers could be different. The interaction between nanoscale layers is evident from the intermixture and formation of compounds at the interfaces between layers. This interaction already takes place upon deposition, but continues and may accelerate upon exposure to intense photon fluxes, which can lead to thermal loading and promote diffusion of atoms. Diffusion induced phenomena in thin films may behave differently due to the effects of interfaces [8] and grain boundaries [9]. Also, multilayer structural changes – such as compound interlayer growth [8], void elimination [10], stress changes [11] and crystallization [9] – can take place due to thermal loading. All these call for studies to understand not only the chemical and the structural properties of multilayers, but also the changes (in the properties) and their effects on multilayer performance.

---

[*] The critical angle – the angle below which all light is reflected from the surface – is given by $\sin\theta_c \simeq \sqrt{2\delta}$. The angle is too small for the EUV range since n is close to unity.

This thesis discusses the physics of multilayer coatings designed for EUVL. The first part of the thesis focuses on understanding the mechanisms of thermally induced structural changes in Mo/Si multilayers with ultra-thin B_4C diffusion barrier layers, designed for 13.5 nm. The highlight is the unraveling of interface reactions that can lead to changes in the multilayer period thickness upon thermal loading. The knowledge acquired has been used to design a Mo/Si-based multilayer system showing a stable temporal behavior at elevated temperatures, by balancing the diffusion-induced multilayer structural changes at the interfaces. The latter part of this thesis focuses on thermally induced structural changes in La/B-based multilayer systems designed for 6.7 nm. Due to the high reactivity of La, intermixing and compound formation takes place at the La/B interfaces, even during deposition [12, 13]. LaN/B multilayers are suggested as candidate multilayers with reduced reactivity at the interfaces, enhancing both the reflectance and thermal stability. The knowledge obtained could be used to further improve the performance of La/B-based optics.

This work is part of the research programme Controlling Photon and Plasma-induced Processes at EUV optical surfaces (CP3E) of the Stichting voor Fundamenteel Onderzoek der Materie (FOM), which is financially supported by the Nederlandse Organisatie voor Wetenschappelijk Onderzoek (NWO). The CP3E programme is co-financed by Carl Zeiss SMT and ASML.

1.2. Multilayer reflective optics

The theoretical reflectance, *r*, for radiation incident perpendicular to a smooth interface between two materials is given by the following equation:

$$r = \left| \frac{\tilde{n}_1 - \tilde{n}_2}{\tilde{n}_1 + \tilde{n}_2} \right|^2 , \tag{1.4}$$

showing that, the reflectance depends on the difference in refractive index. As mentioned in Section 1.1 (see equation 1.2), in the EUV wavelength range, the contrast in $n = 1\text{-}\delta$ for materials is very small while the absorption, related to β, is relatively high. As a result, a single interface reflects only a small fraction of radiation, typically not much more than 1%.

The solution to obtain high reflectance is to design multilayers, which utilize constructive interference of the radiation reflected at the interfaces. An optimal reflectance can be achieved if the optical contrast of the two materials, Δn, is high at a certain target wavelength. For this condition to be fulfilled, firstly, the absorption β of both materials must be as low as possible, and secondly, the difference between δ values must be as high as possible. Basically, multilayer mirrors are designed to have many alternating layers of high and low δ, as shown in Fig. 1.1.

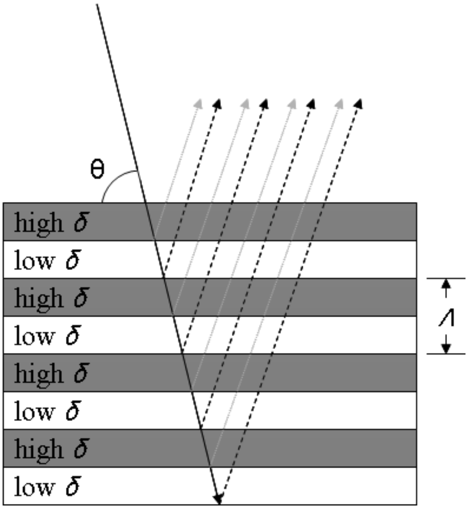

Fig. 1.1: The principle of constructive interference in multilayers.

The thickness of the multilayer period Λ is chosen so that the radiation of wavelength λ is interfering constructively at angles θ_m, satisfying the Bragg equation:

$$m\lambda = 2\Lambda \sin\theta_m \sqrt{1 - \frac{2\overline{\delta}}{\sin^2\theta_m}} \tag{1.5}$$

where, $\overline{\delta}$ is the average δ of the period. For example, for reflecting soft X-rays and EUV radiation at normal near-normal incidence, the period Λ should be approximately $\lambda/2$.

1.3. Extreme Ultraviolet Lithography

For the last half of a century, miniaturization of electronic circuits has continued to follow the trend which is now referred to as ‘Moore’s Law’ [14]. In 1965, Gordon E. Moore observed that the number of transistors per square inch in integrated circuits had doubled every year from 1958, the year integrated circuits were invented, to 1965 [15]. Since then, the semiconductor industry has adopted Moore's observation as a law for guiding the research and the development, in order to keep doubling the number of transistors in the circuits after every 18 months.

The increased number of transistors is a direct result of the decrease in transistor size. Since the integrated circuits are prepared by optical projection lithography, the resolution, R, of the smallest obtainable feature is proportional to the wavelength, λ, as governed by the Rayleigh criterion for a microscope system [6]:

$$R = \frac{0.61\lambda}{NA}, \tag{1.6}$$

where, NA is the numerical aperture, defined as $n \sin \omega$, with ω being the acceptance angle of the microscope and n the refractive index of the surrounding medium (n_{air} = 1). The factor 0.61 is for a perfect lens. Currently, the photolithography process that is used to print semiconductor devices employs a 193-nm wavelength illumination source. The source illuminates a specific reticle pattern, and then the pattern is demagnified and projected by a set of lenses onto Si wafers coated with a photoresist. The illuminated parts of the photoresist are then etched to leave a profile for subsequent steps. For lithography systems, the Rayleigh criterion is written as follows:

$$CD = k_1 \frac{\lambda}{NA} \tag{1.7}$$

where, CD is the critical dimension or the minimum feature size and k_1 is an empirical process constant [16]. The photolithography process has another constraint, namely depth of focus, which restricts the thickness of the photoresist and the topography on the wafer. The depth of focus, D_F, is given by:

$$D_F = k_2 \frac{\lambda}{NA^2}, \tag{1.8}$$

where, k_2 is another empirical process constant [16]. State-of-the-art photolithography, known as immersion photolithography, replaces the air between the final lens element and the wafer with water. This increases the numerical aperture since the refractive index of water (n_{water} = 1.33) is higher than that of air (n_{air} = 1). As a result, the resolution and the depth of focus are improved (see equations 1.7 and 1.8). A resolution of 32 nm has been achieved using immersion photolithography employing an illumination wavelength of 193 nm.

To improve the resolution of the 193 nm immersion lithography to 16 nm, the industry is exploring techniques such as double patterning [17]. Actually, a smaller illumination wavelength would prove more beneficial in terms of a cost effective manufacturing process (i.e. single exposure instead of double exposure). The next-generation lithography (EUVL) equipment will make use of a wavelength of 13.5 nm. As previously discussed (Section 1.1), due to the fact that most materials have high absorption at this wavelength, the refractive optics systems need to be replaced with reflective multilayer coated optics and the equipment should be operating in a high vacuum environment. The highest theoretical normal incidence reflectance for the wavelength of 13.5 nm can be obtained with multilayer coatings that make use of Mo as reflector material and Si as a spacer material. Fig. 1.2 shows a schematic image of an EUVL equipment with reflective Mo/Si-based multilayer coatings employed in illumination and projection optics. A resolution of 22 nm has reportedly been achieved using EUVL employing the wavelength of 13.5 nm [19].

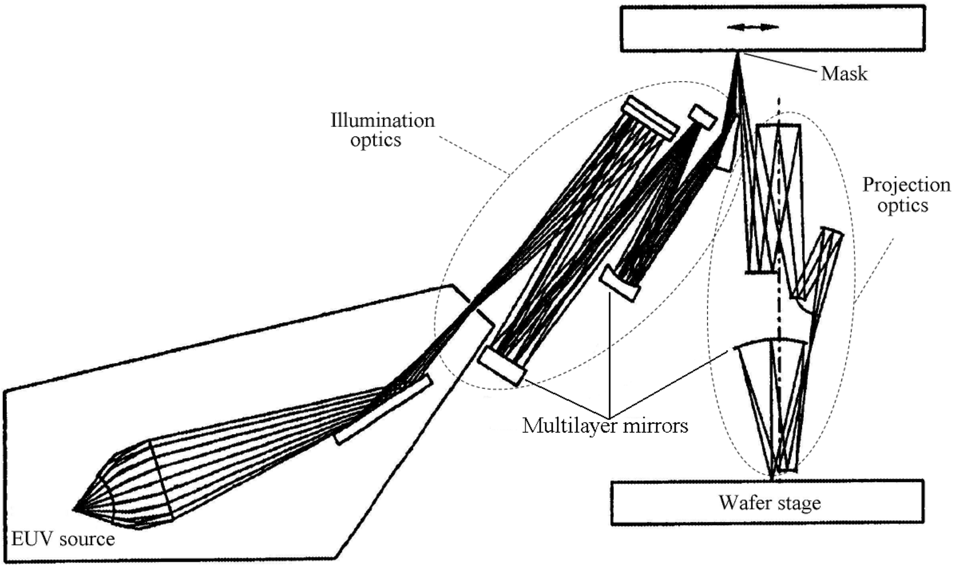

Fig. 1.2: Schematic view of an EUVL equipment operating at $\lambda = 13.5$ nm showing the principle of how Mo/Si-based multilayer coatings are used to focus and defocus light [18].

The EUVL community is also exploring ways to further improve the resolution to the 16 nm node and beyond [20]. The main challenge lies in increasing the numerical aperture up to 0.7 or even higher [20], and employing an even shorter wavelength (~6.7 nm) for the lithography process. The highest theoretical normal incidence reflectance for the wavelength of 6.7 nm can be obtained with multilayer coatings that make use of La layers as reflector material, and B layers as an appropriate spacer material since B has a K-absorption edge at 6.63 nm [21, 22, 23].

Considering that the entire optical path in EUVL tools (Fig. 1.2) consists of as many as 10 multilayer mirrors, it is very important to have a good performance of each single mirror. For instance, a few-percent decrease in reflectance of each mirror would have a significantly huge impact on the throughput. Moreover, each mirror in the projection optics is supposed to match *both* the wavelength and the phase of the employed radiation. All these demands are supposed to be sustained by the optics for several years in an industrial environment that implicitly incorporates several possible causes for optics degradation.

There are several factors that can affect the performance of multilayer coatings in an EUVL tool. The part of the vacuum equipment where the optics reside is in contact with other parts of the tool that can act as sources of contamination. Such contaminants include outgassing of carbon from the photoresist, tin from the EUV source, buffer gases, residual oxygen and hydrocarbons. These contaminants can either directly or through photo-activated processes be deposited onto the surfaces of multilayer coated optics during operation of the tool, resulting in a decrease of the reflectance. Although surface contamination on its own is a serious threat to optics lifetime, the focus of this thesis will actually be on the threat to optics lifetime that is related to damage that occurs *inside* the layered structures, specifically due to thermal loading caused by intense or prolonged exposures of photon fluxes.

1.4. Thermally induced structural changes in EUV multilayers

Although the materials used to fabricate multilayers by design have relatively low absorption coefficients at the wavelengths used for EUVL, the layers absorb a part of the radiation. As a result, intense or prolonged exposures of photon fluxes can cause thermal loading of the multilayer optics. This might lead to changes in the multilayer internal structure due to void elimination [10], changes in stress [11], crystallization [9], interdiffusion of atoms at the interfaces [8] and compound interlayer growth [8]. To observe phenomena like interdiffusion and compound interlayer growth, non-destructive experimental techniques with depth-resolved sub-Ångström accuracy are required. A non-destructive technique with such sensitivity, namely grazing incidence X-ray reflectometry (GIXR), was used *in-situ* during thermal annealing to characterize multilayer period changes as a function of annealing time and temperature. In addition, *ex-situ* wide angle X-ray diffraction (WAXRD) was used to determine changes in layer crystallinity and specifically changes in crystallite sizes. X-ray photoelectron spectroscopy (XPS) and Auger electron spectroscopy (AES) sputter depth profiling was used to probe relative changes in atomic concentrations due to intermixing at the interfaces. The experimental methods are described in more detail in Chapter 2.

In the following sections, mechanisms of multilayer interface diffusion and subsequent compound interlayer growth as well as their effects are discussed in detail. Also, methods to mitigate diffusion and/or its effects on both the multilayer structural changes and performance are outlined.

1.4.1. Diffusion in multilayers

The diffusion of atoms and subsequent compound formation at the interfaces results in changes in the optical contrast of multilayers [6]. For multilayers which consist of reactive materials, a compound with negative formation enthalpy can be formed even during deposition if the local temperature/energy is high enough. For example, in Mo/Si multilayers, amorphous $MoSi_2$ is expected to be formed during deposition [24, 25], deteriorating the optical contrast and therefore reducing the reflectance.

Compound interlayer growth may lead to changes in the multilayer period thickness if the density of the compound formed is different from the average density of the constituent materials. A change in multilayer period, through Bragg's law, results in a change in the optimally reflected wavelength, and therefore a mismatch with the spectral characteristics of the other optical components and the illumination source. For Mo/Si multilayers, densification upon silicide formation at the interfaces would lead to a reduction of the multilayer period. Table 1.1 shows fractional volume changes upon formation of various silicides, from which the consumption of Mo and Si, as well as the expected compaction upon interface formation is obtained. The data for $MoSi_2$ formation has been found to be consistent with the period compaction observed in Mo/Si multilayers during thermal loading experiments up to 300 °C [26].

	A (g/mol)	ρ (g/cm^3)	$V_I/V_{comp.}$	$V_{II}/V_{comp.}$	Fractional Vol. Change
Mo	95.94	10.20	-	-	-
Si	28.085	2.33	-	-	-
Mo_3Si	315.78	8.97	0.80	0.34	-0.14
Mo_5Si_3	563.74	8.20	0.68	0.52	-0.21
$MoSi_2$	152.06	6.24	0.39	0.99	-0.38

Table 1.1: Molecular volumes of Mo and Si consumed in chemical reactions to form various silicides. V_I and V_{II} are molecular volumes of the first element and second element, respectively, and $V_{comp.}$ is the molecular volume of the corresponding formed compound. Calculations are based on bulk density values. Densification/compaction is expected in all reactions between Mo and Si considered here.

In order to quantify the effects of diffusion and growth of compound interlayers, and relate them to the performance of EUVL tools, it is necessary to address parameters such as diffusion constants, activation energies, etc. Fick’s equations are commonly used to describe diffusion of atoms in solids. Fick’s first law postulates that the flux of atoms goes from regions with high concentration to regions with a low concentration, with the magnitude dependent on the gradient of the concentration. The law is written as follows:

$$J = -D\nabla C \tag{1.9}$$

where, J is the magnitude of the flux, D is the diffusion coefficient and C is the concentration. In systems where the total amount of diffusing species can be assumed to be constant, the following condition should be fulfilled:

$$-\nabla \cdot J = \frac{\delta C}{\delta t}. \tag{1.10}$$

Combining this with equation 1.9 yields Fick’s second law:

$$\frac{\delta C}{\delta t} = \nabla\left(D\nabla C\right). \tag{1.11}$$

From the second law, the time dependent concentration of diffusing species can be numerically computed.

Since the mobility of atoms generally increases with increasing temperature, the diffusion coefficients described by Fick’s laws are temperature dependent.

The diffusion coefficient is related to the activation energy for diffusion E_a and temperature T by the Arrhenius equation:

$$D = D_o \exp\left(-\frac{E_a}{kT}\right), \tag{1.12}$$

where, D_o is a pre-exponential factor and k is the Boltzmann constant.

For nanoscale layered systems, the diffusion processes are not straightforward. Firstly, equation 1.10 is often invalid for layered systems due to the fact that there are chemical reactions taking place at the interfaces during thermal loading. As a result, there is a diffusion-reaction mechanism leading to the growth of compound interlayers, making this a moving boundary problem. Gösele *et al* suggested a model explaining two limiting cases for the diffusion-reaction mechanism during the growth of compound interlayers between two materials [27]:

1. At the very initial stages, the compound interface is thin and diffusion through the interfaces is relatively rapid, yielding a sufficiently large supply of atoms for compound formation. Therefore, the chemical reaction to form the compound interlayer is the rate determining step. This step is called 'reaction limited' interface growth, and the interface width x should increase linearly with time t:

$$x \propto t \tag{1.13}$$

2. When a relatively thick compound interlayer is formed, the diffusion flux will have slowed down, and diffusion through the compound interlayer becomes the rate limiting step. This step is called 'diffusion limited' interlayer growth, and the growth of the interlayer width x should follow the parabolic growth law of interlayers:

$$x^2 \propto D't \tag{1.14}$$

   where, D' is an effective diffusion coefficient, related to the real diffusion coefficient.

Moreover, studies by Erdélyi *et al* [28] have shown that nanoscale diffusion effects can strongly depend on the local concentration C. Hence, the diffusion coefficient can be concentration dependent:

$$D(C) \propto D_o \exp(C)\,. \tag{1.15}$$

The diffusion-reaction mechanism in Mo/Si multilayers was recently studied by Bosgra *et al* [29] and it was shown that the diffusion rate decreased as the silicide interlayers grew [29]. Therefore, the simple parabolic growth law of interlayers (equation 1.14) is not valid for all nanoscale multilayered structures and should be applied with caution. In this thesis, we are going to investigate how factors like the availability of diffusing species and/or concentration of layer materials affect the growth of compound interlayers and their structures. As it will be discussed in Chapter 4, in some cases, enrichment of interlayers with one of the constituent layer materials can take place, resulting in a completely different mode of interlayer growth.

1.4.2. Mitigation of diffusion in EUV multilayers

EUVL demands high precision of the multilayer periodicity, and the coatings are required to be stable over many years of operation. For Mo/Si-based illumination optics (Fig. 1.2), a few per mil period change results in a change in the angular response, which makes the highest and the lowest angles of incidence change by 1%. For projection optics, in order to avoid imaging distortions, the reflected wavefront should not be more than a few Ångströms off. Therefore, for the 50-period Mo/Si multilayer coatings, the period thickness should be controlled with a precision of a few tens of picometers during prolonged photon exposure. This is a huge challenge considering the internal structural changes that can take place due to thermal loading.

For mitigation of interdiffusion due to thermal loading, ultra-thin diffusion barriers are often introduced between the layers. Ideal diffusion barriers should have very low diffusion coefficients for multilayer constituent elements, and should be thermodynamically stable with respect to the multilayer materials. Furthermore, for multilayer optics, diffusion barriers should not have high absorption coefficients. The growth properties of diffusion barriers are also crucial. Since the barriers are ultra-thin, materials which have smooth, closed layer growth are preferred. Diffusion barriers which have been proposed for mitigating diffusion in Mo/Si multilayers are B_4C [30], Si_3N_4 [31], C [32] and Mo_2C [33]. From these materials, B_4C is widely used due to its favorable optical properties [30]. In Chapters 3 and 4, B_4C diffusion barriers are investigated and it is shown how their functionality can be understood from the chemical interactions with the Mo and Si layers. Also, the limited efficiency of B_4C layers as diffusion barrier is discussed.

Another method to enhance thermal stability is to replace an entire layer component with a thermodynamically more stable compound. Examples for Mo/Si-based multilayer replacements are Mo_2C/Si [33] and MoN/SiN [34] multilayer structures. This method is also suggested for La/B-based multilayers (designed for $\lambda = 6.7$ nm). As it will be discussed in Chapter 7, LaN/B multilayers have an enhanced optical contrast and thermal stability compared to La/B.

As it will be shown in this thesis, the two mitigation methods suggested here do not completely stop the diffusion induced effects at elevated temperatures or during prolonged photon exposures. To circumvent the period compaction at elevated temperatures, we propose an alternative, self-correcting multilayer design in Chapter 5. The self-correcting process is achieved by balancing the effects of diffusion at the interfaces of multilayers. The design is based on a reference multilayer that exhibits compaction upon thermal loading and includes an additional sub-structure, which expands upon thermal loading to compensate for the basic compaction. Using Mo/Si-based multilayers as an example, the optimization of the ratio of the number of the expanding periods (in this case, Mo/B_4C) to that of compacting periods (Mo/B_4C/Si/B_4C) is demonstrated. Both the average periodicity and the centroid wavelength of the composite multilayer were preserved during annealing at 250 °C for 60 hours.

1.5. Outline

Changes in the optical response of EUV multilayers due to thermally induced structural changes can be adverse for applications. A lot of research has been done to investigate thermal stability of multilayers, but this work presents results that give further insight into nanoscale diffusion phenomena, interface reactions and compound interlayer growth. The experimental methods used to produce and investigate multilayered systems are discussed in detail in Chapter 2.

The introduction of B_4C barrier layers does enhance the thermal stability of Mo/Si multilayers. However, the B_4C-barriered multilayers exhibit a complex behavior of changes in period thickness, with both compaction and expansion being observed during thermal loading. This is due to the fact that B_4C is chemically reactive with both Mo and Si [35, 36]. Using *in-situ* GIXR, WAXRD and XPS depth profiling, the interface reactions are unraveled and their effects on period change are discussed in Chapter 3.

In Chapter 4, the interaction of Mo and B_4C nanoscale layers is investigated further in detail using *in-situ* GIXR, WAXRD, AES depth profiling and stress analysis. Although strong stress relaxation is observed during thermal loading, it is excluded as a cause for period change. It is shown that period changes in Mo/B_4C multilayers depend on the structure of the growing compound interlayers, which is determined by the availability of materials, annealing temperature and annealing time.

The knowledge acquired from the studies of interface interactions of B_4C with both Si and Mo was used to design a self-correcting Mo/Si-based multilayer system, based on the principle of balancing the diffusion-induced multilayer structural changes at the interfaces. The self-correcting design as well as experimental results showing a multilayer with stable temporal behavior at elevated temperatures are presented in Chapter 5

The latter part of this thesis focuses on thermally induced structural changes in La/B-based multilayers. In Chapter 6, the competing effects in terms of period changes, namely, crystallization of compound interlayer (already formed during deposition) and diffusion-induced interlayer growth, are investigated using *in-situ* GIXR, WAXRD and AES depth profiling. In Chapter 7, the interlayer growth in La/B and LaN/B multilayers, designed for $\lambda = 6.7$ nm, is addressed by means of *in-situ* GIXR, GIXR scans and EUV near-normal incidence reflectance measurements. The differences in multilayer optical response are linked to the differences in the rates of interlayer growth.

References

[1] http://www.zyvex.com/nanotech/feynman.html

[2] M. Das, K. H. Shim, S. S. A. An, D. K. Yi, *Toxicology and Environmental Health Sciences* Vol. 3, Issue 4, 193 (2011).

[3] J. Triscone, Ø. Fischer, *Reports on Progress in Physics* **60**, 1673 (1997).

[4] S. S. P. Parkin, *Annual Review of Materials Science* Vol. **25**, 357 (1995).

[5] M. Pessa, A. Tünnermann, *New Journal of Physics* **8**, (2006).

[6] D. Attwood, *Soft X-Rays and Extreme Ultraviolet Radiation, Principles and Applications* (Cambridge University, 1999).

[7] B.L. Henke, E.M. Gullikson, J.C. Davis, *Atomic Data and Nuclear Data Tables* Vol. **54**, 181 (1993).

[8] J. Bosgra, J. Verhoeven, R.W.E. van de Kruijs, A.E. Yakshin, F. Bijkerk, *Thin Solid Films* Vol. **522**, 228 (2012).

[9] V. I. T. A. de Rooij-Lohmann, A. E. Yakshin, R. W. E. van de Kruijs, E. Zoethout, A. W. Kleyn, E. G. Keim, M. Gorgoi, F. Schäfers, H. H. Brongersma, F. Bijkerk, *Journal of Applied Physics* **108**, 014314 (2010).

[10] X. W. Zhou, H. N. G. Wadley, Journal of Applied Physics **87**, 553 (2000).

[11] J. M. Freitag, B. M. Clemens, *Applied Physics Letters* **73**, 43 (1998).

[12] T. Tsarfati, R. W. E. van de Kruijs, E. Zoethout, E. Louis, F. Bijkerk, *Thin Solid Films* **518**(5), 1365 (2009).

[13] T. Tsarfati, R. W. E. van de Kruijs, E. Zoethout, E. Louis, F. Bijkerk, *Thin Solid Films* **518**(24), 7249 (2010).

[14] S. Kumar, N. Krenner, *Journal of Science Education and Technology* Vol. **11** (No. 3), 229 (2002).

[15] G. E. Moore, "Cramming more components onto integrated circuits," *Electronics Magazine*, 4 (1965).

[16] V. Bakshi, *EUV Lithography*, SPIE and John Wiley & Sons, Inc., (2009).

[17] R. F. Pease, S. Y.Chou, *Proceedings of the IEEE* Vol. **96**, (No. 2), 248 (2008).

[18] Singer *et al*, *Illumination System That Suppresses Debris From A Light Source - Patent 6927403* (2005).

[19] O. Wood, C-S Koay, K. Petrillo, H. Mizuno, S. Raghunathan, J. Arnold, D. Horak, M. Burkhardt *et al, Proceedings SPIE* **7636**, 76361M (2010).

[20] N. I. Chkhalo, S. Kunstner, V. N. Polkovnikov, N. N. Salashchenko, F. Schäfers, S. D. Starikov1, *Applied Physics Letters* **102**, 011602 (2013).

[21] A. M. Hawryluk, N. M. Ceglio, *Applied Optics* **32**(34), 7062 (1993).

[22] I. A. Makhotkin, E. Zoethout, E. Louis, A. M. Yakunin, S. Müllender, F. Bijkerk, *Optics Express* **20**(11), 11778 (2012).

[23] C. Michaelsen, J. Wiesmann, R. Bormann, C. Nowak, C. Dieker, S. Hollensteiner, W. Jaeger, *Proceedings SPIE* **4501**, 135 (2001).

[24] R. S. Rosen, D. G. Stearns, M. A. Viliardos, M. E. Kassner, S. P. Vernon, Y. D. Cheng, *Applied Optics* **32**(34), 6975, (1993).

[25] F.R. de Boer, R. Boom, W.C.M. Mattens, A.R. Miedema, A.K. Niessen. *Cohesion in metals – Transition metal alloys* (North-Holland, 1988).

[26] S. Bruijn, R.W.E. van de Kruijs A.E. Yakshin, F. Bijkerk, *Applied Surface Science* Vol. **257**, Issue 7, 2707 (2011).

[27] U. Gosele, K.N. Tu , *Journal of Applied Physics* **53**(4), 3252 (1982).

[28] Z. Erdélyi, D.L. Beke, *Journal of Material Science* **46**, 6465 (2011).

[29] J. Bosgra, J. Verhoeven, R.W.E. van de Kruijs, A.E. Yakshin, F. Bijkerk, *Thin Solid Films* **522**, 228 (2012).

[30] Saša Bajt, Jennifer B. Alameda, Troy W. Barbee, Jr., James A. Folta, Ben Kaufmann, Eberhard A. Spiller, *Optical Engineering* **41**, 1792 (2002).

[31] I. Nedelcu, R. W. E. van de Kruijs, A. E. Yakshin, F. Bijkerk, *Journal of Applied Physics* Vol. **103**, Issue 8, 083549 (2008).

[32] S. Yulin, N. Benoit, T. Feigl, N. Kaiser, *Microelectronic Engineering* **83**(4-9), 692 (2006).

[33] T. Feigl**,** H. Lauth, S. Yulin, N. Kaiser**,** *Microelectronic Engineering Microelectronic Engineering* Vol. **57-58**, 3 (2000).

[34] H. Nakajima, M. Ikebe, Y. Muto, S. Yamaguchi, H. Fujimori, *MRS Int'l. on Adv. Mats.* **10**, 405 (1989).

[35] V.I.T.A. de Rooij-Lohmann, L. W. Veldhuizen, E. Zoethout, A. E. Yakshin, R. W. E. van de Kruijs, B. J. Thijsse, M. Gorgoi, F. Schäfers, F. Bijkerk, *Journal of Applied Physics* **108**, 094314 (2010).

[36] V. I. T. A. de Rooij-Lohmann, A. E. Yakshin, R. W. E. van de Kruijs, E.

Zoethout, A. W. Kleyn, E. G. Keim, M. Gorgoi, F. Schäfers, H. H. Brongersma, F. Bijkerk, *Journal of Applied Physics* **108**, 014314 (2010).

2. Experimental

2.1. Deposition of multilayered structures

The multilayered structures discussed in this thesis were deposited at a coating facility of the nanolayer Surfaces and Interfaces (nSI) department of the FOM Dutch Institute for Fundamental Energy Research (DIFFER). The schematic diagram of the facility is shown in Fig. 2.1. The multilayers were deposited in an Ultra High Vacuum (UHV) setup using two physical vapor deposition techniques: DC magnetron sputtering deposition and electron beam (e-beam) deposition.

Magnetron sputtering deposition is widely used to deposit thin films and nanoscale multilayered structures, and most of the multilayers in this thesis were deposited using this method. The base pressure of the setup was below 10^{-8} mbar to prevent contamination of layers during growth. During deposition, the Kr gas above the magnetron target is ionized by electrons emitted by a cathode. As the target material is negatively biased, the Kr ions are accelerated towards the target and sputter the target. The kinetic energy of sputtered particles ranges between 1 and 10 eV, which may induce atom intermixing at shallow interfaces. The distance between the target and the substrate holder is ~30 cm – larger than the distance in traditional magnetron sputtering setups. The large distance, combined with an increased pressure in the chamber, reduces the energy of sputtered atoms through collisions with gas atoms, and thus reducing the chances of surface damage during deposition.

Using e-beam deposition, an electron beam evaporates a solid target material placed in a crucible. The evaporated material atoms arriving at the substrate

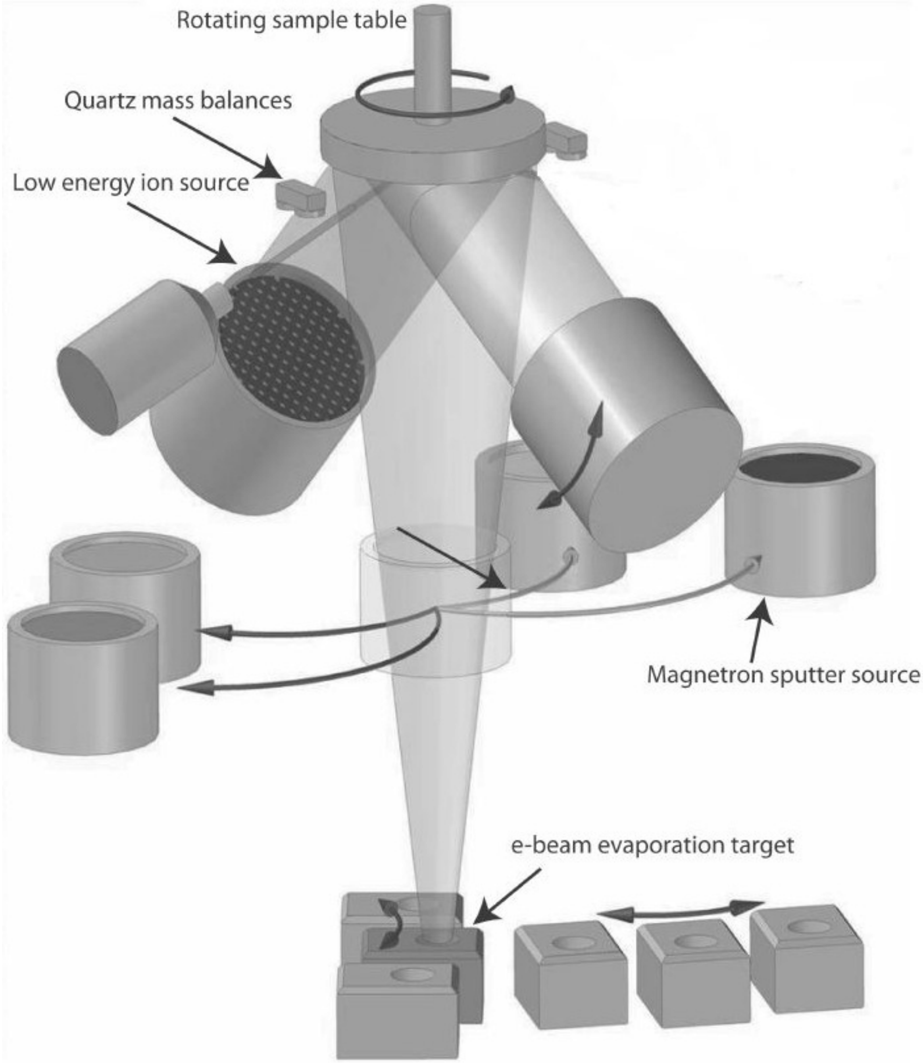

Fig. 2.1: A schematic diagram of the coating facility.

have a low adatom energy (~0.1 eV) [1], which reduces sub-surface atom implantantion and intermixing effects with the previous layer or the substrate. However, the low adatom energy may lead to development of roughness and lower densities due to build up of porosity in the layers. For smoothening the layers and preventing the build up of porosity, a low energy ion treatment can be used during or after the growth of each individual layer. The ion treatment has been shown to produce layers with densities and interface roughness comparable to those produced by DC magnetron sputtering [2]. Note that the ion treatment is generally more suitable for amorphous layers since crystalline layers may show preferential sputtering that can actually further increase the roughness. To obtain optimal layer properties, the incident angle, the energy and the flux of impinging ions should be optimized.

Accurate control of the thickness of the layers deposited by magnetron sputtering is achieved by using specified sputter process times based on calibrated deposition rates.

Since e-beam deposition cannot use calibrated rates, controlling the layer thickness during growth is done by using multiple quartz mass balances mounted near the sample holder. The quartzes vibrate at a certain resonance frequency depending on their mass. When extra mass is added during deposition a thin films, the frequency changes and can be used to determine the mass deposited on the quartzes. Using the density of the deposited material, an accurate measure of the deposited layer thickness can be determined. The accuracy of this method is about 0.3 Å due to variations in temperature and pressure, uncertainty in density values and instabilities in the deposition plume. In our experiments, magnetron sputtering was preferred to e-beam deposition due to higher stability and better reproducibility.

Several methods were used to study the structural and chemical changes in multilayers at enhanced temperatures and their effects on the performance. To investigate diffusion and compound interlayer growth during annealing treatment, *in-situ* grazing incidence X-ray reflectometry (GIXR) was used. This technique characterizes multilayer period changes with picometer accuracy. *Ex-situ* wide angle X-ray diffraction (WAXRD) was used to determine changes in crystallinity and specifically changes in crystallite size. The two techniques were used together with a complimentary destructive chemical analysis technique, either X-ray photoelectron spectroscopy (XPS) or Auger electron spectroscopy (AES) depth profiling, which could probe relative changes in atomic concentrations due to intermixing at the interfaces. The X-ray diffraction and reflection experimental methods and the chemical analysis techniques are described in detail in Sections 2.3 and 2.4. EUV reflectometry (AOI = 1.5°) measurements were performed at the soft X-ray beam line of Physikalisch-Technische Bundesanstalt (PTB), Berlin.

2.2. Annealing treatment for diffusion studies

The structural changes in multilayers during annealing were investigated using an annealing setup inside a hard X-ray diffractometer (Cu-Kα radiation, λ = 0.154 nm), shown in Fig. 2.2. The setup is equipped with an Anton Paar heating stage located under a dome made of the X-ray transparent material PEEK. The setup enables *in-situ* diffusion studies during annealing. The stage can heat up a sample up to 900 °C, with the temperature control, stability and reproducibility being within 0.5 °C. Due to variations in thermal conductivity, the temperature on top of the sample can deviate. However, at temperatures lower than 300 °C this deviation is limited to < 2 °C, and the effects of these deviations are negligible for the experiments discussed in this thesis. The setup is suitable for diffraction and reflection studies during annealing since the annealing stage can rotate in all directions. Further details of the annealing setup can be found in ref. [3].

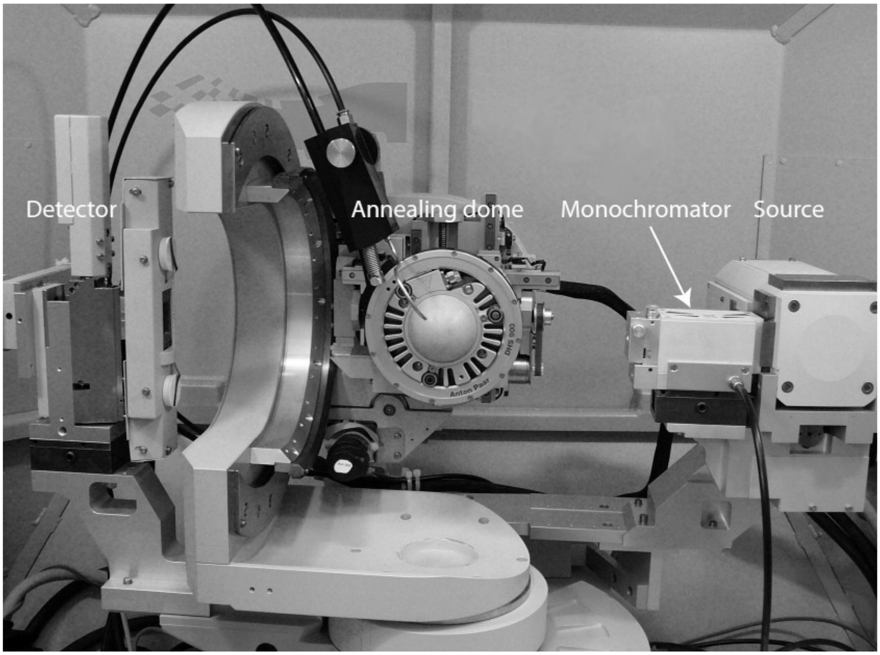

Fig. 2.2: Cu-Kα diffractometer with an annealing setup for *in-situ* diffusion studies. The heating plate is located under the annealing dome, which is made of the X-ray transparent material PEEK.

The annealing experiments were performed in a nitrogen gas environment (constant flow of 1 l/min) in order to prevent surface contamination during annealing. The gas flow significantly reduces contamination and specifically limits the effects of oxidation to the top few nanometers of the multilayer samples. XPS analysis on annealed Mo/Si samples ($\Lambda = 7$ nm) shows that below 400 °C the oxidation is limited to the first layer while above 400 °C one bilayer is oxidized [4]. Such oxidation effects were ignored in the analysis due to the focus of this thesis on the multilayer internal structure and the fact that Cu-Kα radiation penetrates all the layers.

2.3. Hard X-ray diffraction and reflection

Hard X-rays (Cu-Kα radiation, $\lambda = 0.154$ nm) penetrate all the layers, therefore revealing information about the internal structure of the whole multilayer. Moreover, X-ray diffraction and reflection measurement techniques are non-destructive, making them ideal for investigating thermally induced changes in multilayers during the annealing treatment. The two techniques use different measurement geometries to probe different structural information, as discussed in detail in the following sections.

2.3.1. Wide angle X-ray diffraction

WAXRD is used to study the crystalline structure of multilayers. Properties such as crystalline phase, preferred lattice orientation in nanocrystallites, crystallite size and lattice strain can be obtained from WAXRD scans. From these properties, information about crystallinity, diffusion/compound interlayer growth and link between microstrains and macroscopic substrate deformation can be deduced. For instance, Mo layers in multilayers investigated in Chapters 3 and 4 have a polycrystalline structure, while the Si and B_4C layers are amorphous. From the widths of diffraction peaks (see Fig. 2.3), Mo crystallites size can be obtained. The crystallites size can be used as a tool to monitor the changes in Mo layer thickness, which is relevant for understanding diffusion processes and compound interlayer growth [5].

WAXRD measurements on Mo containing multilayers (Chapters 3 and 4) were performed using a PANalytical X'Pert X-ray diffractometer, with a 4-bounce asymmetrically cut Ge (220) monochromator that monochromates the radiation from the X-ray tube to only the Cu-Kα_1 line. A programmable receiving slit and a programmable anti-scatter slit were placed at the detector. An automated attenuator was mounted in front of the detector to avoid damage during direct illumination (Fig. 2.2). WAXRD measurements on La/B-based multilayers (Chapters 6 and 7) were performed using a PANalytical Empyrean X-ray diffractometer (Cu-Kα radiation, 0.154 nm), with a parallel beam mirror at the source and a parallel plate collimator at the detector. The parallel beam mirror was introduced to improve the collection efficiency. The measurements do not suffer from resolution losses due to the introduction of parallel plate collimator and broad peaks from small crystals to start with.

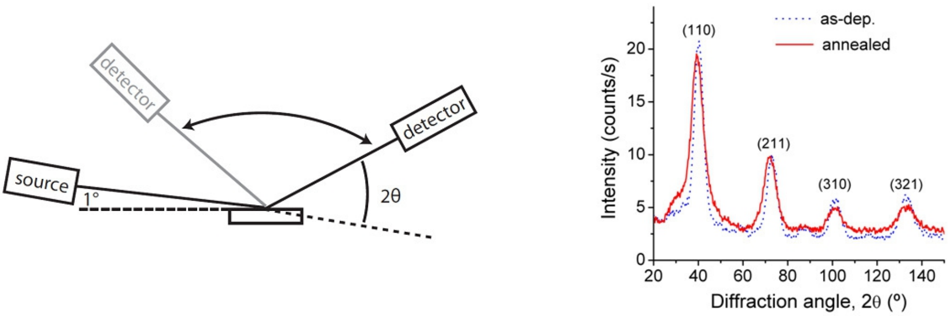

Fig. 2.3: WAXRD measurement geometry, with an example of scans for as-deposited and annealed Mo/Si multilayers with B_4C diffusion barriers.

Fig. 2.3 shows the WAXRD measurement geometry. A fixed grazing incidence source angle of 1° is used in order to maximize the illumination area and collection efficiency. However, this angle gives a peak broadening of ~1°. The multilayers were routinely deposited onto crystalline Si substrates to obtain smooth growth conditions. However, the crystalline Si substrate will also lead to diffraction peaks. To suppress in particular the (311) and (422) diffraction peaks from the Si substrate, the samples are rotated by 20° in plane with respect to the (100) axis.

The crystallite size *X* can be calculated using the Scherrer equation:

$$X = \frac{K\lambda}{L\cos(\theta)} \tag{2.1}$$

where, *L* is the full width at half-maximum of the peak at diffraction angle 2θ, λ is the wavelength and $K = 0.94$ for lattices with cubic symmetry (for e.g. bcc Mo) [6]. The size of a crystallite may depend on the orientation of the crystallite in the multilayer. This is defined by the angle ψ between the surface normal and the normal vector of the diffraction planes. For accurate determination of crystallite size, the instrumental peak broadening should be small compared to *L*.

The widths of diffraction peaks from the studied multilayers are generally much broader than 3°, significantly larger than the instrumental broadening of typically 1°. Although the results presented in this thesis were not corrected for instrumental broadening, which may result in an underestimation of approximately 10-20% of the crystallite size, the changes in crystallite size as a result of annealing can be determined with a much higher accuracy (~5%).

2.3.2. Grazing incidence X-ray reflection

GIXR measurements were performed using the PANalytical X'Pert X-ray diffractometer, whose details are provided in Section 2.3.1. X-rays interacting with matter are specifically sensitive to electron density fluctuations. The used θ-2θ geometry is sensitive to the electron density profile perpendicular to the surface (i.e. scattering vector perpendicular to the surface), providing information like layer thicknesses, densities and roughness.

A multilayer is a special periodic example of an electron density profile. Constructive interference from the multilayer interfaces is amplified when Bragg's law is met. Fig. 2.4 shows the GIXR measurement geometry and an example of a GIXR scan. The positions of Bragg peaks from a multilayer can be described using the following equation:

$$m\lambda = 2\Lambda \sin\theta_m \sqrt{1 - \frac{2\overline{\delta}}{\sin^2\theta_m}} \tag{2.2}$$

where, $\overline{\delta}$ is the weighted average over δ values of the materials (with $\delta = 1\text{-}n$) and Λ is the multilayer period thickness. Furthermore, scan features like peak intensities/widths and peak intensity ratios can provide information about the optical contrast and density modulation inside a period. All these features can be measured and used to explain the effects of diffusion on the multilayer structure. For example, growth of dense compound interlayers would cause the multilayer period thickness to decrease, causing the Bragg peak positions to shift to larger grazing angles; intermixing of atoms at the interfaces can lead to a drop in peak intensities and a decrease in peak widths, etc. Also, the complete spectrum can be compared to model simulations – e.g. by using a program like IMD [7] – and model parameters such as the thickness of compound interlayers/intermixed regions, and interface and surface roughness can be extracted.

It should be noted at this point that GIXR is highly sensitive to in-depth density fluctuations but in principle insensitive to lateral density fluctuations.

For this reason, GIXR cannot distinguish between morphological interface roughness and interface concentration gradients. Measurement of off-specular reflectivity scans and comparison with more extended scattering theories within for e.g. (Distorted Wave) Born approximation could help to distinguish between morphological and graded interface roughness but are beyond the scope of this thesis. Furthermore, GIXR is in principle not sensitive to specific chemical environment, i.e. it is the combination of density and X-ray scattering cross-section that is probed; without knowing one, the other cannot uniquely be identified. Therefore, to fully explain the changes in the internal structure, in this thesis GIXR will be complemented with chemical analysis techniques such as XPS or AES.

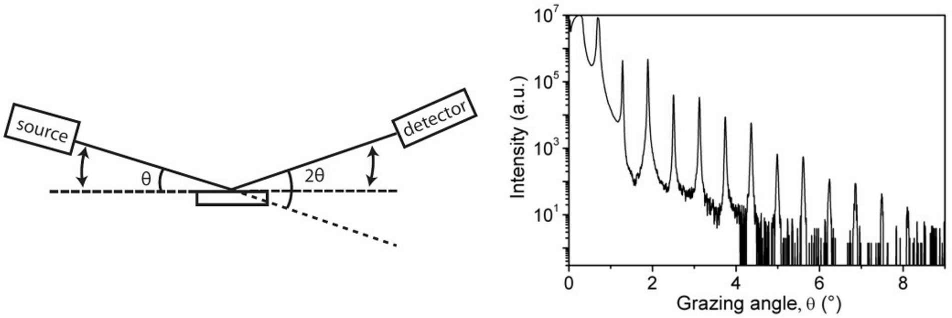

Fig. 2.4: GIXR measurement geometry, with an example of a scan for an as-deposited Mo/Si multilayer with B_4C diffusion barriers. The grazing angle, θ, ranges from 0° to 10°.

2.3.3. *in-situ* grazing incidence X-ray reflection during annealing

GIXR scans were performed *in-situ* during annealing to study the multilayer structural changes in real time, using the annealing and measurement setup described in Section 2.2 (see Fig. 2.2). Before thermal loading, alignment of the sample position with respect to the incident X-ray beam is performed, followed by measurement of a reference GIXR scan. The sample is then heated up to the target temperature. To correct for alignment errors introduced by thermal expansion of the sample stage and/or mechanical deformation of the sample at enhanced temperature, the sample position with respect to the X-ray beam is again aligned at the enhanced temperature. After that, GIXR scans are continuously recorded during the annealing treatment. Possible misalignment in θ can be corrected for by the data fitting procedure described below.

To speed up data collection, only partial GIXR scans are recorded during annealing. This reduces the impact of changes during measurements. The data is analyzed by comparing the angular positions of specific low and high order diffraction peaks to those obtained for the reference scan. The change in multilayer period is then calculated using a simplified version of Equation 2.2, in which it is assumed that the average δ remains unchanged (therefore neglected) and $\sin\theta \approx \theta$ for small angles:

$$\Delta\theta_2 - \Delta\theta_1 = \lambda(\Delta m)\left(\frac{1}{2\Lambda_0} - \frac{1}{2\Lambda}\right), \qquad (2.4)$$

where Δm is the Bragg order difference of the peaks recorded, Λ_o is the period before annealing, Λ is the period during annealing, and $\Delta\theta_1$ and $\Delta\theta_2$ are peak shifts of the low order and high order Bragg peaks with respect to the respective reference angular positions of those Bragg peaks. This method is independent of small possible sample misalignment in θ since the relative shifts in the positions of Bragg peaks are used in the analysis and the misalignment is equal for both peaks. Nevertheless, the change in the shapes of observed peaks can introduce errors. The accuracy of the determined period changes can be as good as 1 pm for materials with high optical contrast, for example Mo and Si [4, 8]. For materials with poorer optical contrast like Si and C, the accuracy is ~2.5 pm.

2.4. Atomic concentration depth profiling

GIXR is a very accurate analysis technique for determining multilayer period thickness, and to a lesser extent individual layer thicknesses and densities, but it is insensitive to atomic concentrations and chemical environment. Therefore, XPS and AES depth profiling techniques were employed to complement GIXR (and WAXRD) analysis in order to explain thermally induced changes in multilayers. For instance, in Chapter 3, Mo-B_4C multilayers appeared stable when analyzed using *in-situ* GIXR due to the absence of significant changes in the Mo/B_4C multilayer period thickness, but XPS depth profiles showed significant intermixing.

2.4.1. X-ray photoelectron spectroscopy

XPS is generally used to obtain information about the elemental composition and the chemical states of elements in a surface layer. For XPS measurements, a Theta Probe instrument employing Al-Kα radiation (hν = 1486.6 eV) was used.

The radiation removes core electrons from atoms in the sample. Considering the elastic mean free path of the photoelectrons is in the order of a few nm, XPS analysis probes only a depth of 5 to 10 nm, depending on the kinetic energy of the emitted electrons. The binding energy of the photoelectrons is determined from the difference between the energy of the impinging photons and the kinetic energy of the electrons. Since each element has a distinct set of binding energies, XPS can be used to determine the elements and their concentrations. Moreover, the environment of the elements can lead to shifts in their binding energies, which can be used to indentify the chemical states.

Angular resolved XPS (ARXPS) is a non-destructive method used to obtain information from a probed depth. At grazing angles, the photoelectrons will have originated from close to the surface, while at larger angles the photoelectrons originate from deeper locations in the sample. Therefore, ARXPS effectively provides information about the atomic concentration profile over a certain probed depth. However, we are interested in the concentration profiles over several periods of multilayers with period thickness of 4 – 7 nm. Furthermore, as mentioned before (Section 2.2), the top few layers of the multilayer samples are often contaminated with oxygen. These two factors make ARXPS not suitable for obtaining the atomic concentration depth profiles of multilayers.

In order to obtain the atomic concentration depth profiles of multilayers over several periods, XPS measurements are combined with ion beam sputtering. In our studies (Chapter 3), a 0.5 keV Ar^+ beam, impinging at 45°, was used to erode a thin layer from the surface and subsequently an XPS measurement was performed. The alternative sequence of eroding and measurement provides in-depth information on the multilayer composition. It should be noted that the ion beam does intermix the layers and the sampling depth is larger than the individual layer thickness. Thus, the analysis results in profiles with a gradual transition between the materials rather than a sharp one. Although this method does not provide absolute atomic concentration profiles, it does provide information on the relative changes due to intermixing at the interfaces induced by elevated temperatures.

2.4.2. Auger electron spectroscopy

AES can also be used to obtain information about the elemental composition and the chemical state in a surface layer. In contrast to XPS, AES uses an electron beam of a typically a few keV to remove core electrons from atoms in the sample. The kinetic energy of the Auger electrons, emitted as a result of relaxation of the ionized atoms to the ground state, contains information about the difference in binding energies between the core level and the immediate/next upper shell together with the outer shell.

Similar to XPS, in order to obtain the atomic depth profiles of multilayers over several periods, AES measurements are combined with ion beam sputtering. In our studies, an electron beam of 5 keV was used with sputter erosion performed using 250 eV Ar^+ ions impinging at 45º. Also, this method does not provide absolute atomic concentration profiles but gives information about relative changes due to intermixing at the interfaces, albeit with higher resolution due to the fact AES probing depth is lower compared to XPS. AES depth profiling was used in Chapter 6 to investigate atom diffusion at the interfaces of La/B multilayers (Λ = 7 nm) at different annealing temperatures. The results provided qualitative information on the differences in intermixing at 300 °C and 400 °C – the former showed only marginal intermixing while the latter showed significant intermixing.

References

[1] P. J. Martin, *Journal of Materials Science* **21**, 1 (1986).

[2] S. Bruijn, R. W. E van de Kruijs, A. E. Yakshin, F. Bijkerk, *Journal of Applied Physics* **111**, 064303 (2012).

[3] R. Resel, E. Tamas, B. Sonderegger, P. Hofbauer, and J. Keckes, *Journal of Applied Crystallography* **36**, 80 (2003).

[4] S. Bruijn, *Diffusion phenomena in chemically stabilized multilayer structures* (Ipskamp Drukkers, 2011).

[5] J. Bosgra, J. Verhoeven, R.W.E. van de Kruijs, A.E. Yakshin, F. Bijkerk, *Thin Solid Films* **522**, 228 (2012).

[6] A. L. Patterson, *Physics Review* **56**, 978 (1939).

[7] D. L. Windt, *Computers in Physics* **12**(4), 360 (1998).

[8] S. Bruijn, R.W.E. van de Kruijs, A.E. Yakshin and F. Bijkerk, *Applied Surface Science* **257**, Issue 7, 2707 (2011).

3. Thermally induced interface chemistry in Mo/B_4C/Si/B_4C multilayered films

Abstract

B_4C diffusion barrier layers are often introduced into Mo/Si multilayered films for enhancement of thermal stability. It is observed that, such multilayered films exhibit both period expansion and period compaction upon annealing at temperatures below 300 ºC, depending on the annealing temperature and time. Using *in-situ* grazing incidence X-ray reflection measurements during sequential annealing, we resolved picometer periodicity changes in Mo/B_4C/Si/B_4C, Si/B_4C and Mo/B_4C multilayer films, and show that the two opposite period-change effects are a result of interaction of Si with B_4C layers, leading to expansion, and Mo_xSi_y formation, leading to compaction. The study of Si/B and Si/C multilayer sub-systems suggests that the cause of expansion is the formation of relatively low density Si_xB_y compounds at the Si-B_4C interface. Although the Mo-B_4C interface seems to be stable based on reflectometry data, other techniques such as depth profiling X-ray photoelectron spectroscopy and wide angle X-ray diffraction measurements show that Mo and B_4C actually intermix.

3.1. Introduction

Interactions at interfaces in thin films and multilayers play an important role for current day nanoscale devices. Free electron lasers, astrophysics research and extreme ultra-violet lithography (EUVL) tools are examples of applications that make use of Mo/Si multilayers as reflective coatings, requiring control of interface interactions at the atomic level. The high-flux photon exposures in applications provide thermal load onto the coatings, causing interdiffusion of Mo and Si atoms. Formation of molybdenum silicides at the interfaces [1] leads to reduced optical contrast and a lower reflectance [2]. In addition, densification upon silicide formation at the interfaces leads to a reduction of the multilayer period, which through Bragg's law leads to a reduction of the wavelength that is reflected.

The Mo/Si multilayer structure and interlayer growth at high temperatures [1, 3] have been studied extensively, including development of scaling laws for diffusion-reaction mechanisms [4]. In order to mitigate the degradation of multilayer optics under thermal loading, thin Si_3N_4, Mo_2C or B_4C layers [1, 5, 6] can be introduced as diffusion barriers. B_4C is widely used due to its favorable optical properties, and 1-nm-thick B_4C barriers have been shown to improve the thermal stability of the multilayers [6, 9].

Although there is significant reduction of interdiffusion rates and formation of molybdenum silicides, the Mo/B_4C/Si/B_4C system, designed for EUVL applications ($\lambda = 13.5$ nm), exhibits unexpected behavior upon annealing. When the system is subjected to temperatures higher than 300 ºC, only period compaction is observed, similar to what is observed in Mo/Si multilayers. However at lower temperatures, the system exhibits period expansion as well as period compaction upon annealing, depending on the annealing temperature and time. Most of the previous works concentrated on investigating this system at high temperatures (more than 300 ºC) for determining diffusion constants [6, 7, 8], with the structural changes observed at low temperatures being not yet understood. In this chapter, we present results from low-temperature annealing studies on Mo/B_4C/Si/B_4C multilayers and address the chemical interactions at the interfaces during annealing in order to explain the competing mechanisms of multilayer expansion and compaction below 300 ºC.

3.2. Experimental

Several 50-period multilayer systems were deposited onto 25 mm × 25 mm super-polished Si substrates. Initially the following systems were prepared:

Mo/B_4C/Si/B_4C, Mo/B_4C and Si/B_4C. Following the investigation, the following sub-systems were added: Mo/B, Mo/C, Si/B and Si/C. For all systems the layer thicknesses of Mo and Si were selected to be 3 nm and 4 nm, respectively, which are typical values for several applications. 1-nm-thick B_4C barrier layers have proven to successfully enhance thermal stability by reducing Mo and Si interdiffusion at the interfaces [6, 9]. Therefore, B_4C, B and C layer thicknesses were chosen to be 1 nm.

All the layers, except for B, were deposited by DC magnetron sputtering in a deposition setup with base pressure $< 1 \cdot 10^{-8}$ mbar. Since B could not be ignited by a DC power supply at low target temperature, electron beam deposition of boron was used instead. The B layers were deposited with noble gas (Kr) ion-beam assistance (beam voltage 60 V, flux 7×10^{13} cm^{-2} s^{-1}, angle of incidence 45º) for smoothening and preventing the build up of porosity. This process has been shown to produce layers with densities and surface roughness comparable to those produced with DC sputtering. Layer thicknesses were monitored during deposition using quartz mass balances, and deposition speeds were fixed at the rate of 20 pm/s. To ensure homogenous coating on the substrates, the sample holder was rotated at 1 Hz.

To study the multilayer structure during thermal loading, grazing incidence X-ray reflection (GIXR) measurements were conducted *in-situ* during annealing using a PANanalytical X'Pert X-ray diffractometer (Cu-Kα radiation, 0.154 nm).

Before annealing, the alignment of the sample position with respect to the impinging X-ray beam was performed and a reference GIXR scan was recorded. After that, the sample was heated up to the required temperature. The sample position was aligned again with respect to the X-ray beam to correct for thermal expansion of the sample stage, and subsequent GIXR scans were recorded during annealing. Detailed descriptions of the *in-situ* annealing setup (Anton Paar stage) are found in reference [10].

Mo/B_4C/Si/B_4C, Mo/B_4C and Si/B_4C multilayer samples were sequentially annealed from 75 ºC to 300 ºC, in steps of 25 ºC. Mo/B, Mo/C, Si/B and Si/C samples were sequentially annealed from 100 ºC to 250 ºC, in steps of 50 ºC. The duration of each annealing cycle in all experiments was 8 hours. Multilayer periods during annealing were extracted from changes in measured Bragg peak positions. Further details about the experimental method, determination of positions and relative shifts of Bragg peaks and period change are found in reference [4]. This method can resolve period changes with picometer accuracy and is therefore sensitive enough to detect structural changes at relatively low annealing temperatures. The period changes presented in this chapter were corrected for thermal expansion using bulk thermal expansion coefficients. The coefficients of Mo, Si and B_4C were taken from ref [11], and those of B and C were taken from refs. [12] and [13], respectively. The corrected period changes were verified by obtained periods of as-deposited and annealed samples, measured at room temperature.

Before and after annealing, Mo-containing multilayer samples were characterized by wide angle X-ray diffraction (WAXRD) and X-ray photoelectron spectroscopy (XPS) sputter depth profiling. The sample was rotated in plane of the substrate by a fixed angle during WAXRD measurements in order to suppress the diffraction peak of the monocrystalline Si substrate. For XPS measurements, a Theta Probe instrument using Al-Kα radiation (hν = 1486.6 eV) was used, with sputter erosion performed using 0.5 keV Ar^+ ions impinging at 45º.

3.3. Results and discussion

The results are presented in three sections. We start with the $Mo/B_4C/Si/B_4C$ multilayer system, and compare this to Mo/Si, Mo/B_4C and Si/B_4C multilayers. Secondly, simple binary multilayer systems of Si/B and Si/C will be investigated and compared to Si/B_4C. Similarly, Mo/B and Mo/C multilayers are compared to Mo/B_4C.

3.3.1. $Mo/B_4C/Si/B_4C$, Mo/B_4C and Si/B_4C

Fig. 3.1 shows the period changes for the $Mo/B_4C/Si/B_4C$ multilayer upon sequential annealing at different temperatures. Period changes observed in Mo/Si multilayers, taken from ref [1], are shown as reference. Although it is evident that the introduction of thin B_4C barriers in Mo/Si multilayers reduces the period changes, the temperature dependent behavior appears quite complex, dominated by period expansion below 225 ºC, and switching to period compaction above 250 ºC. It should be noted that such behavior is not observed in Mo/Si multilayers, where only compaction is observed due to $MoSi_2$ formation at the interfaces during annealing [1].

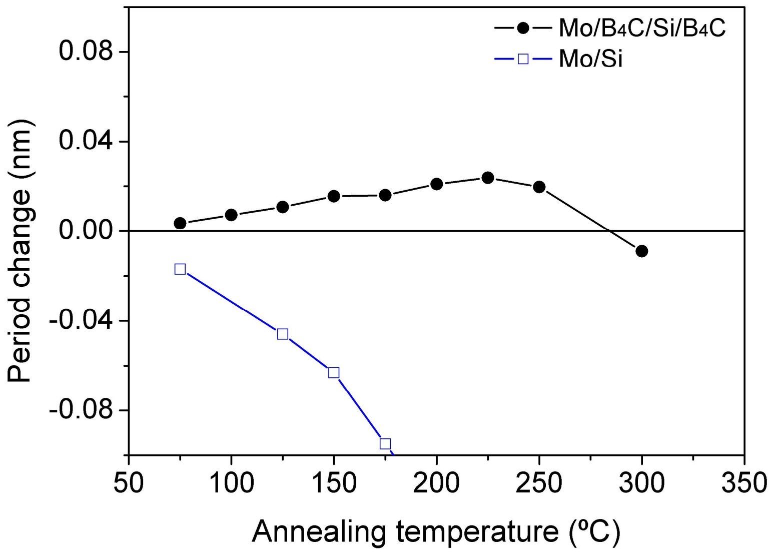

Fig. 3.1: Period change as a function of annealing temperature for Mo/B_4C/Si/B_4C multilayer system. Each data point was measured after an annealing cycle of 8 hours. Previous results of Mo/Si multilayers are added for comparison.

Studies performed by de Rooij-Lohmann *et al* [7, 8] have shown that B_4C is chemically reactive with both Mo and Si and various compounds can be formed at the interfaces of Mo/B_4C/Si/B_4C. Depending on the densities of the constituent species and the densities of the compounds formed, either compaction or expansion could occur. Table 3.1 shows binary compounds that could be formed and the volumetric effects, based on bulk densities provided by literature [12]. Densification/period compaction is observed in all reactions, and therefore bulk densities cannot be used to predict the observed period change behavior of Mo/B_4C/Si/B_4C.

Since the behavior of the system cannot be explained by volumetric effects calculated from literature density values, additional experiments were carried out to separately investigate the behavior of Si-B_4C and Mo-B_4C interfaces. For this purpose, Si/B_4C and Mo/B_4C multilayers were prepared and subjected to thermal annealing and analysis.

	A (g/mol)	ρ (g/cm^3)	$V_I/V_{comp.}$	$V_{II}/V_{comp.}$	Fractional Vol. Change
Mo	95.94	10.20	-	-	-
Si	28.085	2.33	-	-	-
B	10.811	2.34	-	-	-
C	12.01	1.80	-	-	-
MoB	106.75	8.65	0.76	0.37	-0.14
MoB_2	117.56	7.12	0.57	0.56	-0.13
Mo_2B	202.69	9.26	0.86	0.21	-0.07
MoC	107.95	8.2	0.71	0.51	-0.22
Mo_2C	203.89	8.20	0.82	0.29	-0.11
SiB_3	60.52	2.52	0.50	0.58	-0.08
SiB_6	92.95	2.47	0.32	0.74	-0.06
SiC	40.10	3.22	0.97	0.53	-0.50
Mo_3Si	315.78	8.97	0.80	0.34	-0.14
Mo_5Si_3	563.74	8.20	0.68	0.52	-0.21
$MoSi_2$	152.06	6.24	0.39	0.99	-0.38

Table 3.1: Molecular volumes of Mo, B, C and Si consumed in chemical reactions to form various binary compounds. V_I and V_{II} are molecular volumes of the first element and second element, respectively, and $V_{comp.}$ is the molecular volume of the corresponding formed compound. Calculations are based on bulk density values. Densification/compaction is observed in all reactions. For example, 0.76 nm of Mo and 0.37 nm of B are consumed to form 1 nm of MoB.

Fig. 3.2 shows the period changes observed in Si/B_4C and Mo/B_4C multilayers as a function of the annealing temperature. The Mo-B_4C interfaces seem to be thermally more stable than the Si-B_4C interfaces as the period of Mo/B_4C does not change significantly during annealing, with only a small decrease in period being observed at temperatures > 200 ºC. When comparing Figs. 3.1 and 3.2, it can be concluded that the behavior of Mo/B_4C/Si/B_4C cannot be explained by simply adding the separate contributions from Mo-B_4C and Si-B_4C interfaces. Doing so would result in expansion (interactions at the Si-B_4C interfaces), with no compaction expected as observed in Mo/B_4C/Si/B_4C at temperatures above 250 ºC.

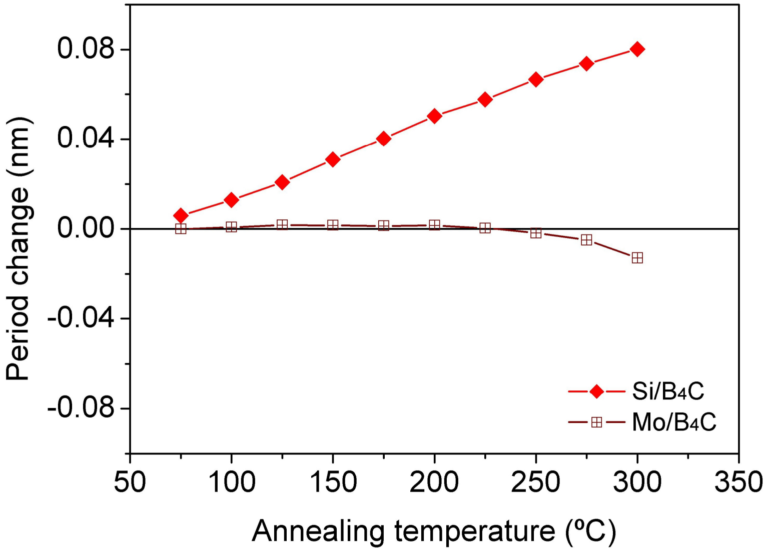

Fig. 3.2: Period change as a function of annealing temperature for Si/B_4C and Mo/B_4C multilayers.

Since the presence of B_4C only slows down (but does not completely prevent) the interdiffusion of Mo and Si [7, 8, 14, 15], Mo_xSi_y formation should be considered when addressing the temperature behavior of the full Mo/B_4C/Si/B_4C system. To investigate possible contribution from Mo_xSi_y formation in Mo/B_4C/Si/B_4C, the period changes due to interactions at the Mo-B_4C and Si-B_4C interfaces were subtracted from the period changes in Mo/B_4C/Si/B_4C. The resulting calculated temperature dependence is shown in Fig. 3.3, as data set (4). We found that this resembles the temperature dependence observed for Mo/Si multilayers, when reducing the Mo/Si data by a factor of five. This indicates that there is five times less Mo_xSi_y interlayer growth in Mo/Si multilayers with B_4C barriers than in multilayers without such barriers. The observed temperature dependence for Mo/B_4C/Si/B_4C is now explained as a combined effect of chemical interactions at the Si-B_4C interfaces and simultaneous formation of Mo_xSi_y.

In fact considering again the data shown in Fig. 3.2, it is surprising that period expansion is observed in Si/B_4C, since volumetric calculations of formation of silicon borides and silicon carbides is expected to result in period reduction. However, such volumetric calculations assume bulk densities, and it should be noted that a reduced density (for example 5 % lower) of the formed compounds

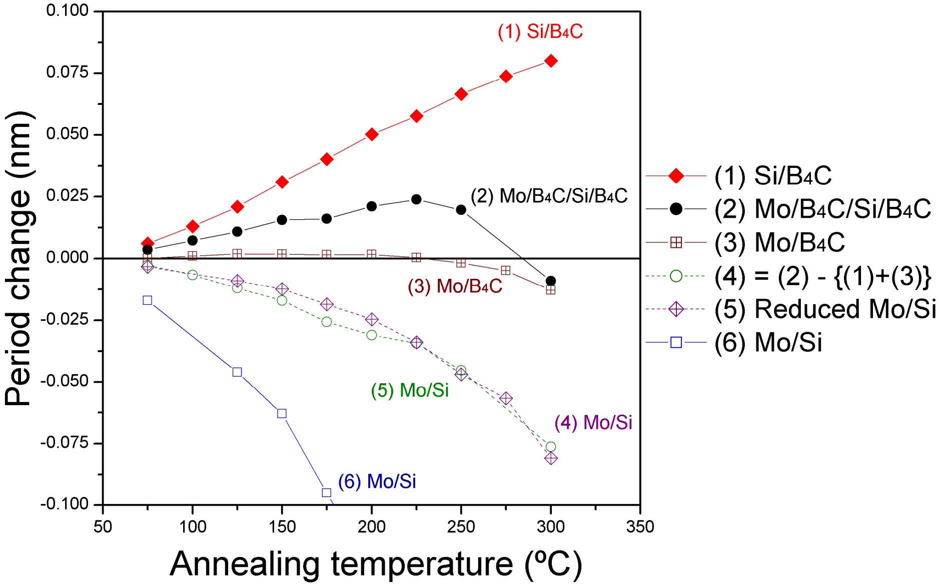

Fig. 3.3: An overview of period change as a function of annealing temperature for the following multilayer systems: Si/B_4C, $Mo/B_4C/Si/B_4C$, Mo/B_4C and Mo/Si.

would already result in period expansion instead of compaction. Since the densities of the deposited films and formed compounds are actually not known to this accuracy, this makes it impossible to link a period change directly to the formation of a specific compound during annealing.

To further explore the chemistry at the interfaces of $Mo/B_4C/Si/B_4C$ multilayers, elementary multilayer systems of Si/B and Si/C were investigated and compared to Si/B_4C. Similarly, Mo/B and Mo/C multilayers were compared to Mo/B_4C.

3.3.2. Si/B, Si/C and Si/B_4C

Fig. 3.4 shows period changes as a function of annealing temperature for Si/B, Si/C and Si/B_4C multilayers. Samples were annealed for 8 hours at each temperature. The expansion in Si/C is relatively small, while that observed in Si/B is very similar to that observed in Si/B_4C.

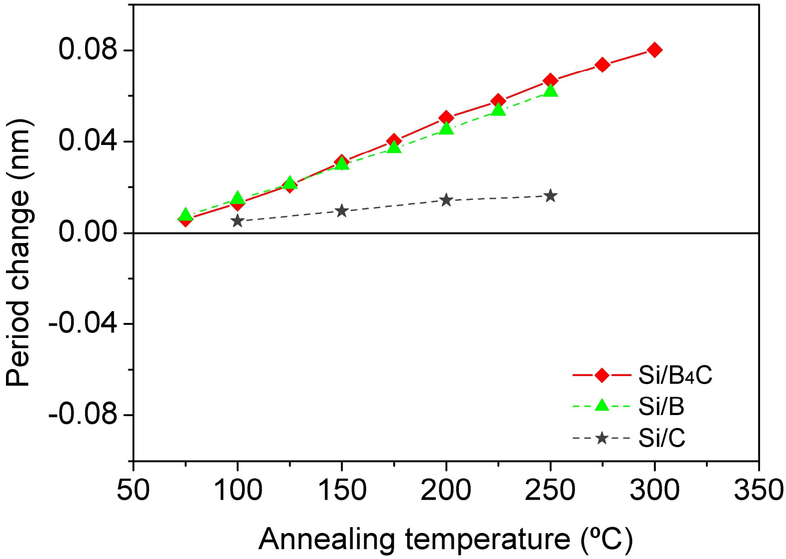

Fig. 3.4: Period change as a function of annealing temperature for Si/B, Si/C and Si/B_4C multilayers.

The similarity between Si/B and Si/B_4C suggests that period expansion in Si/B_4C, and by extension, the low temperature behavior of Mo/B_4C/Si/B_4C, is explained by the formation of low density Si_xB_y compounds. The exact boride(s) being formed, as well as the density of the interface compound, cannot be identified from these results since the amounts of initial materials consumed to form compounds are not known. However, for period expansion to be observed, the densities of, for instance, SiB_6 or SiB_3 formed should be at least 5% to 7% respectively lower than the bulk values. This is calculated based on bulk densities of the initial components (Si and B). High temperature studies, increasing the amount of reacted material, may allow identification of the formed compounds through for example XPS studies, but it may prove difficult to link such results to the current low temperature studies due to possible differences in the formed interface composition.

3.3.3. Mo/B, Mo/C and Mo/B_4C

Fig. 3.5 shows Mo/B, Mo/C, and Mo/B_4C multilayer period change as a function of the annealing temperature. In contrast to the observed absence of period changes in Mo/B_4C, the periods of both Mo/B and Mo/C multilayers do decrease upon sequential annealing, with changes in Mo/B multilayers being dominant. This indicates that the growth of Mo_xB_y and Mo_xC_y interlayers results in period compaction. Since the behavior of Mo/B_4C cannot be directly explained by its elementary sub-components, these results suggest that the densities of the Mo_xB_y and Mo_xC_y compounds formed in the Mo/B and Mo/C systems could be different from those formed in the Mo/B_4C system. Namely, since formation of Mo_xB_y and Mo_xC_y compounds induce compaction, their densities should be significantly higher than the densities of the compounds formed in the Mo/B_4C system. Another explanation for the difference in behavior between Mo/B_4C and Mo/B or Mo/C could be that the formation rates, and therefore thicknesses of formed Mo_xB_y and Mo_xC_y compounds are much lower in Mo/B_4C than in Mo/B or Mo/C. To obtain information on the chemical changes at the interfaces, XPS sputter depth profiling was used.

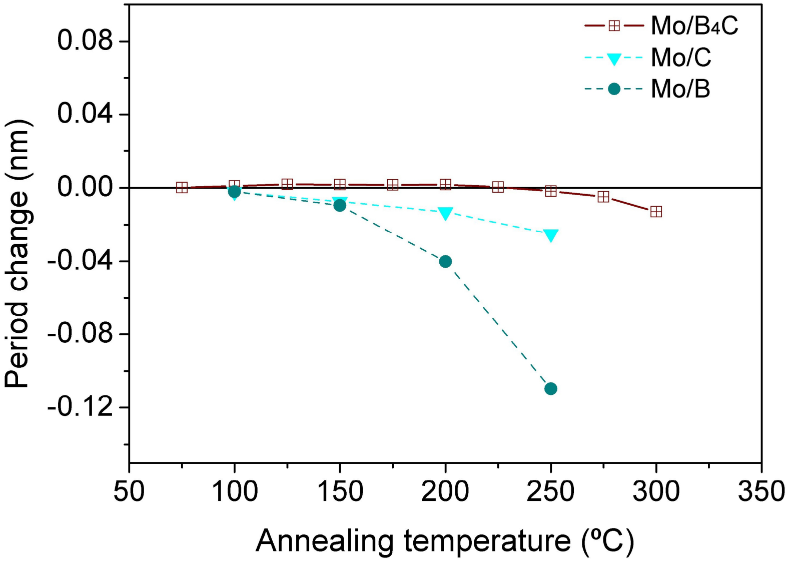

Fig. 3.5: Period change as a function of annealing temperature for Mo/B, Mo/C and Mo/B_4C multilayers.

The results of XPS studies on Mo/B, Mo/C and Mo/B_4C, before and after annealing are shown in Fig. 3.6. The in-depth traces of the atomic concentrations of the elements depict the changes in contrast the multilayers undergo during annealing. Fig. 3.6(a) and 3.6(b) show the results for Mo/B and Mo/C multilayers. Significant intermixing is observed for the case of Mo/B, while less intermixing is observed for Mo/C, fully consistent with the large period changes for Mo/B and small period changes for Mo/C that were observed in Fig. 3.5. Surprisingly, the XPS results for Mo/B$_4$C (Fig. 3.6(c)) also indicate intermixing at the interfaces, while the multilayer period remains virtually unchanged as shown in Fig. 3.5. To resolve this apparent inconsistency, additional WAXRD measurements were performed to study the multilayer crystalline structure of Mo/B, Mo/C and Mo/B$_4$C before and after annealing.

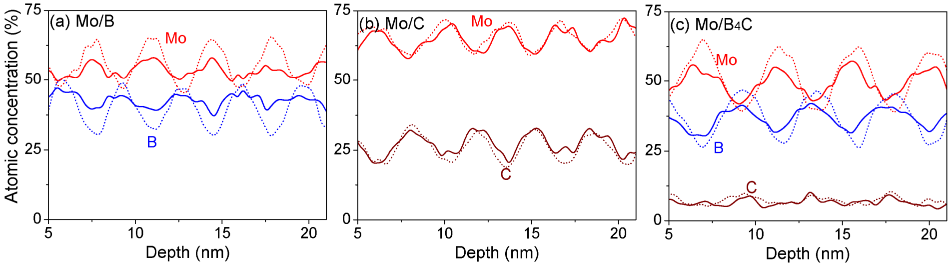

Fig. 3.6: XPS depth profiles before (dotted lines) and after annealing (solid lines) for (a) Mo/B, (b) Mo/C and (c) Mo/B$_4$C multilayers.

Fig. 3.7 shows WAXRD data from Mo/B, Mo/C and Mo/B$_4$C. The crystalline structure changes in Mo/B are more prominent than changes in Mo/C (see Fig. 3.7(a)); consistent with the observed period changes (Fig. 3.5) as well as obtained XPS depth profiles (Fig. 3.6(a) and 3.6(b)). The XRD scan from Mo/B$_4$C (Fig. 3.7(b)) show significant changes in crystalline structure the multilayer undergoes during annealing. The diffraction patterns (of Mo/B$_4$C) are identified as polycrystalline bcc-Mo. Mo crystallites sizes in the direction of film growth, *X*, were obtained using Scherrer's formula,

$$X = \frac{0.94\lambda}{L\cos(\theta)} \tag{3.1}$$

where, $\lambda = 0.154$ nm, L is the full width at half-maximum determined for the (110) peak, and 2θ is the diffraction angle. It was found that the Mo crystallites size decreased by 0.5 nm during annealing treatment. This means that B and C atoms diffuse into Mo and consume Mo to form Mo$_x$B$_y$ and Mo$_x$C$_y$ or MoB$_x$C$_y$. The fact that such compound formation is clearly taking place, combined with the absence of significant period change, suggests that interface compounds formed in Mo/B$_4$C do have lower densities compared to those formed in Mo/B and Mo/C.

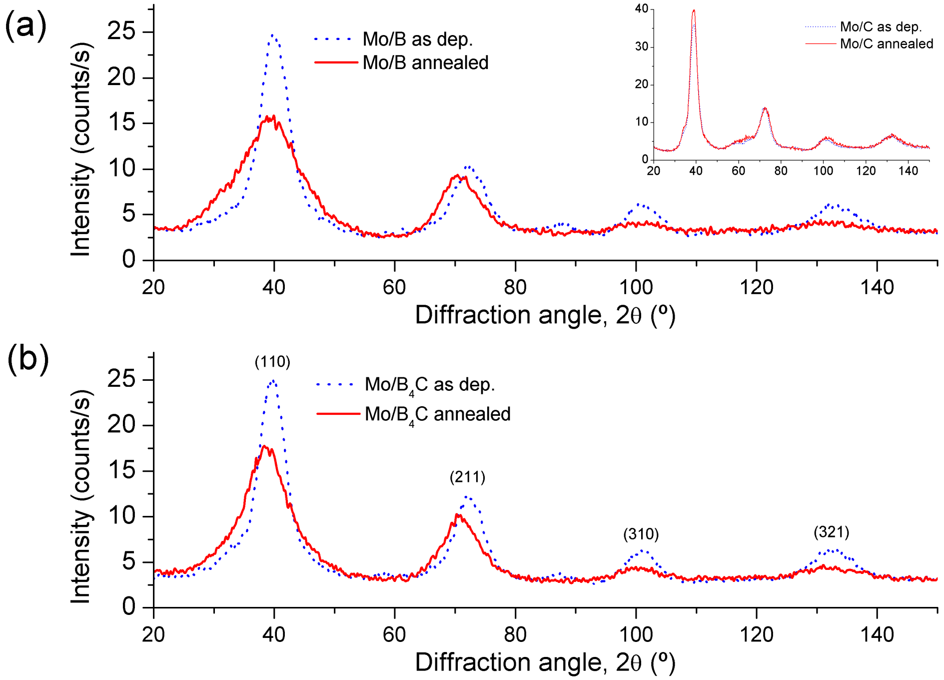

Fig. 3.7: WAXRD scans for (a) Mo/B, Mo/C and (b) Mo/B_4C multilayers before (blue, dotted lines) and after annealing (red, solid lines).

3.4. Conclusions

In-situ GIXR measurements during sequential annealing enabled us to resolve picometer scale changes in Mo/B_4C/Si/B_4C multilayer structures, which were analyzed to reveal the complex chemical behavior of the system at temperatures below 300 ºC. Depending on annealing temperature and time, period expansion as well as period compaction can be observed. By systematically breaking up the total multilayer effects into two-component model systems, we found that the two effects are a net result of competing processes of interaction of Si with B_4C layers, leading to expansion, and Mo_xSi_y formation, leading to compaction.

The period expansion, which occurs at the Si-B_4C interface, arises from formation of low density silicon borides. The seemingly good stability of the Mo-B_4C interface is the result of formation of Mo_xB_y and Mo_xC_y or MoB_xC_y compounds, whose densities are low. This results in an insignificant period change, while in fact intermixing does take place, as shown by both XPS depth profiling and WAXRD.

References

[1] I. Nedelcu, R. W. E. van de Kruijs, A. E. Yakshin and F. Bijkerk, *Journal of Applied Physics* Vol. **103**, Issue 8, 083549 (2008).

[2] D. Attwood, *Soft X-Rays and Extreme Ultraviolet Radiation, Principles and Applications* (Cambridge University, 1999).

[3] I. Nedelcu, R. W. E. van de Kruijs, A. E. Yakshin, and F. Bijkerk, *Physics Review B* Vol. **76**, 245404 (2007).

[4] S. Bruijn, R.W.E. van de Kruijs, A.E. Yakshin and F. Bijkerk, *Applied Surface Science* Vol. **257**, Issue 7, 2707 (2011).

[5] T. Feigl**,** H. Lauth, S. Yulin and N. Kaiser**,** *Microelectronic Engineering* Vol. **57-58**, 3 (2000).

[6] Saša Bajt, Jennifer B. Alameda, Troy W. Barbee, Jr., James A. Folta, Ben Kaufmann, and Eberhard A. Spiller, *Optical Engineering* **41**, 1792 (2002).

[7] V.I.T.A. de Rooij-Lohmann, L. W. Veldhuizen, E. Zoethout, A. E. Yakshin, R. W. E. van de Kruijs, B. J. Thijsse, M. Gorgoi, F. Schäfers, and F. Bijkerk, *Journal of Applied Physics* **108**, 094314 (2010).

[8] V. I. T. A. de Rooij-Lohmann, A. E. Yakshin, R. W. E. van de Kruijs, E. Zoethout, A. W. Kleyn, E. G. Keim, M. Gorgoi, F. Schäfers, H. H. Brongersma, and F. Bijkerk, *Journal of Applied Physics* **108**, 014314 (2010).

[9] T. Böttger, D.C. Meyer, P. Paufler, S. Braun, M. Moss, H. Mai, E. Beyer, *Thin solid films* **444**, 165 (2003).

[10] R. Resel, E. Tamas, B. Sonderegger, P. Hofbauer, J. Keckes, *Journal of Applied. Crystallography* **36** (Part 1), 80 (2003).

[11] R. C. Weast, *Handbook of Chemistry and Physics*, 64th ed. (CRC, 1984).

[12] T. Lundström, B. Lönnber, J. Bauer, *Journal of Alloys and Compounds* **267**, 54 (1998).

[13] F. C. Marques, R. G. Lacerda, and A. Champi, *Applied Physics Letters* Vol. **83**, Issue 15, 3099 (2003).

[14] S. Bruijn, R.W.E. van de Kruijs, A.E. Yakshin, E. Zoethout and F. Bijkerk, *Surface & Coatings Technology* **205**, 2469 (2010).

[15] I. Nedelcu, R.W.E. van de Kruijs, A.E. Yakshin and F. Bijkerk, *Applied Optics* Vol. **48** Issue 2, 155 (2009).

4. Interlayer growth in Mo/B_4C multilayered structures upon thermal annealing

Abstract

Both multilayer period thickness expansion and compaction was observed in Mo/B_4C multilayers upon annealing, and the physical causes for this were explored in detail. Using *in-situ* time-dependent grazing incidence X-ray reflectometry, period changes down to picometer-scale were resolved. It was shown that the changes depend on the thickness of the B_4C layers, annealing temperature and annealing time. Although strong stress relaxation during annealing was observed, it was excluded as a cause for period expansion. Auger electron spectroscopy and wide angle X-ray diffraction measurements revealed the growth of interlayers, with associated period changes influenced by the supply of B and C atoms to the growing compound interlayers. For multilayers with a Mo thickness of 3 nm, two regimes were recognized, depending on the deposited B_4C thickness: in multilayers with $B_4C \leq 1.5$ nm, the supply of additional Mo into the already formed MoB_xC_y interlayer was dominant and led to densification, resulting in period compaction. For multilayers with $B_4C \geq 2$ nm, the B and C enrichment of interlayers formed low density compounds and yielded period expansion.

4.1. Introduction

Multilayers have proven to be viable as reflective (and transmissive) coatings in both current and next generation advanced optical applications, notably in the short wavelength range. Synchrotrons, free electron lasers and extreme ultraviolet lithography (EUVL) are examples in which multilayers are used as optical coatings [1, 2]. These applications demand high precision optical performance. Particularly for high photon flux applications, thermal loading of the optics may lead to interdiffusion of atoms and subsequent compound formation at the interfaces of multilayers [3], consequently reducing optical contrast and causing a lower reflectance [4]. Moreover, multilayer period thickness reduction, due to densification upon compound formation, results in reduction of the optimally reflected wavelength. For many applications functioning at high thermal loads, it is critical to understand and control the nature of the interface interactions with sub-ångström precision in order to implement mitigation strategies such as diffusion barriers or thermal conditioning.

The interaction between nano-scaled Mo and B_4C layers plays a crucial role in several high thermal load optics applications. For instance, free electron lasers operating at $\lambda = 6.6–7$ nm make use of Mo/B_4C multilayers [5]. Also, due to their favorable optical properties, B_4C layers are suggested as diffusion barriers in Mo/Si multilayers (designed for EUVL, $\lambda = 13.5$ nm) to mitigate the degradation of optical contrast under thermal loading [6, 7].

Upon thermal loading, both increases and decreases in the period thickness have been reported in Mo/B_4C multilayer structures. M. Barthelmess and S. Bajt observed period expansion in Mo/B_4C multilayers upon annealing [5], while a recent study of Mo/B_4C showed a stable period upon annealing below 250 °C, followed by period compaction at temperatures higher than 275 °C [8]. In this chapter, we present *in-situ* time-dependent grazing incidence X-ray reflectometry, Auger electron spectroscopy, X-ray diffraction and stress analysis studies and address structural changes in Mo/B_4C multilayers. The results reveal diffusion and interlayer growth and explain the expansion and compaction results observed in literature.

4.2. Experimental

Six types of 50-period Mo/B_4C multilayers were deposited onto super-polished Si substrates, with each type having a different B_4C layer thickness in order to distinguish between bulk and interface effects. Multilayers with the following B_4C thicknesses were prepared: 1 nm, 1.5 nm, 2 nm, 2.5 nm, 3 nm and 4 nm.

The thickness of Mo layers in all multilayers was chosen such that the Mo layers have a polycrystalline structure, as it provides additional information on changes in the structure of multilayers due to thermally induced diffusion and compound formation at interfaces. Since Mo layers crystallize at a relatively larger thickness when in contact with B$_4$C [9, 10], compared to ~2 nm in Mo/Si [11, 12], the thickness of Mo layers was chosen to be 3 nm.

DC magnetron sputtering was used to deposit all the layers in a UHV setup with base pressure $< 1 \cdot 10^{-8}$ mbar. Quartz microbalances were used to monitor layer thicknesses during deposition, with calibrated deposition rates fixed at 20 pm/s. The substrate holder was rotated at 1 Hz during deposition to achieve a homogenous coating.

A PANalytical X'Pert X-ray diffractometer (Cu-Kα radiation, 0.154 nm) was used to measure grazing incidence X-ray reflection (GIXR) scans *in-situ*, during annealing treatment. The alignment of the sample position with respect to the incident X-ray beam was performed before thermal loading, followed by measurement of a reference GIXR scan. The sample was then heated up to 300 °C – a temperature where from previous studies significant intermixing is expected, while remaining well below temperatures where phase transformations start to play a role [3, 8]. To correct for thermal expansion of the sample stage, the sample position with respect to the X-ray beam was again aligned at the enhanced temperature. Subsequently, GIXR scans were continuously recorded during 48 hours of annealing. Ref. [13] provides a more detailed description of the *in-situ* annealing setup, equipped with Anton Paar thermal stage.

Period changes in multilayers during annealing were calculated from the shifts in measured Bragg peak positions. More details about the method, which allows determination of the multilayer period with picometer accuracy, can be found in ref. [14]. The changes in multilayer periods discussed in this chapter were corrected for thermal expansion using bulk thermal expansion coefficients of Mo and B$_4$C obtained from ref. [15], and were verified for each sample by comparing GIXR scans during annealing with those taken at room temperature, before and after the 48-hour annealing cycle.

Multilayer stress for each of the systems was measured *ex-situ* at room temperature after the following annealing times: 5 minutes, 4 hours and 48 hours. An interferometry-based set up was used to obtain substrate curvature, from which the multilayer film stress was calculated using Stoney's formula:

$$\sigma_f = \frac{1}{6}\left(\frac{E_s}{1-v_s}\right)\frac{t_s^{\,2}}{t_f}\left(\frac{1}{R_1}-\frac{1}{R_2}\right) \tag{4.1}$$

where, σ_f is the stress in the multilayer, $E_s/(1-v_s)$ is the biaxial modulus of the substrate, t_s is the substrate thickness, t_f is the multilayer film thickness and R_1 and R_2 are the substrate curvatures before and after deposition (or annealing treatment), respectively.

Wide angle X-ray diffraction (WAXRD) scans were performed to characterize witness samples *ex-situ* at room temperature after each annealing stage. The scans were used to determine Mo crystallite sizes. A fixed grazing angle of 1° was set to maximize the collection efficiency. In order to suppress the diffraction peaks of the monocrystalline Si substrate, the samples were rotated in-plane by a fixed angle of 20° before starting the sample alignment procedure.

Before and after annealing, the samples were characterized by Auger electron spectroscopy (AES) sputter depth profiling. A Theta Probe instrument using radiation of 5 keV was used with sputter erosion performed using 250 eV Ar^+ ions impinging at 45º.

4.3. Results and discussion

4.3.1. Period changes

Fig. 4.1 shows changes in period thickness for Mo/B_4C multilayers with different B_4C thicknesses, as a function of time upon annealing at 300 °C. The first surprising observation is that both period expansion and compaction are observed. This is in contrast to for instance Mo/Si multilayers which show only compaction, regardless of annealing time, temperature or thickness of Mo (or Si) [16]. For Mo/B_4C multilayers, systems with $B_4C < 2$ nm exhibit compaction, while the systems with $B_4C > 2.5$ nm expand. In addition, the period of multilayers with B_4C thicknesses of 2 nm and 2.5 nm initially expand and over time start to compact. It is evident that period change in Mo/B_4C multilayers depends on both the thickness of the B_4C layers and the annealing time.

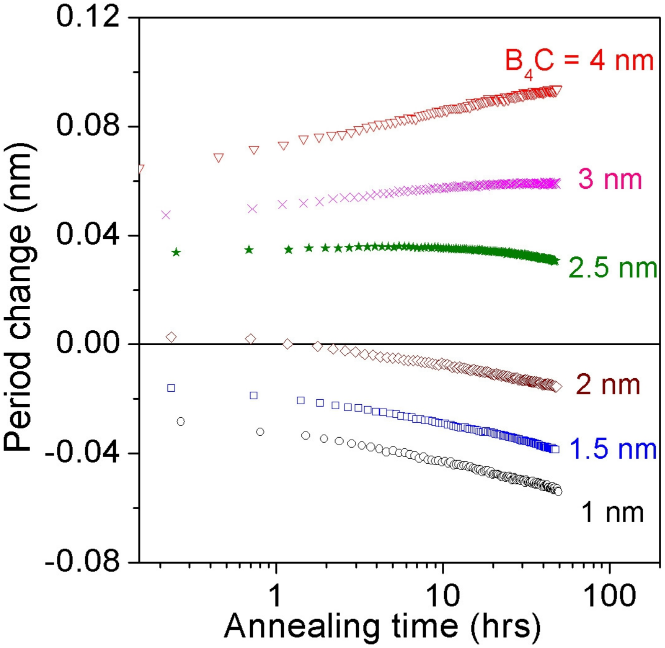

Fig. 4.1: Period change as a function of annealing time at 300 °C in various Mo/B$_4$C multilayers. The as-deposited thickness of Mo layers in all multilayers is 3 nm. The as-deposited B$_4$C thicknesses in corresponding multilayers are indicated on the plot.

4.3.2. Stress relaxation

Fig. 4.2(a) shows the measured Mo/B$_4$C multilayer stress as a function of B$_4$C thickness. The general trend of more intrinsic compressive stress for larger B$_4$C thickness agrees with the expected tensile stress for 3-nm Mo layers [17] and strongly compressive stress for the B$_4$C layers [5, 18]. Morawe *et al.* [18] observed a similar trend in Ru/B$_4$C multilayers, whose compressive stress also increased with the thickness of the B$_4$C layers.

Fig. 4.2(b) shows multilayer stress as a function of annealing time. Depending on the deposited B$_4$C thickness, two regimes of changes in multilayer stress can be recognized, namely: B$_4$C $\leq$ 1.5 nm and B$_4$C $\geq$ 2 nm, referred to as I and II, respectively. The two regimes can be linked with observed period changes (Fig. 4.1) as the multilayers with B$_4$C $\leq$ 1.5 nm show compaction, while the multilayers with B$_4$C $\geq$ 2 nm initially expand. The stress in the former regime

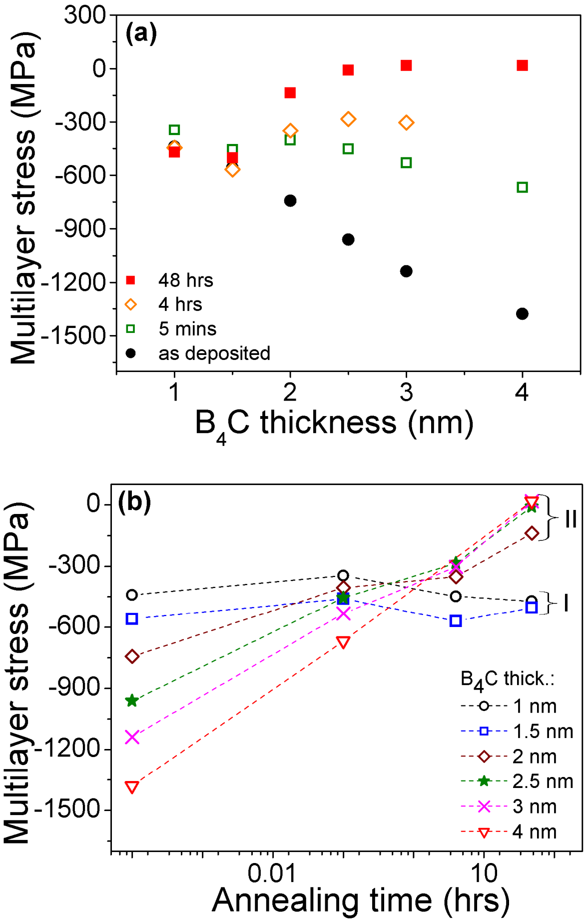

Fig. 4.2: (a) Mo/B_4C multilayer stress as a function of B_4C thickness for as-deposited state and various stages after annealing at 300 °C. (b) Mo/B_4C multilayer stress as a function of annealing time at 300 °C. As-deposited Mo thickness in all multilayers is 3 nm. The B_4C thicknesses are indicated on the graph.

does not relax, while the latter shows stress relaxation, with the strongest relaxation observed for the largest initial stress. Such strong stress relaxation would result in a change of film strain and may actually be (partially) responsible for the observed period changes. To distinguish period changes due to stress relaxation from period changes due to interfacial intermixing and compound formation, the stress-relaxation induced film strain changes, and resulting period changes, have been estimated. The strain parallel to the film, $\varepsilon_{||}$, can be calculated using the relation:

$$\sigma_{||} = \frac{E_l}{1 - v_l}\varepsilon_{||} \tag{4.2}$$

where, $\sigma_{||}$ is the stress parallel to the layer plane, and E_l and v_l are the Young's elastic modulus and Poisson's ratio of the layer, respectively. The strain perpendicular to the film plane, which contributes to layer thickness changes and thus period change, can be obtained using the following relation:

$$\varepsilon_{\perp} = \frac{-2v_l}{1 - v_l}\varepsilon_{||} \tag{4.3}$$

Using bulk elastic constants E_{Mo} = 329 GPa, v_{Mo} = 0.31, E_{B4C} = 450 GPa and v_{B4C} = 0.207, stress-relaxation induced multilayer period changes due to strain changes were found to be negligible compared to the changes shown in Fig. 4.1. For instance, in a Mo/B$_4$C multilayer with Mo = 3 nm and B$_4$C = 4 nm, the measured stress relaxation of 1400 MPa would result in a period expansion of only 4 pm, while up to ~100 pm expansion is observed. P. Sharma and S. Ganti have shown that elastic moduli of nanocrystalline materials do decrease with grain size [19]. Also, grain-boundary sliding leads to reduction of the apparent elastic moduli [19]. These changes in elastic properties could possibly lead to an increase of period expansion due to changes in film strain. However, in order to explain at least the order of magnitude of the observed period expansion (Fig. 4.1), the elastic moduli of both Mo and B$_4$C layers would have to be reduced by at least one order of magnitude, which is highly unlikely. Hence, it can be concluded that the observed period expansion is not due to changes in strains in the bulk of Mo and B$_4$C layers that take place as a result of stress relaxation upon thermal loading.

4.3.3. Diffusion and interlayer growth

Various studies have shown that Mo is chemically reactive with B$_4$C [8, 20, 21]. Thermal loading generally leads to interdiffusion of atoms and compound formation at Mo-B$_4$C interfaces. AES sputter depth profiling was performed to determine the atomic depth profiles before and after annealing (for 48 hrs). As an example, Fig. 4.3(a) shows AES depth profiles before and after annealing for a Mo/B$_4$C multilayer with B$_4$C = 3 nm. The reduction in contrast (reduced amplitudes) after annealing depicts significant intermixing. The amount of intermixing was quantified by modeling the atomic concentrations and extracting interlayer thicknesses for multilayers with B_4C thickness ≥ 2 nm. The obtained interlayer thicknesses for various Mo/B_4C multilayers before and after annealing are shown in Fig. 4.3(b). (The depth profile of the annealed multilayer with B_4C = 2 nm could not be modeled.) It is evident that the compound interlayers grow during annealing.

Based on bulk density values, volumetric effects upon formation of possible binary compounds at interfaces should yield compaction due to densification (Table 4.1). However, it may not be straightforward to refer to bulk densities of Mo, B_4C and interlayer compounds in order to explain period changes for Mo/B_4C multilayers as period expansion is not predicted from Table 4.1, but can clearly be observed in Fig. 4.1.

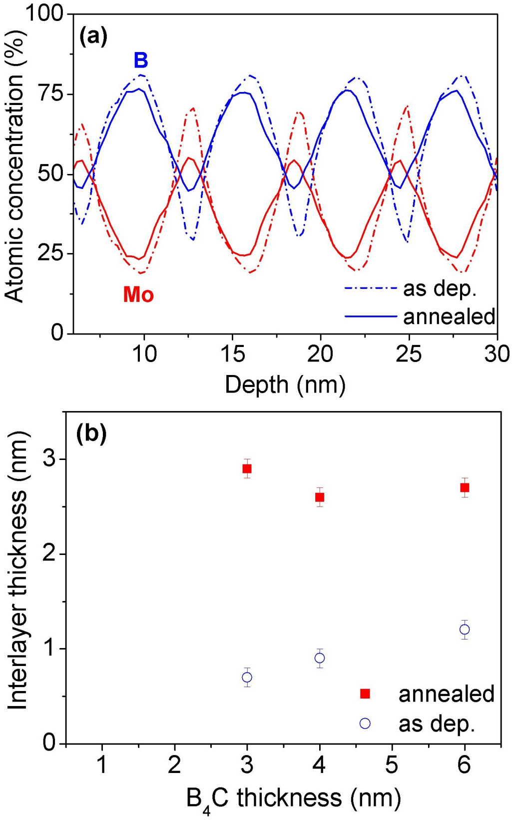

Fig. 4.3: (a) AES depth profiles before (dotted lines) and after annealing (solid lines) for Mo/B_4C multilayer with B_4C thickness of 3 nm. (b) Compound interlayer thickness in Mo/B_4C multilayers as a function of B_4C thickness.

	A (g/mol)	ρ (g/cm^3)	$V_I/V_{comp.}$	$V_{II}/V_{comp.}$	Fractional Vol. Change
Mo	95.94	10.20	-	-	-
B	10.811	2.34	-	-	-
C	12.01	1.80	-	-	-
Mo_2B_5	245.98	7.01	0.54	0.66	-0.20
MoB	106.75	8.65	0.76	0.37	-0.14
MoB_2	117.56	7.12	0.57	0.56	-0.13
Mo_2B	202.69	9.26	0.86	0.21	-0.07
MoC	107.95	8.2	0.71	0.51	-0.22
Mo_2C	203.89	8.20	0.82	0.29	-0.11

Table 4.1: Molecular volumes of Mo, B and C consumed in chemical reactions to form various binary compounds. V_I and V_{II} are molecular volumes of the first element and second element, respectively, and $V_{comp.}$ is the molecular volume of the corresponding formed compound. Calculations are based on bulk density values. Densification is expected for all reactions.

WAXRD measurements were performed to investigate the changes in crystalline structure of multilayers during annealing. The diffraction scans are identified as polycrystalline bcc-Mo. The average Mo crystallite size in the direction of film growth, *X*, is obtained using Scherrer's formula:

$$X = \frac{0.94\lambda}{L\cos(\theta)} \tag{4.4}$$

where, $\lambda = 0.154$ nm, L is the full width at half-maximum determined for the (110) peak, and 2θ is the diffraction angle. The as-deposited average Mo crystallite size in all multilayers is (2.0 ± 0.1) nm, which is less than the deposited 3 nm. Clearly, interlayers of Mo_xB_y, Mo_xC_y or MoB_xC_y compounds are already formed during deposition [9, 10], which is consistent with calculated as-deposited interlayer thicknesses shown on Fig. 4.3(b). Fig. 4.4 shows the change in Mo crystallite size as a function of annealing time at T = 300 °C for various Mo/B_4C multilayers. A reduction of the crystallite size is observed; suggesting that diffusion of B and C atoms into Mo layers consumes “pure” Mo and results in growth of the compound interlayer, again consistent with results in Fig. 4.3(b). Also, it is observed that the rate of Mo consumption increases with deposited B_4C thickness, and saturates for multilayers with $B_4C \geq 2$ nm. Depending on the deposited B_4C thickness, two regimes of changes in the crystalline structure of multilayers can be recognized, namely: $B_4C \leq 1.5$ nm and $B_4C \geq 2$ nm (I and II, respectively). The two regimes are the same for multilayer stress relaxation observed in Fig. 4.2(b), and can also be linked with observed period changes (Fig. 4.1).

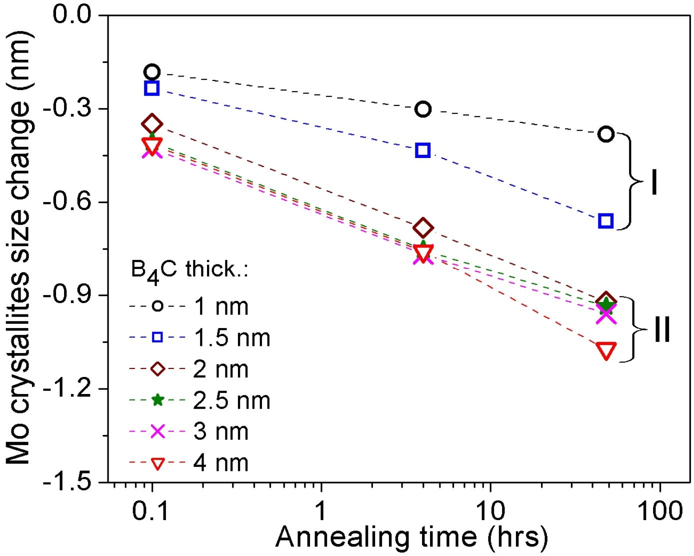

Fig. 4.4: Change in Mo crystallite size as a function of annealing time at 300 °C in various Mo/B_4C multilayers. The as-deposited Mo crystallites size in all multilayers is (2.0 ± 0.1) nm.

It should be noted that stress relaxation would not be observed if the volumetric effects upon compound formation were completely anisotropic, with expansion or compaction only occurring in the direction perpendicular to the film plane [17]. Fig. 4.5 shows Mo/B_4C multilayer film stress relaxation as a function of period change, obtained at three different annealing times. It is observed that, for multilayers with $B_4C \geq 2$ nm, stress relaxation increases with interlayer growth. As demonstrated in studies by J. M. Freitag and B. M. Clemens [17], the interlayer growth during thermal loading allows multilayer films to relieve most of the intrinsic stress. In addition (for multilayers with $B_4C \geq 2$), the same Mo crystallites size change suggest that the interlayers have the same Mo content (Fig. 4.4).

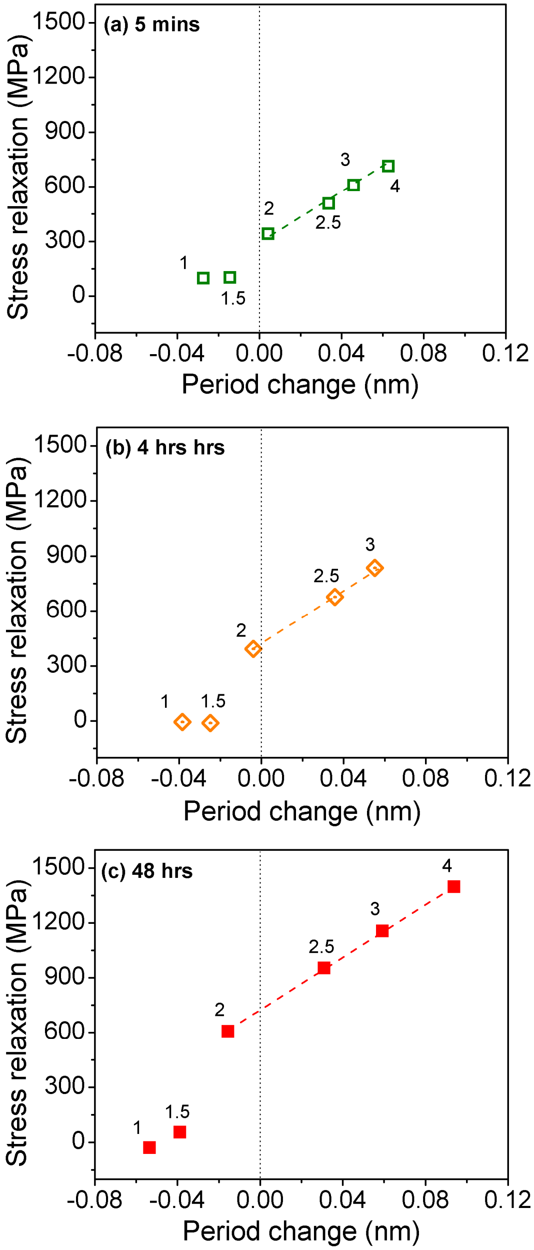

Fig. 4.5: Stress relaxation versus period change in Mo/B_4C multilayers after the following annealing stages: (a) 5 minutes (b) 4 hours and (c) 48 hours. For each data point, the corresponding as-deposited B_4C thickness (in nanometers) is indicated on the plot. The dotted lines are a guide to the eye.

4.3.4. B and C enrichment of interlayers

Considering the fact that relatively thick interlayers are already formed in Mo/B_4C multilayers during deposition, it is expected that the supply of Mo, B and C atoms into the growing interlayers influences the exact interlayer structure and therefore the associated period changes during thermal loading.

As previously mentioned, for multilayers with as-deposited Mo thickness of 3 nm, two regimes of multilayer stress relaxation (Fig. 4.2(b)) and crystalline structural changes (Fig. 4.4) have been recognized. Before annealing, the multilayers with $B_4C \leq 1.5$ nm would have no or little pure B_4C left, while the multilayers with $B_4C \geq 2$ nm would still have pure B_4C left (see Fig. 4.6). During annealing, Mo, B and C atoms diffuse into the MoB_xC_y interlayer, with diffusion rates of B and C atoms being higher due to the fact that their mobility is much higher than that of Mo atoms [20]. For multilayers with $B_4C \leq 1.5$ nm, the slow supply of additional Mo into the MoB_xC_y interlayer is dominant and apparently results in densification, and thus period compaction.

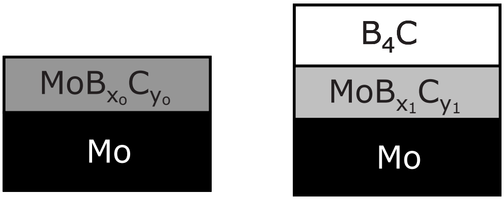

I: $B_4C \leq 1.5$ nm II: $B_4C \geq 2$ nm

Fig. 4.6: Model depicting structural differences in as-deposited Mo/B_4C multilayers with different as-deposited B_4C thicknesses.

For multilayers with $B_4C \geq 2$ nm, since the interlayers should have the same Mo content (Fig. 4.4), the differences in period changes are determined by the supply of B and C. Apparently, the enrichment of interlayers with B and C leads to formation of relatively low density compounds, and therefore period expansion, as observed at initial annealing stages. At large annealing times, after most B_4C would have been consumed, Mo enrichment would again result in densification. This is observed in multilayers with as-deposited B_4C thicknesses of 2 nm and 2.5 nm, with the latter exhibiting period compaction at a later stage (Fig. 4.1). Accelerating the diffusion kinetics in multilayers with B_4C thicknesses of 3 nm and 4 nm should yield similar results, i.e. expansion then followed by compaction. Fig. 4.7 shows period change as function of annealing time at 350 °C for the above mentioned multilayers. Indeed, initially the periods expand and over time start to compact, with the multilayer with larger B_4C thickness starting to compact at a later stage.

A more detailed analysis of the exact interlayer compounds formed during annealing and their structures is challenging, because they would require analytical tools with sub-ångström resolution as well as chemical sensitivity. In practice, one could investigate diffusion phenomena at higher temperatures to amplify the structural changes in order to use techniques such as AES or X-ray photoelectron spectroscopy (XPS) that do not exhibit sub-ångström resolution. For example, according to studies by P. Rogl and H. Bittermann (at ~1,200 °C) [22], the interaction of Mo and B_4C is dominated by formation of ternary boron carbides (MoB_xC_y) rather than binary compounds. Also, the MoB_xC_y structure depends on the ratio of Mo to B and C [22], where increasing B and C content tends to form larger nonmetal aggregations. It remains questionable if such results are useful to describe the phenomena observed at much lower temperatures.

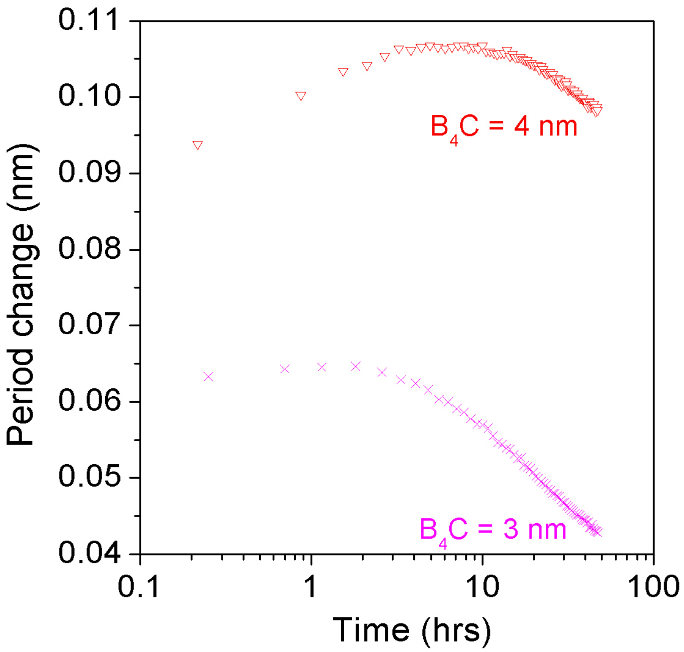

Fig. 4.7: Period change as a function of annealing time at 350 °C in Mo/B_4C multilayers. The thickness of Mo layers in all multilayers is 3 nm, while the as-deposited B_4C thicknesses in corresponding multilayers are indicated on the plot.

4.4. Conclusions

Time-dependent *in situ* GIXR measurements have been performed on Mo/B_4C multilayer structures. Picometer scale period changes are observed during annealing, where both period expansion and period compaction can be obtained, depending on the thickness of the B_4C layers, annealing temperature and annealing time. Strong stress relaxation during annealing was observed. However, the contribution of stress-relaxation induced changes in multilayer film strains, which could lead to period expansion, was estimated and found to be negligible.

AES and WAXRD measurements revealed the growth of interlayers, with associated period changes influenced by the supply of B and C to the growing compound interlayers. For multilayers with Mo thickness of 3 nm, two regimes were recognized, depending on the deposited B_4C thickness. In multilayers with $B_4C \leq 1.5$ nm, the supply of additional Mo into the already formed MoB_xC_y interlayer was dominant and led to densification, resulting in period compaction. For multilayers with $B_4C \geq 2$ nm, the B and C enrichment of interlayers formed low density compounds and yielded period expansion.

References

[1] S. Bajt, H. N. Chapman, E. A. Spiller, J. B. Alameda, B. W. Woods, M. Frank, M. J. Bogan, S. Boutet, S. Marchesini, S. P. Hau-Riege, J. Hajdu, D. Shapiro, *Applied Optics* **47**(10), 1673 (2008).

[2] E. Louis, A.E. Yakshin, T. Tsarfati, F. Bijkerk, *Progress in Surface Science* **86**, 255 (2011).

[3] I. Nedelcu, R. W. E. van de Kruijs, A. E. Yakshin and F. Bijkerk, *Journal of Applied Physics.* **103**(8), 083549 (2008).

[4] D. Attwood, *Soft X-Rays and Extreme Ultraviolet Radiation, Principles and Applications* (Cambridge University, 1999).

[5] M. Barthelmess, S. Bajt, *Applied Optics* **50**(11), 1620 (2011)

[6] S. Bajt, J. B. Alameda, T. W. Barbee, Jr., J. A. Folta, B. Kaufmann, E. A. Spiller, *Optical Engineering* **41**, 1792 (2002).

[7] T. Böttger, D. C. Meyer, P. Paufler, S. Braun, M. Moss, H. Mai, and E. Beyer, *Thin Solid Films* **444**, 165 (2003).

[8] S. L. Nyabero, R. W. E. van de Kruijs, A. E. Yakshin, E. Zoethout and F. Bijkerk, *Journal of Applied Physics* **112**, 054317 (2012).

[9] S. A. Patelli, J. Ravagnan, V. Rigato, G. Salmaso, D. Silvestrini, E. Bontempi, L.E. Depero, *Applied Surface Science* **238**, 262 (2004).

[10] A. Patelli, V. Rigato, G. Salmaso, N. J. M. Carvalho, J. Th. M. De Hosson, E. Bontempi, L. E. Depero, *Surface Coating Technology* **210**, 143 (2006).

[11] S. Bajt, D. G. Stearns, and P. A. Kearney, *Journal of Applied Physics* **90**, 1017 (2001)

[12] R. W. E. van de Kruijs, E. Zoethout, A. E. Yakshin, I. Nedelcu, E. Louis, H. Enkisch, G. Sipos, S. Mullender, F. Bijkerk, *Thin Solid Films* **515**(2), 430 (2006).

[13] R. Resel, E. Tamas, B. Sonderegger, P. Hofbauer, and J. Keckes, *Journal of Applied Crystallography* **36**, 80 (2003).

[14] S. Bruijn, R. W. E. van de Kruijs, A. E. Yakshin, and F. Bijkerk, *Applied. Surface Science*. **257**(7), 2707 (2011).

[15] R. C. Weast, *Handbook of Chemistry and Physics*, 64th ed. (CRC, 1984).

[16] I. Nedelcu, R. W. E. van de Kruijs, A. E. Yakshin, and F. Bijkerk, *Physics Review B* **76**, 245404 (2007).

[17] J. M. Freitag, B. M. Clemens, *Applied Physics Letters* **73**, 43 (1998).

[18] Ch. Morawe, J.-Ch. Peffen, K. Friedrich , *Proceedings SPIE* **7802,**78020B1 (2010).

[19] P. Sharma, S. Ganti, *Journal of Materials Research* **18**(8), 1823 (2003).

[20] V. I. T. A. de Rooij-Lohmann, L. W. Veldhuizen, E. Zoethout, A. E. Yakshin, R. W. E. van de Kruijs, B. J. Thijsse, M. Gorgoi, F. Schäfers, F. Bijkerk, *Journal of Applied Physics* **108**, 094314 (2010).

[21] V. I. T. A. de Rooij-Lohmann, A. E. Yakshin, R. W. E. van de Kruijs, E. Zoethout, A. W. Kleyn, E. G. Keim, M. Gorgoi, F. Schäfers, H. H. Brongersma, F. Bijkerk, *Journal Applied Physics* **108**, 014314 (2010).

[22] P. Rogl, H. Bittermann, *International Journal of Refractory Metals & Hard Materials* **17**, 27 (1999).

5. Enhanced thermal stability of EUV multilayers by balancing diffusion-induced structural changes

Abstract

A new multilayer design that compensates period thickness compaction at elevated temperatures is presented. The design is based on a reference multilayer that exhibits compaction upon thermal loading and includes an additional sub-structure, which expands upon thermal loading to compensate for the basic compaction. Using extreme ultraviolet reflecting multilayers as an example, the optimization of the ratio of the number of the expanding Mo/B_4C periods to that of compacting B_4C-barriered Mo/Si periods is demonstrated. Both the average periodicity and the centroid wavelength of the composite multilayer were preserved during annealing at 250 °C for 60 hours.

5.1. Introduction

Periodic Mo/Si multilayers have been realized as reflecting coatings for the optics of next-generation lithography equipment operating at $\lambda = 13.5$ nm – also known as extreme ultraviolet lithography (EUVL) [1]. EUVL demands sub-ångström precision of the multilayer coating periodicity and the multilayer coating should be stable over many years of operation under intense photon loads. The high photon fluxes during prolonged exposure provide thermal loading, which causes interdiffusion of Mo and Si atoms and compound formation at the multilayer interfaces [2]. For Mo/Si multilayers, densification upon $MoSi_2$ formation leads to reduction of the multilayer period thickness, and hence reduction of the reflected wavelength, unacceptable from application point of view.

In order to mitigate Mo and Si interdiffusion and period compaction, B_4C diffusion barrier layers are introduced due to their favorable optical properties [3, 4]. The diffusion barriers lead to multilayers exhibiting a complex temporal behavior due to the fact that B_4C is chemically reactive with both Mo and Si [5]. Recent studies suggest that, at low temperatures and/or initial stages of photon exposure, formation of low density silicon borides at Si-B_4C interfaces results in period expansion [7]. At elevated temperatures and/or later stages of prolonged photon exposure, formation of dense molybdenum silicide becomes dominant and results in period compaction [7]. As a result of both expansion and subsequent compaction, angular dependent reflected wavelength, intensity and wavefront will change, generally deteriorating the optical performance of the multilayer coating. In this chapter, a design to circumvent period compaction in EUV multilayers at elevated temperatures is presented.

5.2. Results and discussion

5.2.1. Diffusion-induced structural changes in Mo/B_4C/Si/B_4C multilayers

The characteristic temporal behavior of regular EUV multilayers with barriers is demonstrated. For this purpose, a 50-period Mo/B_4C/Si/B_4C multilayer was prepared using DC magnetron sputtering in a UHV setup with base pressure $< 1 \cdot 10^{-8}$ mbar. The multilayer period thickness was 6.9 nm, with nominal values for Mo = 1.9 nm, B_4C = 1 nm and Si = 3 nm. For determination of period changes, grazing incidence X-ray reflection (GIXR) scans were recorded *in-situ* during the annealing treatment using a PANalytical X'Pert X-ray diffractometer

(Cu-Kα radiation, 0.154 nm), equipped with an Anton Paar thermal stage [8]. Before heating up the sample, the alignment of the sample position with respect to the incident X-ray beam was performed, followed by the measurement of the GIXR scan. The temperature was then ramped up to 250 °C. The sample position with respect to the beam was aligned again to correct for alignment errors introduced by thermal expansion of the sample stage and/or mechanical deformation of the sample at enhanced temperature. After that, GIXR scans were continuously recorded during 60 hours of annealing.

The changes in multilayer period thickness were calculated from the measured shifts in the Bragg peak positions, as explained in ref [9]. This method allows determination of period changes with picometer accuracy. Period changes were corrected for thermal expansion using thermal coefficients of Mo, Si and B_4C from ref. [10], and verified after cooling down to room temperature. Hence, the observed changes are due to reactions taking place at multilayer interfaces.

Fig. 5.1 shows period change in Mo/B_4C/Si/B_4C during annealing at 250 °C for duration of 60 hours. The initial period expansion is attributed to reactions at the Si-B_4C interfaces; afterwards the period starts to compact when molybdenum silicide is formed [6, 7]. It should be noted that, the period changes induced by molybdenum silicide formation at the interfaces are much smaller than those observed in reference Mo/Si multilayer. For further reduction of the silicide growth, the thickness of the B_4C barrier layers could be increased, but would lead to more reflectance loss as the loss increases quadratically with the thickness of the barrier. An alternative method is proposed, involving the addition of layers which expand upon annealing.

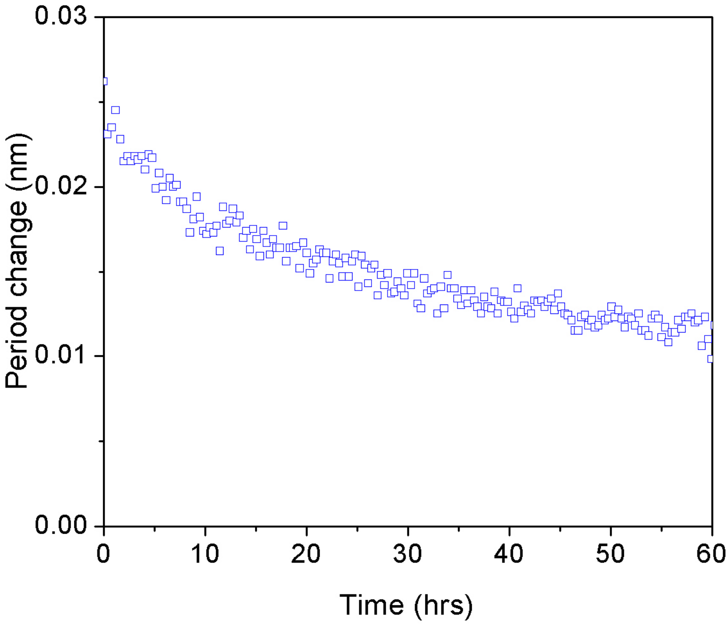

Fig. 5.1: Period change in Mo/B_4C/Si/B_4C multilayer as a function of time during annealing treatment at 250 °C.

5.2.2. Diffusion-induced structural changes in Mo/B_4C multilayers

It has been recently shown that the period thickness of Mo/B_4C multilayers can either expand or compact upon thermal loading, depending on the thickness of the B_4C layers, the annealing temperature and annealing time [11]. For Mo/B_4C multilayers with an as-deposited Mo thickness of 3 nm, period expansion can be observed when the thickness of B_4C is equal or larger than 3 nm, and has been attributed to the formation of low density, B and C-rich compounds at the interfaces [11]. Thus a 50-period Mo/B_4C multilayer with a period thickness of 7.2 nm – with Mo = 3 nm, B_4C = 4.2 nm – was prepared and annealed at 250 °C. Fig. 5.2 shows the period change in the Mo/B_4C multilayer during the annealing treatment, and is compared to the period change observed in Mo/B_4C/Si/B_4C. As expected, the period of the Mo/B_4C multilayer expands during annealing.

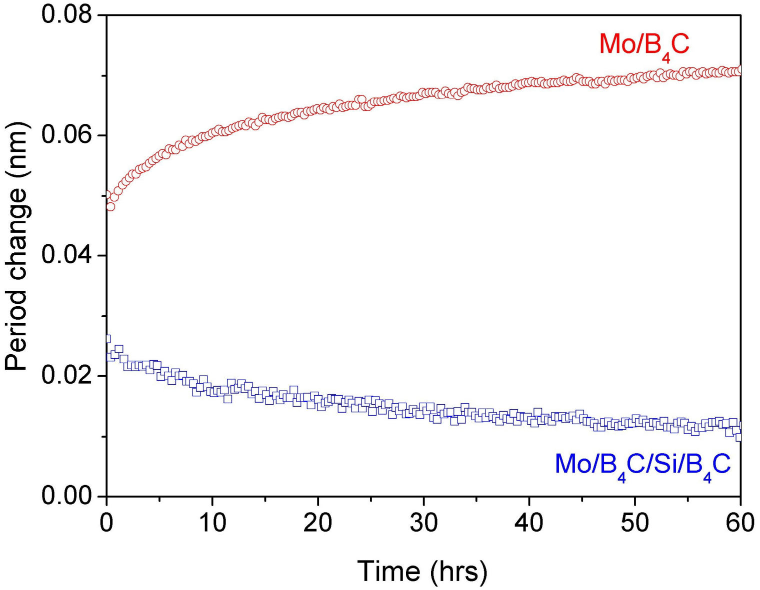

Fig. 5.2: Period change in Mo/B_4C and $Mo/B_4C/Si/B_4C$ multilayers during annealing treatment at 250 °C. The as-deposited period thicknesses are 7.2 nm and 6.9 nm, respectively.

5.2.3. Balancing period compaction and expansion

A new design is proposed that combines periods of $Mo/B_4C/Si/B_4C$ with periods of Mo/B_4C, where upon thermal loading the expansion in Mo/B_4C fully compensates the compaction in $Mo/B_4C/Si/B_4C$. If this can be realized, the multilayer surface position with respect to the substrate remains constant, and this design would preserve the reflected intensity and the wavefront. In order to achieve this at 250 °C for the two multilayers discussed above (Fig. 5.2), the optimal ratio of the number of periods of Mo/B_4C and that of $Mo/B_4C/Si/B_4C$ is 2:4. The complete design of the composite multilayer is depicted in Fig. 5.3.

To demonstrate the functionality of a composite multilayer coating, a multilayer was prepared according to the design shown in Fig. 5.3. The thicknesses of individual layers were the same as for separate multilayers discussed above (Fig. 5.2). Fig. 5.4 shows the measured period changes in the composite multilayer as a function of time, during annealing at 250 °C. Apart from the initial expansion of ~37 pm, which is attributed to the

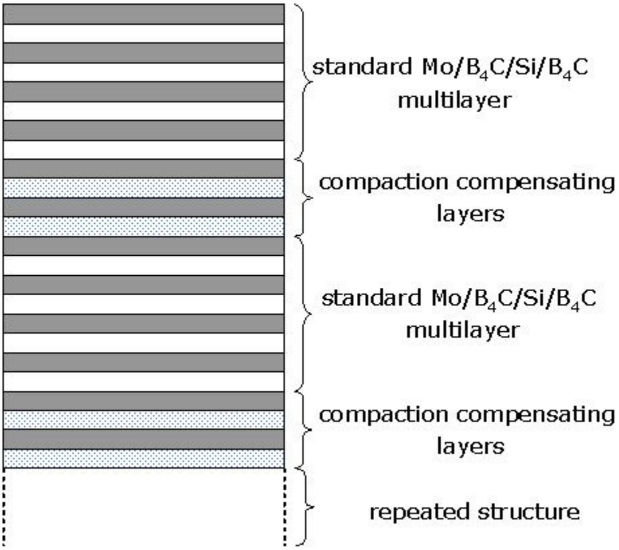

Fig. 5.3: Design of multilayers with compaction compensating layers. Mo/B_4C multilayers, which expand upon annealing, are introduced to compensate for the compaction in Mo/B_4C/Si/B_4C. For clarity, the B_4C barrier layers in the standard Mo/B_4C/Si/B_4C multilayers are not shown.

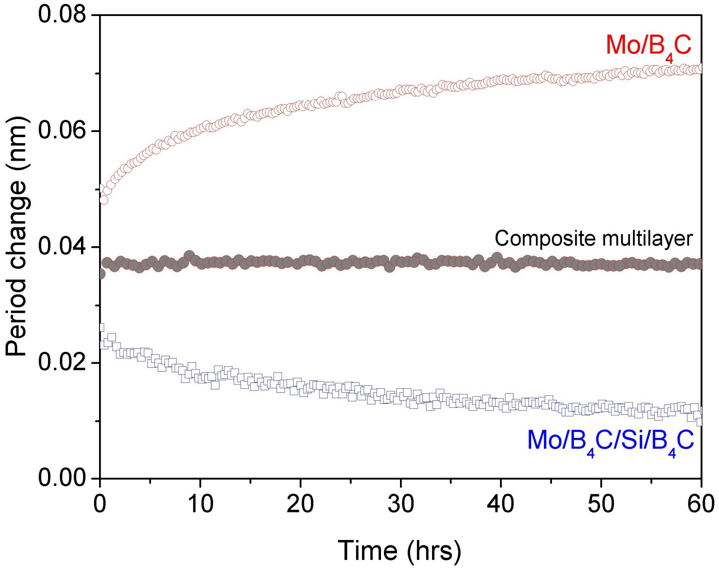

Fig. 5.4: Period change in composite multilayer during annealing at 250 °C, compared to separate multilayer systems (Mo/B_4C and Mo/B_4C/Si/B_4C).

interactions at the Si-B_4C and the Mo-B_4C interfaces, it is observed that the average period thickness does not change over the duration of 60 hours (root mean square value of only 0.5 pm).

5.2.4. Reflectance of the compaction-compensating multilayer

EUV reflectometry (AOI = 1.5°) of the composite sample was performed at the soft X-ray beam line of Physikalisch-Technische Bundesanstalt (PTB), Berlin. Fig. 5.5 shows the EUV reflectometry spectra of the composite multilayer before and after annealing for 10 minutes and 60 hours. As previously discussed, the observed spectrum shift from as-deposited to after annealing for only 10 minutes is attributed to the initial expansion due to interactions at the Si-B_4C and Mo-B_4C interfaces, which are inevitable (but could be compensated for in a design for the purpose of wavelength matching). Afterwards, it is observed that the composite multilayer preserves both the centroid wavelength and reflectance (58% at λ =13.7 nm) throughout the duration of thermal treatment.

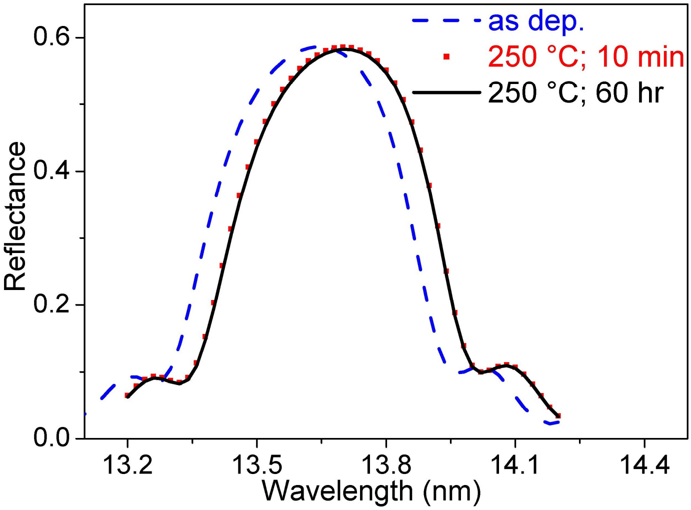

Fig. 5.5: Measured reflectance for compaction-compensating multilayer before and after annealing at 250 °C for 10 minutes and 60 hours. IMD calculation [12] of the designed structure, with roughness/diffuseness $\sigma = 3\text{Å}$ at all the interfaces, gives a reflectance of 57%, which is comparable with the experimental results.

5.3. Conclusions

A multilayer design to compensate for period compaction has been devised and demonstrated. The method introduces to the standard multilayer stack additional layers whose periods expand upon thermal loading. The introduction of the expanding layers to the multilayer – whose period thickness compacts – is optimized such that the composite multilayer has zero net change in the average periodicity during thermal loading. This ensures that the multilayer surface position with respect to the substrate remains constant, and preserving the angular dependent reflected wavelength, reflected intensity and the wavefront over time. Both the placement and the number of periods of the expanding component may be varied within the limit that the optical performance of the composite design is not severely impaired. As a proof-of-principle, a composite multilayer containing both compacting Mo/B_4C/Si/B_4C and expanding Mo/B_4C periods was constructed and thermal loading demonstrates effective cancellation of expansion and compaction (after the initial expansion), with centroid wavelength and reflectance (58%) remaining unchanged for over 60 hours.

References

[1] E. Louis, A.E. Yakshin, T. Tsarfati, F. Bijkerk, *Progress in Surface Science* **86**, 255 (2011).

[2] I. Nedelcu, R. W. E. van de Kruijs, A. E. Yakshin, F. Bijkerk, *Physics Review B* **76**, 245404 (2007).

[3] S. Bajt, J. B. Alameda, T. W. Barbee, Jr., J. A. Folta, B. Kaufmann, E. A. Spiller, *Optical Engineering* **41**, 1792 (2002).

[4] T. Böttger, D. C. Meyer, P. Paufler, S. Braun, M. Moss, H. Mai, and E. Beyer, *Thin Solid Films* **444**, 165 (2003).

[5] V. I. T. A. de Rooij-Lohmann, L. W. Veldhuizen, E. Zoethout, A. E. Yakshin, R. W. E. van de Kruijs, B. J. Thijsse, M. Gorgoi, F. Schäfers, F. Bijkerk, *Journal of Applied Physics* **108**, 094314 (2010).

[6] V. I. T. A. de Rooij-Lohmann, A. E. Yakshin, R. W. E. van de Kruijs, E. Zoethout, A. W. Kleyn, E. G. Keim, M. Gorgoi, F. Schäfers, H. H. Brongersma, F. Bijkerk, *Journal of Applied Physics* **108**, 014314 (2010).

[7] S. L. Nyabero, R. W. E. van de Kruijs, A. E. Yakshin, E. Zoethout and F. Bijkerk, *Journal of Applied Physics* **112**, 054317 (2012).

[8] R. Resel, E. Tamas, B. Sonderegger, P. Hofbauer, and J. Keckes, *Journal of Applied Crystallography* **36**, 80 (2003).

[9] S. Bruijn, R. W. E. van de Kruijs, A. E. Yakshin, and F. Bijkerk, *Applied Surface Science* **257**(7), 2707 (2011).

[10] R. C. Weast, *Handbook of Chemistry and Physics*, 64th ed., (CRC, 1984).

[11] S. L. Nyabero, R. W. E. van de Kruijs, A. E. Yakshin, E. Zoethout, G. van Blanckenhagen, J. Bosgra, R. A. Loch, and F. Bijkerk, *Journal of Applied Physics* **113**, 144310 (2013).

[12] D. L. Windt, *Computers in Physics* **12**(4), 360 (1998).

6. Thermally induced interlayer structural changes in La/B multilayers

Abstract

Thermally induced structural changes in La/B multilayers were studied using *in-situ* X-ray reflectometry, Auger electron spectroscopy and X-ray diffraction. The results reveal two competing processes with opposite effects on the level of picometer scale multilayer period thickness changes, i.e. expansion and compaction. It was found that, the period changes depend on annealing temperature, annealing time and amount of La and/or B. Studies on the multilayers with period thickness of 7 nm reveal two competing processes: crystallization of the compound interlayers formed during deposition and further growth of the compound interlayer due to diffusion. At 300 °C, the continuous crystallization of the lanthanum boride interlayers is dominant throughout the annealing treatment, forming LaB_6 crystallites and consequently leading to period compaction. At 400 °C, crystallization of lanthanum boride interlayers (to form LaB_6 crystallites) is dominant during the initial 10 minutes of annealing, exhibiting compaction. Afterwards the diffusion-induced growth of amorphous, low density lanthanum boride interlayers is prominent, resulting in expansion. For multilayers with $\Lambda = 3.5$ nm, no crystallization of the compound interlayers was observed.

6.1. Introduction

In the EUV and soft x-ray wavelength range, thin film multilayer structures are of interest as reflective coatings for various optical applications. In particular for the 6.7-6.9 nm wavelength range, the highest theoretical normal incidence reflectance can be obtained with multilayer coatings that make use of La layers as reflector material, and B layers as an appropriate spacer material, since B has a K-absorption edge at 6.6 nm [1, 2, 3, 4]. Examples of applications that may use La/B-based multilayers include free electron lasers and extreme ultra-violet lithography (EUVL). Although Mo/Si multilayer coatings are currently proving to be feasible for EUVL optics operating at $\lambda = 13.5$ nm [5, 6], achieving spatial resolutions better than 22 nm might require a shorter wavelength (~6.7 nm) [1].

The optical response of multilayers consisting of up to hundreds of pairs of nanometer thin layers is particularly sensitive to the quality of the interfaces between the layers. High-flux photon exposures in applications result in thermal loading, which may cause interdiffusion of La and B atoms and subsequent compound formation at the multilayer interfaces [1, 4], leading to deterioration of the optical contrast [7]. In addition, the period thickness of multilayers might change upon compound formation [8, 9], leading to a mismatch between the multilayer period and the wavelength of incident light. It is crucial to understand the underlying thermally induced interface effects in order to control and mitigate such effects with sub-ångström precision.

In this chapter, we present *in-situ* time-dependent grazing incidence X-ray reflectometry, Auger electron spectroscopy and X-ray diffraction studies, and discuss thermally induced structural changes in La/B multilayers.

6.2. Experimental

Fifty-period La/B multilayers were deposited onto super-polished Si substrates. The period thickness of the multilayers was $\Lambda = 3.5$ nm, with a La layer fraction of $\Gamma = \Lambda_{La}/\Lambda = 0.4$. In order to distinguish between bulk and interface effects during thermal loading, fifty-period La/B multilayers with period thickness of $\Lambda = 7$ nm (with $\Gamma = 0.4$) were also investigated. The multilayers were coated using DC magnetron sputtering in a UHV setup with base pressure $< 1 \cdot 10^{-8}$ mbar.

Grazing incidence X-ray reflection (GIXR) scans were measured *in-situ* during annealing using a PANalytical X'Pert X-ray diffractometer with a four-bounce monochromator (Cu-Kα radiation, 0.154 nm). The diffractometer was equipped with an Anton Paar thermal stage whose detailed description is found in ref. [10]. Before annealing the alignment of the sample was performed and a reference measurement was performed. After temperature ramping, the sample position was realigned to correct for alignment errors introduced by thermal expansion of the sample stage and mechanical deformation of the sample at elevated temperatures. Subsequent to realignment, GIXR scans were continuously recorded during annealing. The multilayers were annealed for more than 20 hours in the temperature range of 250 °C – 400 °C.

The changes in multilayer period thickness during annealing were obtained from the shifts in measured Bragg peak positions, as described in detail in ref. [11]. This method enables determination of the period changes with picometer accuracy. The period changes recorded during annealing were corrected for thermal expansion using bulk thermal coefficients of La and B from ref [12] and [13], and were verified by comparing GIXR scans during annealing with those taken at room temperature, before and after the annealing treatment.

To study La and B interdiffusion during annealing, witness samples with Λ = 7 nm and Γ = 0.4 were characterized *ex-situ* at room temperature by Auger electron spectroscopy (AES) sputter depth profiling. A Theta Probe instrument using radiation of 5 keV was used with sputter erosion performed using 250 eV Ar^+ impinging at 45º. The atomic depth concentration profiles of as-deposited multilayers were compared with those after annealing at 300 °C and 400 °C.

Grazing incidence wide angle X-ray diffraction (GI-WAXRD) scans on witness samples of multilayers were performed *ex-situ* at room temperature using a PANalytical Empyrean X-ray diffractometer (Cu-Kα radiation, 0.154 nm), with a parallel beam mirror at the source and a parallel plate collimator at the detector. A fixed grazing angle of 1° was set to maximize the collection efficiency. In order to suppress the diffraction peaks of the monocrystalline Si substrate, the samples were rotated in-plane by a fixed angle of 20°. The WAXRD scans were recorded both directly after deposition as well as after several specific annealing times at 300 °C and 400 °C.

6.3. Results and discussion

6.3.1. Changes in layered structures

Fig. 6.1(a) shows multilayer period change as a function of annealing time at 250 – 400 °C for La/B multilayers with as-deposited period thickness Λ = 3.5 nm. Only period expansion is observed. La and B are chemically reactive [14, 15, 16], and it has been shown that La and B atoms tend to intermix and form lanthanum borides at the interfaces already during deposition of the multilayers [3, 15, 16]. Fig. 6.1(b) shows WAXRD scans of the La/B multilayer directly after deposition and after annealing at 400 °C for 20 hours. The scan after annealing shows clearly pronounced (100) and (110) diffraction peaks from simple cubic LaB_6 (WAXRD analysis and results are discussed in detail in section 6.3.3). The formation of LaB_6, combined with the observed period expansion, could be used to suggest that B diffuses into La and forms LaB_6 interlayers. Based on bulk densities and molecular volumes of La and B, formation of lanthanum borides is expected to yield compaction. For instance, formation of 1 nm of LaB_6 ($\rho = 4.72$ g/cm^3) is expected to consume 0.52 nm of La and 0.64 nm of B, resulting in a compaction of 16%. For expansion to be observed, the density of the formed LaB_6 should be at least 15% lower than the above mentioned bulk value. Period expansion upon thermal loading was previously also reported for Si/B_4C and Si/B multilayers, and was attributed to formation of low density borides at the interfaces [8].

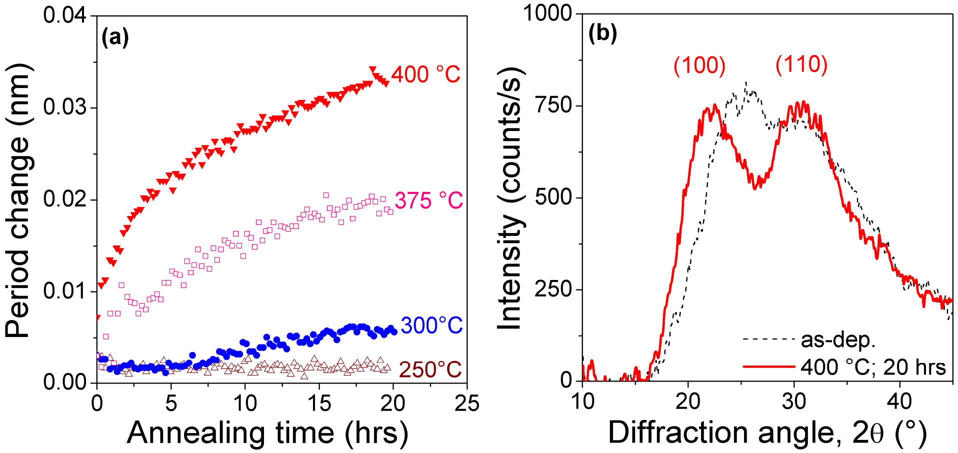

Fig. 6.1: (a) La/B multilayer period change as a function of annealing time. (b) WAXRD scans of as-deposited and annealed multilayers. The as-deposited multilayer period thickness is $\Lambda = 3.5$ nm, with $\Gamma = 0.4$.

Note that, apart from the changes in period caused by thermally induced growth of interfaces, also changes in the bulk structure of the layers may contribute to the observed changes in the multilayer period. For the La/B multilayer system, bulk La is known to undergo phase transformation from hexagonal closed-packed (hcp) to face-centered cubic (fcc) at 310 °C [12]. The hcp-to-fcc phase transformation in zirconium nanocrystals is associated with approximately 9% increase in volume per atom [17]. In order to discriminate the effects of La and B intermixing at the interfaces from bulk effects in the La and B layers, multilayers with much thicker individual layers (Λ = 7 nm) were investigated.

Fig. 6.2 shows multilayer period change as a function of annealing time at 300 °C – 400 °C for La/B multilayers with an as-deposited period thickness of Λ = 7 nm. Surprisingly, both period expansion and compaction are observed. At 300 °C the period compacts (which is not the case for multilayers with Λ = 3.5 nm (Fig. 6.1(a))). At 400 °C, after rapid period compaction at the initial stages of annealing (the first two measurement points), the period starts to expand. Moreover, at 350 °C the period compacts in the first 4 hours and then starts to show expansion. Comparing these results with the Λ = 3.5 nm multilayer, it can be concluded that period changes in La/B depend not only on annealing temperature, but also on annealing time and amount of La and/or B.

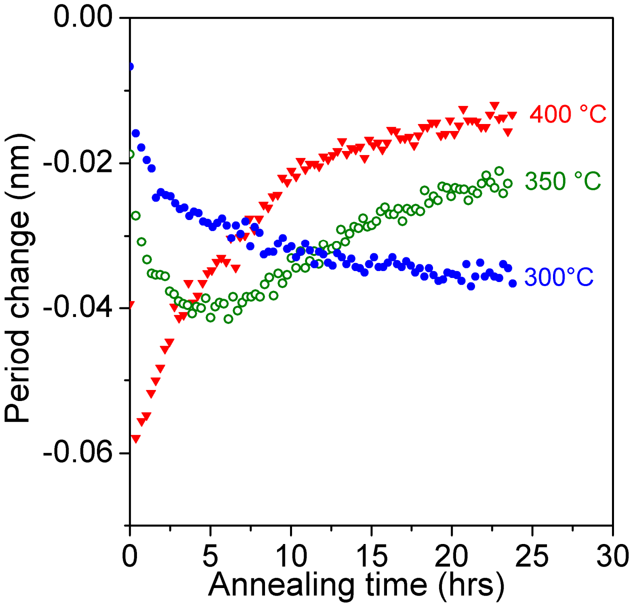

Fig. 6.2: La/B multilayer period change as a function of annealing time at 300 °C – 400 °C. The as-deposited multilayer period thickness Λ = 7 nm, with Γ = 0.4.

6.3.2. La and B interdiffusion

AES depth profiling measurements were performed to investigate La and B interdiffusion by comparing atomic depth profiles before and after annealing for multilayers with Λ = 7 nm. Fig. 6.3 shows the results of AES depth profiles of La/B multilayers before and after annealing for 24 hours at both 300 °C and 400 °C. For samples annealed at 400 °C, significant La and B intermixing is observed. In contrast, for 300 °C the difference between as-deposited and annealed samples is marginal. From this and the period changes observed in Fig. 6.2, it can be concluded that expansion pronouncedly visible at higher temperatures is related to diffusion-induced growth of the (low density) compound interlayers, while compaction, pronouncedly visible at lower temperatures and/or shorter annealing times, must be caused by mostly the densification of the layers and/or compound interlayers formed during deposition.

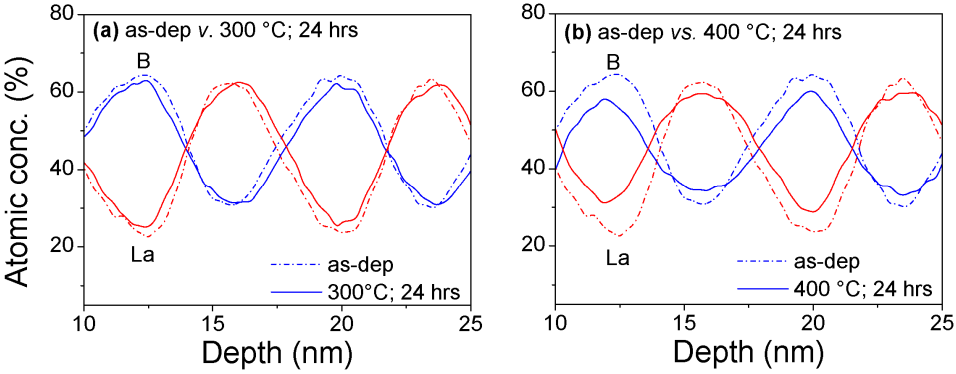

Fig. 6.3: AES atomic concentration profiles for La/B multilayers (Λ = 7 nm).

6.3.3. Crystallization and compound interlayer growth

WAXRD measurements were performed after various stages of annealing treatment at 300 °C and 400 °C to investigate changes in crystalline structure in multilayers with Λ = 7 nm. Due to overlapping diffraction peaks from different compositions, deconvolution of WAXRD scans was performed. A minimum number of Gaussians describing the diffraction scans was determined over a large set of data at different annealing times and temperatures. Fig. 6.4 shows resulting positions of the Gaussians for as-deposited and annealed multilayers (400 °C for 1 hour) as examples, with contributions from cubic LaB_6 and fcc La (reference from powder diffraction). The fourth peak (denoted as "La (200) +

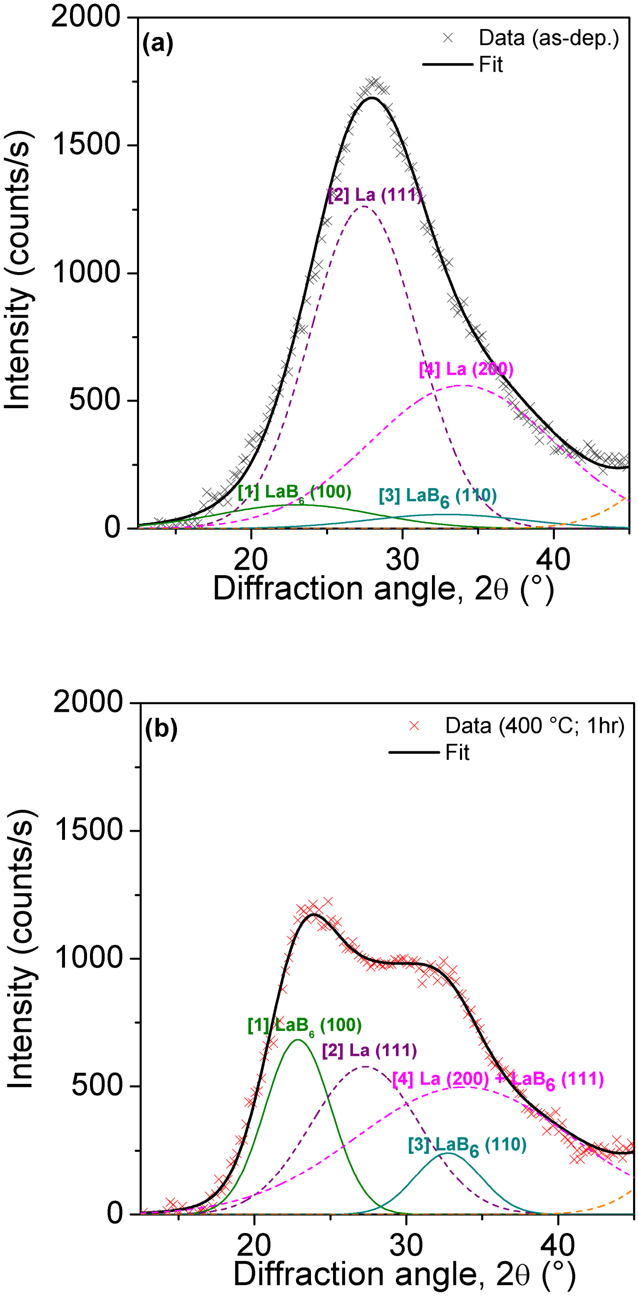

Fig. 6.4: WAXRD scans of La/B multilayers with $\Lambda = 7$ nm and $\Gamma = 0.4$ (a) after deposition, and (b) after annealing treatment at 400 °C for 1 hour. Contributions from fcc La, simple cubic LaB_6 peaks and resulting fits are displayed on the plots.

LaB_6 (111)" on Fig. 6.4(b)), which was needed to describe the scans, was effectively attributed to two contributions, from fcc La and cubic LaB_6. The second possible La hcp phase has not been observed. Therefore, the hcp-to-fcc phase transformation of La layers (discussed in Section 6.3.1) is ruled out as the cause of period expansion for multilayers with $\Lambda = 7$ nm and $\Gamma = 0.4$.

For the data fitting procedure, the relative positions of all Gaussians were fixed. Also, the widths of the two LaB_6 peaks were set to be the same at time t_i for annealing temperature T_j. The amplitudes of the LaB_6 peaks are related by a constant factor c for all annealing times and temperatures. The diffracted intensity I at angle 2θ is thus given by:

$$I(2\theta \mid t_i, T_j) = \sum_{n=1}^{4} a_i(t_i, T_j) \exp\left(-\frac{\left(2\theta - b_i(T_j)\right)^2}{2\sigma_i^2(t_i, T_j)} \right) \tag{6.1}$$

$$a_1(t_i, T_j) = c a_3(t_i, T_j) \tag{6.2}$$

$$\sigma_1(t_i, T_j) = \sigma_3(t_i, T_j) \tag{6.3}$$

$$b_2(T_j) = b_1(T_j) + o_2 \tag{6.4}$$

$$b_3(T_j) = b_1(T_j) + o_3 \tag{6.5}$$

$$b_4(T_j) = b_1(T_j) + o_4 \tag{6.6}$$

where, σ_i is the standard deviation, b_i is the position of the center of the peak, and o_2, o_3 and o_4 are offsets with respect to the position of the center of the first peak (b_1).

The crystallite sizes were calculated using Scherrer's formula. Fig. 6.5 shows the calculated La and LaB_6 crystallite sizes as a function annealing time for multilayers annealed at 300 °C and 400 °C. At 400 °C (Fig. 5(b)), two regimes of crystallites size change can be recognized for both La and LaB_6. The LaB_6 crystallite size initially increases rapidly during annealing (first ten minutes of annealing) and saturates at longer annealing times, while the La crystallite size initially increases slightly, followed by a strong decrease in the second stage. At 300 °C (Fig. 6.5(a)), the continuous increase in LaB_6 size, combined with no significant decrease in La size, is consistent with the effects observed in the first stage of annealing at 400 °C.

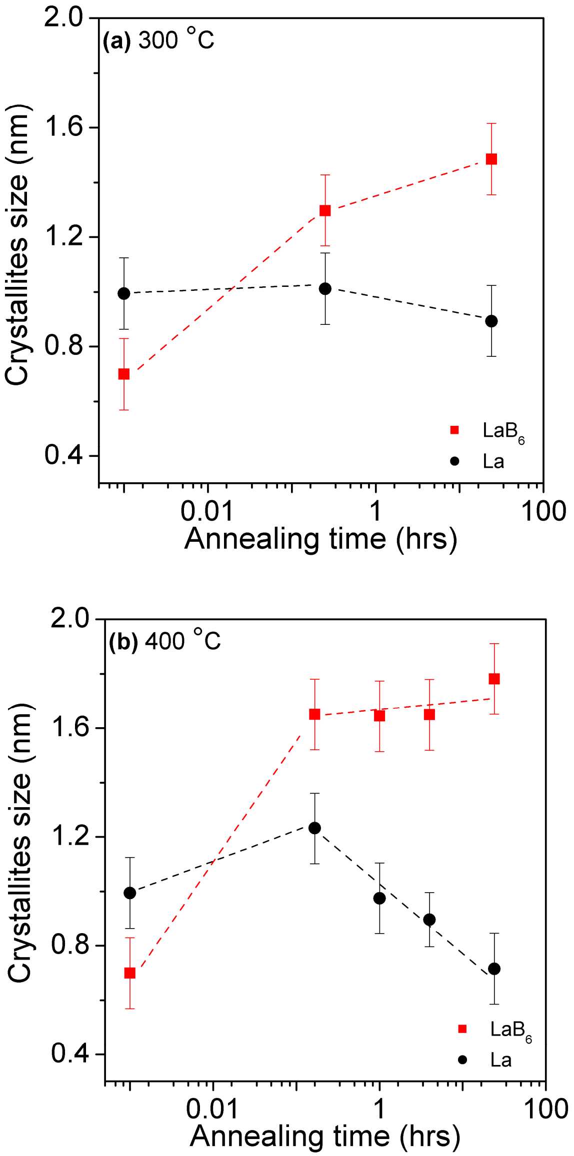

Fig. 6.5: La and LaB_6 crystallite size as a function of annealing time for La/B multilayers with $\Lambda = 7$ nm and $\Gamma = 0.4$; annealing temperatures (a) 300 °C and (b) 400 °C. The first data point of every series represents the as-deposited sample. The dashed lines are guides to the eye.

These results reveal two processes with opposite effects in terms of multilayer period thickness changes at the two temperatures mentioned above (Fig. 6.2). At 300 °C, where La and B interdiffusion is marginal (Fig. 6.3(a)), the continuous crystallization-induced densification of already formed lanthanum boride interlayers – to form LaB_6 crystallites – causes period compaction. At 400 °C, the crystallization of lanthanum boride interlayer (to form LaB_6 crystallites) occurs only in the first ten minutes of annealing, leading to relatively fast period compaction. Further annealing (at 400 °C) leads to slow growth of LaB_6 crystallites and a significant decrease in La crystallite size (Fig 6.5(b)). The reduction of La crystallite size suggests B diffuses into the La layer and consumes La to form a lanthanum boride interlayer. This is consistent with AES depth profiles which show significant La and B interdiffusion at 400 °C (Fig. 6.3(b)).

As previously discussed (Section 6.3.1), based on bulk densities and molecular volumes, formation of 1 nm of LaB_6 is expected to consume 0.52 nm of La and 0.64 nm of B. If the observed expansion (Fig. 6.2) is due to formation of LaB_6 with a density which is 15% lower than the bulk density, formation of a 1-nm-thick interlayer of LaB_6 would consume 0.44 nm of La. This cannot be the case since the rates of La crystallite consumption and LaB_6 crystallite growth do not correspond to the above mentioned ratio. Apparently, the lanthanum boride formed as a result of the diffusion process has an amorphous structure. Hence, it can be concluded that, thermally induced period changes in La/B multilayers are a result of two competing processes, namely, crystallization of lanthanum boride interlayers formed during deposition and growth of diffusion-induced amorphous lanthanum boride. At 300 °C the crystallization of the already formed boride interlayers is dominant throughout the annealing treatment, leading to period compaction. In contrast, at 400 °C, after the fast crystallization of the already formed lanthanum boride interlayers (to form LaB_6 crystallites), growth of low density, amorphous lanthanum boride interlayers is prominent, causing period expansion. It should be noted that, for multilayers with $\Lambda = 3.5$ nm, the as-deposited LaB_6 crystallite size is (1±0.1) nm, and no crystallization of the interlayers is observed during annealing. This explains why the multilayers do not exhibit period compaction (Fig. 6.1(a)).

6.4. Conclusions

Thermally induced period changes in La/B multilayer systems were found to depend on annealing temperature, annealing time and amount of La and/or B. Detailed AES and WAXRD studies on La/B multilayers with period thickness $\Lambda = 7$ nm reveal two competing processes, namely crystallization, leading to compaction, and diffusion-induced compound interlayer growth, leading to expansion of the multilayer period thickness. At 300 °C, crystallization of the lanthanum boride interlayers formed during deposition was found to be dominant throughout the annealing treatment, forming LaB_6 crystallites and consequently leading to period compaction. At 400 °C, crystallization of lanthanum boride interlayers formed during deposition (to form LaB_6 crystallites) was dominant during the initial 10 minutes of annealing, exhibiting period compaction. Afterwards the diffusion-induced growth of amorphous, low density lanthanum boride interlayers was prominent, resulting in period expansion. For multilayers with $\Lambda = 3.5$ nm, no crystallization of the compound interlayers is observed, and thus the multilayers exhibits only period expansion due to diffusion-induced lanthanum boride interlayer growth.

References

[1] N. I. Chkhalo, S. Kunstner, V. N. Polkovnikov, N. N. Salashchenko, F. Schäfers, S. D. Starikov1, *Applied Physics Letters* **102**, 011602 (2013).

[2] A. M. Hawryluk and N. M. Ceglio, *Applied Optics* **32**(34), 7062 (1993).

[3] I. A. Makhotkin, E. Zoethout, E. Louis, A. M. Yakunin, S. Müllender, F. Bijkerk, *Optics Express* **20**(11), 11778 (2012).

[4] C. Michaelsen, J. Wiesmann, R. Bormann, C. Nowak, C. Dieker, S. Hollensteiner, W. Jaeger, *Proceedings SPIE* **4501**, 135 (2001).

[5] E. Louis, A.E. Yakshin, T. Tsarfati, F. Bijkerk, *Progress in Surface Science* **86**, 255 (2011).

[6] O. Wood, C-S Koay, K. Petrillo, H. Mizuno, S. Raghunathan, J. Arnold, D. Horak, M. Burkhardt *et al, Proceedings SPIE* **7636,** 76361M (2010).

[7] D. Attwood, *Soft X-Rays and Extreme Ultraviolet Radiation, Principles and Applications* (Cambridge University, 1999).

[8] S. L. Nyabero, R. W. E. van de Kruijs, A. E. Yakshin, E. Zoethout and F. Bijkerk, *Journal of Applied Physics* **112**, 054317 (2012).

[9] S. L. Nyabero, R. W. E. van de Kruijs, A. E. Yakshin, E. Zoethout, G. van Blanckenhagen, J. Bosgra, R. A. Loch, and F. Bijkerk *Journal of Applied Physics* **113**, 144310 (2013).

[10] R. Resel, E. Tamas, B. Sonderegger, P. Hofbauer, and J. Keckes, *Journal of Applied Crystallography* 36, 80 (2003).

[11] S. Bruijn, R. W. E. van de Kruijs, A. E. Yakshin, and F. Bijkerk, *Applied Surface Science* **257**(7), 2707 (2011).

[12] R. C. Weast, *Handbook of Chemistry and Physics*, 64th ed. (CRC, 1984).

[13] T. Lundström, B. Lönnberg, J. Bauer, *Journal of Alloys and Compounds* 267, 54 (1998).

[14] R. W. Johnson , A. H. Daane, *Journal of Physical Chemistry* **65**(6), 909 (1961).

[15] T. Tsarfati, R. W. E. van de Kruijs, E. Zoethout, E. Louis, and F. Bijkerk, *Thin Solid Films* **518**(5), 1365 (2009).

[16] T. Tsarfati, R. W. E. van de Kruijs, E. Zoethout, E. Louis, and F. Bijkerk, *Thin Solid Films* **518**(24), 7249 (2010).

[17] I. Manna, P. P. Chattopadhyay, F. Banhart, and H.-J. Fecht, *Applied Physics Letters* **81**(22), 4136 (2002).

7. Diffusion induced structural changes in La/B-based multilayers for 6.7 nm radiation

Abstract

Thermal stability of La/B and LaN/B multilayers was investigated. The two multilayer systems were found to have comparable sub-ångström period expansion upon annealing in the temperature range of 250 °C – 400 °C. For La/B multilayers, wide angle X-ray diffraction analysis revealed that the size of LaB_6 crystallites present did not change significantly upon thermal treatment. Using grazing incidence X-ray reflectometry, strong change in the internal structure due to interdiffusion at the interfaces of La/B multilayers was observed after annealing. This, coupled to the unchanged crystallinity, suggested the growth of amorphous lanthanum boride interlayers. At-wavelength reflectance measurements showed that as-deposited LaN/B multilayers had an enhanced optical contrast compared to La/B. During thermal loading, the rate of diffusion-induced reflectance decrease in LaN/B multilayers was slower than in La/B. The enhanced thermal stability of LaN/B was attributed to the slower growth of LaN-B interfaces compared to La-B.

7.1. Introduction

Periodic Mo/Si-based multilayers are currently used as reflective coatings for the optics of next generation lithography tools, also known as extreme ultraviolet lithography (EUVL), operating at λ = 13.5 nm [1]. With a spatial resolution of 22 nm reported [2], the EUVL community is committed to further improving the spatial resolution to the 16 nm node and beyond [3]. The main challenge there lies in continuously increasing the numerical aperture up to a value of 0.7 or even higher [3], and employing an even shorter wavelength (~6.7 nm) for the lithography process.

The highest theoretical normal incidence reflectance for the 6.7-6.9 nm wavelength range can be obtained with multilayers that make use of La layers as reflector material, and B layers as an appropriate spacer material since B has a K-absorption at 6.6 nm [4, 5, 6]. Thermal stability of La/B-based reflective multilayer coatings will be an important requirement for performance since the optics are expected to be exposed to increased power densities compared to optics exposed to current 13.5 nm sources. Generally, nanoscale multilayers are sensitive to small structural changes at the interfaces. High-flux or prolonged photon exposures provide thermal loading, which may lead to interdiffusion of atoms and subsequent formation of compounds at the interfaces of multilayers [1, 3, 6]. This deteriorates the multilayer optical contrast, and thus decreases the reflectance [7]. Moreover, the multilayer period thickness might change upon compound formation, resulting in a mismatch between the multilayer period and the target wavelength [8, 9]. For mitigating such effects with sub-ångström precision, it is important to understand the effects induced by thermal loading.

La and B are highly reactive, and lanthanum borides are known to be formed at the multilayer interfaces even during deposition [5, 10, 11]. One of the methods to mitigate lanthanum boride formation is to replace the La layers with LaN, which is thermodynamically more stable [10, 11]. As a result, the formation of lanthanum boride during deposition is significantly suppressed, leading to increased optical contrast and reflectance at λ ≈ 6.7 nm. Based on the reduced interaction at the interfaces in LaN/B multilayer upon deposition, it may be expected that LaN/B multilayers would also exhibit increased thermal stability upon thermal loading. In this chapter, we present a study on the interaction of B with both La and LaN nanoscale layers. Using *in-situ* time-dependent grazing incidence X-ray reflectometry, X-ray diffraction and EUV reflectance measurements, we address the thermally induced changes in the internal structure and their effect on the performance of La/B-based multilayers designed for λ ≈ 6.7 nm.

7.2. Experimental

Two types of fifty-period multilayers were prepared, namely La/B and LaN/B multilayers, deposited on super-polished Si substrates. The nominal period thickness of the multilayers was $\Lambda = 3.45$ nm, with a La or LaN layer fraction of $\Gamma = 0.4$. The multilayers were prepared in a UHV deposition setup with base pressure $< 1 \cdot 10^{-8}$ mbar using DC magnetron sputtering. For LaN/B multilayers, LaN layers were deposited using reactive magnetron sputtering of La using a N_2 and Ar gas mixture.

Multilayer period thickness changes during annealing were monitored by measuring grazing incidence X-ray reflection (GIXR) scans *in-situ* using a PANalytical X'Pert X-ray diffractometer using a four-bounce monochromator (Cu-Kα radiation, 0.154 nm). The diffractometer was equipped with an Anton Paar thermal stage. The detailed description of the thermal stage can be found in ref. [12]. Before annealing, the alignment of the sample was performed and a reference GIXR scan was measured. After ramping to the target temperature, the sample position was realigned to correct for alignment errors introduced by thermal expansion of the sample stage and mechanical deformation of the sample at elevated temperature. At the target temperature, GIXR scans were continuously recorded during annealing. The multilayers were annealed for 20 hours at the following temperatures: 250 °C, 300 °C, 350 °C and 400 °C.

The period thickness changes during annealing were obtained from the shifts in measured Bragg peak positions, according to the method described in ref. [13]. This method allows determination of period changes with picometer accuracy. The obtained period changes were corrected for thermal expansion using bulk thermal coefficients of respective layer materials from ref. [14] and [15], and were verified by comparing GIXR scans during annealing with those measured at room temperature before and after the annealing treatment.

To study the changes in the crystalline structure of multilayers due to thermal loading, wide angle X-ray diffraction (WAXRD) scans were performed *ex-situ* (before and after annealing) at room temperature using a PANalytical Empyrean X-ray diffractometer (Cu-Kα radiation, 0.154 nm) – with a parallel beam mirror at the source and a parallel plate collimator at the detector. A fixed grazing incidence angle of 1° was set to maximize the collection efficiency. The samples were rotated in-plane by a fixed angle of 20° in order to suppress the diffraction peaks of the monocrystalline Si substrate.

EUV reflectometry (AOI = 1.5°) of the as-deposited and the annealed multilayer samples was performed at Physikalisch-Technische Bundesanstalt

(PTB), Berlin. It should be noted that, in applications, at least 175 periods would be required to achieve maximum normal incidence reflectance. However, multilayers with 50 periods were studied since they suffer less from periodicity variations. For instance, the measured peak reflectance of as-deposited 175-period LaN/B multilayer was 57.3% at $\lambda = 6.7$ nm [16].

7.3. Results and discussion

7.3.1. Changes in La/B multilayered structures

La and B are chemically reactive [10, 11], and studies have shown that La and B atoms tend to interdiffuse and form lanthanum borides at the interfaces even during deposition of La/B multilayers [5, 10, 11]. Recent studies by Makhotkin *et al* [5, 16] suggest that the effective thickness of intermixed regions (i.e. boride interlayers) of as-deposited La/B multilayers ($\Lambda = 3.45$ nm; $\Gamma = 0.4$) is approximately 1 nm. Thermal loading is expected to cause further interdiffusion and subsequent growth of the boride interlayers.

Fig. 7.1 shows multilayer period thickness change as a function of annealing time at various temperatures for La/B multilayers, compared with Mo/Si multilayers. Only period expansion is observed in La/B while only period compaction is observed in Mo/Si. In addition, the period changes in La/B are in the order of a few picometers to tens of picometers (at 250 °C – 400 °C), while the changes in Mo/Si are in the order of tens of picometers to a few ångströms (at 100 °C – 300 °C), suggesting that La/B multilayers are more stable than Mo/Si.

For Mo/Si, it is well understood that densification upon amorphous $MoSi_2$ interlayer growth at the interfaces is responsible for the observed period compaction in the temperature range 100 °C - 300 °C. (Fig. 7.1) [13, 17]. More importantly, at annealing temperatures above 300 °C, the silicide interlayers are known to undergo a phase transformation and form polycrystalline, *h*-$MoSi_2$ [17], accompanied by a much larger period compaction [17].

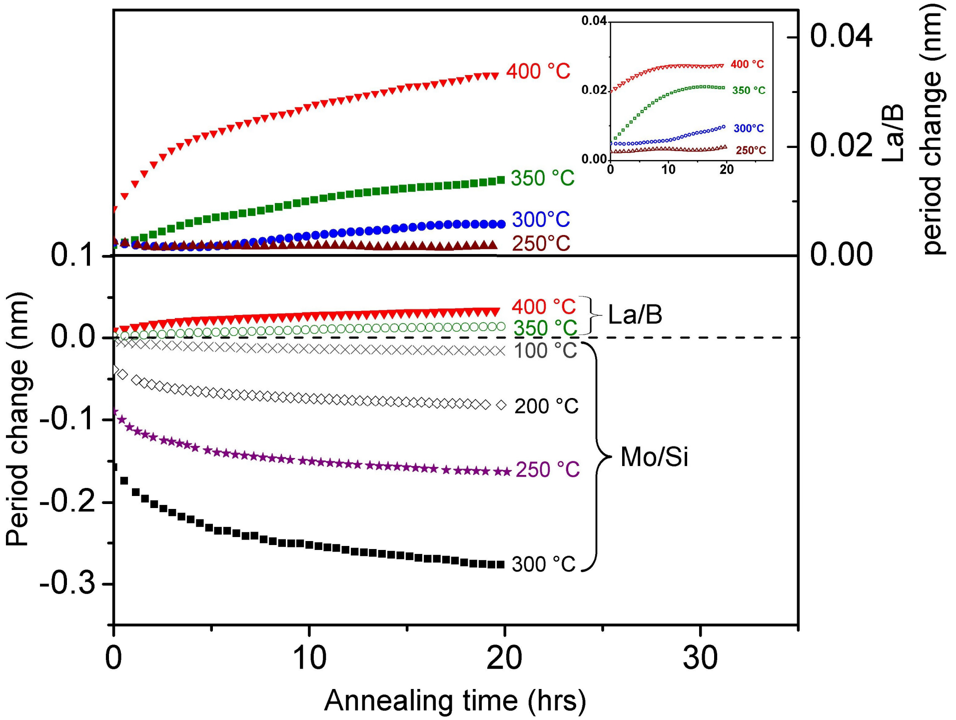

Fig. 7.1: Period change as a function of annealing time at various temperatures for La/B multilayers (Λ = 3.45 nm; Γ = 0.4), compared with Mo/Si multilayers (Λ = 6.9 nm; Γ = 0.4). Insert: Period changes for LaN/B multilayers (discussed in Section 7.3.2).

WAXRD measurements were performed before and after annealing treatment to investigate the crystalline structure of as-deposited La/B multilayers and the changes induced by thermal loading. Fig. 7.2 shows the WAXRD scans of as-deposited and annealed La/B multilayers, as well as a deconvolution of the scans into Gaussian functions. The scans of the samples (Fig. 7.2) show (100), (110) and (111) diffraction peaks from simple cubic LaB_6. The LaB_6 crystallite size is calculated using the Scherrer equation. For the as-deposited multilayer, the crystallite size is (1 ± 0.1) nm, which is consistent with the thickness of the intermixed regions obtained by Makhotkin *et al* [5, 16] using GIXR analysis. When annealed at the temperature range between 250 °C and 400 °C, there are only minor changes in the peak widths (crystallite size) and peak intensities. The most significant difference between as-deposited and annealed samples is observed in the positions of the diffraction peaks, with the LaB_6 peak positions of annealed multilayers being closer to the reference values for bulk LaB_6 [18]. The shift to lower diffraction angle (2θ) values indicates that the atomic lattice spacings are increasing, a phenomenon which suggests residual compressive stress relaxation is taking place [19]. The lack of significant increase in the size of crystallites suggests that the observed La/B period expansion (Fig. 7.1) cannot be explained by growth of polycrystalline compound interlayers.

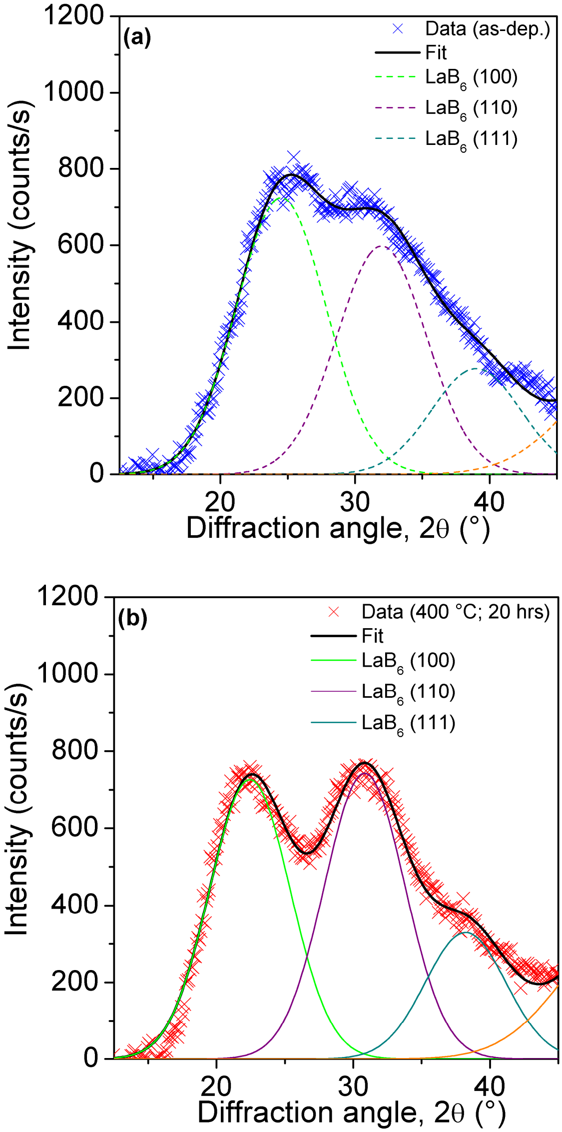

Fig. 7.2: WAXRD scans (markers) of La/B multilayers with $\Lambda = 3.45$ nm; (a) as-deposited, and (b) after annealing at 400 °C for 20 hours. Contributions from cubic LaB_6 peaks and resulting fits are displayed as lines.

Fig. 7.3 shows the GIXR scans of as-deposited as well as annealed La/B multilayers. The strong decrease in the intensities of Bragg peaks at higher angles indicates there are significant changes in the internal structure, which suggests a lot of interdiffusion may take place upon annealing. The interdiffusion at the interfaces, together with the lack of significant increase in LaB_6 crystallites size, indicates that the La/B period expansion is due to diffusion-induced growth of amorphous lanthanum boride interfaces with a relatively low density in order to explain multilayer expansion upon annealing.

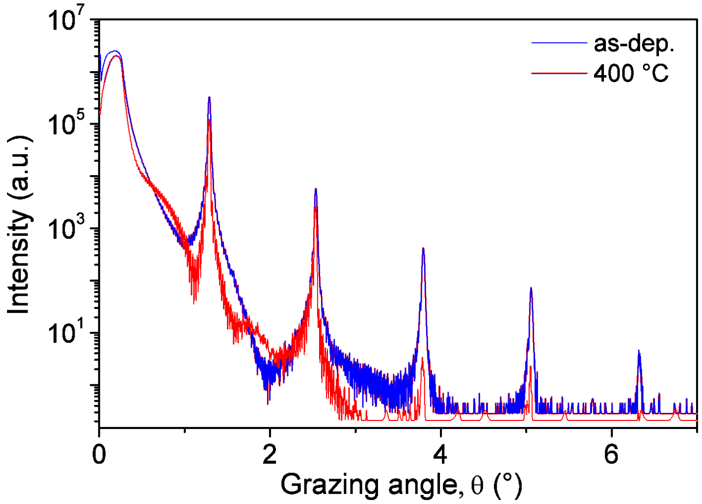

Fig. 7.3: GIXR scans of as-deposited and annealed La/B multilayers.

EUV reflectometry (AOI = 1.5°) of the as-deposited and the annealed La/B multilayer samples was performed to investigate how the diffusion-induced lanthanum boride interlayer growth affects the reflectance of multilayers. The measured peak reflectance of the as-deposited 50-period La/B multilayer is 11.2% at $\lambda = 6.9$ nm, which is significantly lower than the theoretical value (~27 %; with interface roughness/diffuseness $\sigma = 0.3$ nm), and consistent with strong intermixing at the La/B interfaces. Fig. 7.4 shows the measured peak reflectances of La/B multilayers as a function of annealing temperature. Evidently, the La/B multilayer reflectance decreases with increasing temperature, and by extension, with the diffusion-induced growth of lanthanum boride at the interfaces.

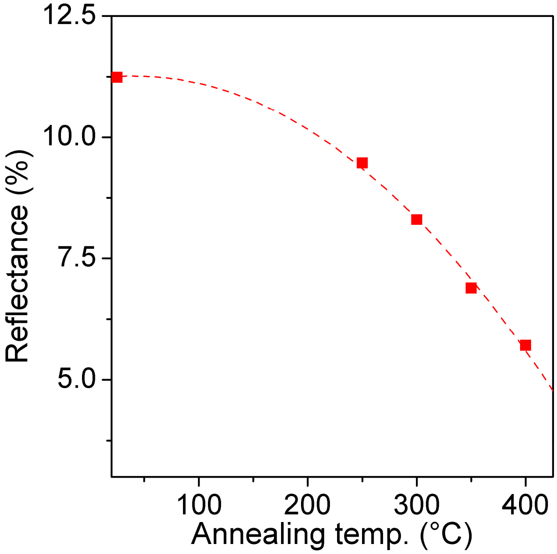

Fig. 7.4: Measured La/B multilayer reflectance (at λ = 6.9 nm) as a function of annealing temperature. Each data point was measured after annealing for 20 hours.

In summary, although La/B period changes are only in the order of a few tens of picometers, the performance of the multilayers is very sensitive to diffusion-induced interface chemistry. This makes La/B multilayers less suited for applications that require high near-normal-incidence reflectance during extended periods of operation at elevated temperatures. To mitigate La and B interdiffusion and boride formation at the interfaces during deposition *and* thermal loading, replacement of La layers with LaN has been suggested. In addition to LaN being thermodynamically more stable than lanthanum borides (Table 7.1) [10, 11], the theoretical LaN/B reflectance is comparable to that of La/B. In the next section, the effect of thermal loading on LaN/B multilayers will be addressed.

Compound	LaN	LaB_6
ΔH^{for} (kJ/mol)	-303	-130

Table 7.1: Formation enthalpies of LaN and LaB_6.

7.3.2. Changes in LaN/B multilayered structures

Fig. 7.1 (insert) shows multilayer period thickness change as a function of annealing time at various temperatures for LaN/B multilayers. The multilayer period increases upon annealing in the temperature range between 250 °C and 400 °C, with period changes comparable to the changes observed in La/B multilayers. In contrast to La/B multilayers, where WAXRD shows the existence of LaB_6 crystallites (Fig. 7.2), the WAXRD scans of both as-deposited and annealed LaN/B multilayers show only an amorphous structure. This indicates that the presence of N prevents crystallization at the interfaces [20], probably by suppressing the formation of critical crystal nuclei [21]. Fig. 7.5 shows the GIXR scans of as-deposited and annealed LaN/B multilayers. The reduction of Bragg peak intensities after annealing again indicates changes in the internal structure. However, the decrease in intensities after annealing is much smaller than that observed for La/B multilayers (Fig. 7.3), especially for higher order Bragg peaks, indicating that the annealing treatment of LaN/B has less impact on the internal structure than a same treatment of La/B multilayers.

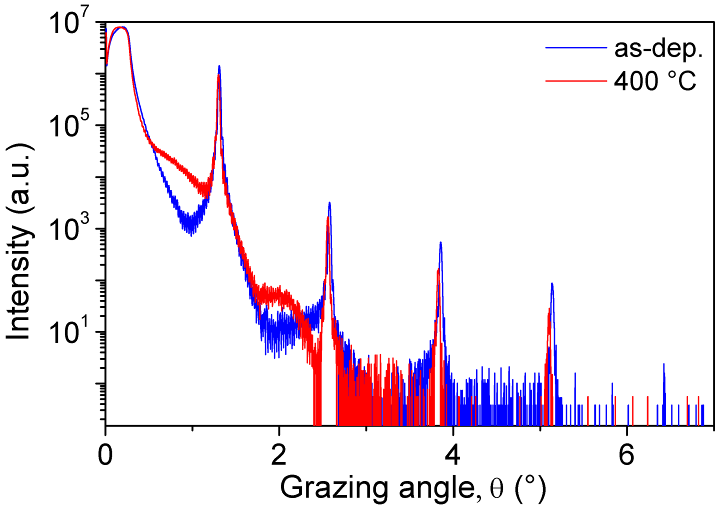

Fig. 7.5: GIXR scans of as-deposited and annealed LaN/B multilayers.

In order to quantify the effect of diffusion induced structural changes on the optical performance, at-wavelength reflectance measurements were performed. A peak reflectance of 17.7% at $\lambda = 6.8$ nm was measured for the as-deposited LaN/B multilayer, a significant increase over the 11.2% at $\lambda = 6.9$ nm for La/B. This is attributed to the improved optical contrast for LaN/B. Fig. 7.6 shows the

LaN/B and La/B multilayer reflectance as a function of annealing temperature, normalized to the respective as-deposited reflectance values. It is clear that the rate of diffusion-induced reflectance decrease in LaN/B multilayers is slower than in La/B. The enhanced thermal stability of LaN/B is attributed to the slower growth of LaN-B interfaces (in LaN/B multilayers) compared to La-B (in La/B multilayers).

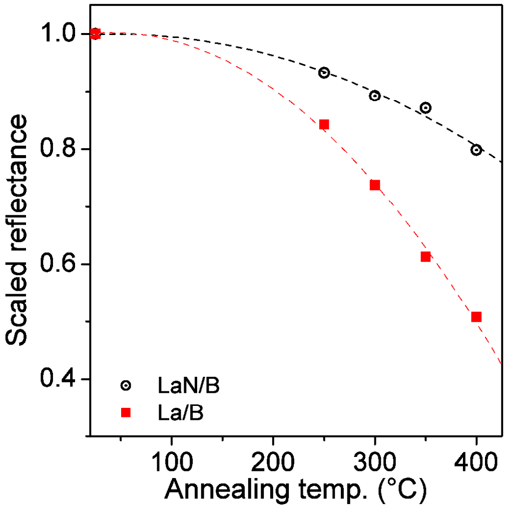

Fig. 7.6: La/B and LaN/B multilayer scaled reflectance as a function of annealing temperature. The as-deposited reflectance of La/B multilayer is 11.2% ($\lambda = 6.9$ nm) and that of LaN/B multilayer is 17.7% (at $\lambda = 6.8$ nm).

7.4. Conclusions

La/B and LaN/B multilayers exhibit sub-ångström period changes upon annealing in the temperature range of 250 °C – 400 °C. The period changes for La/B and LaN/B are much smaller than those observed for Mo/Si, and of opposite sign, i.e. period expansion is observed for La/B and LaN/B, while period compaction was observed for Mo/Si. WAXRD analysis revealed that the size of LaB_6 crystallites present in La/B multilayers does not change significantly upon thermal treatment. However, from GIXR, a strong change in the La/B multilayer internal structure due to interdiffusion was observed after annealing. This, coupled to the unchanging crystallinity, suggests the growth of amorphous lanthanum boride interlayers.

At-wavelength reflectance measurements showed that as-deposited LaN/B multilayers had an enhanced optical contrast compared to La/B, which indicates less La and B interdiffusion during deposition. During thermal loading, it was found that the rate of diffusion-induced reflectance decrease in LaN/B multilayers was slower than in La/B. The enhanced thermal stability of LaN/B was attributed to the slower growth of LaN-B interfaces (in LaN/B multilayers) compared to La-B (in La/B multilayers). The results presented here are of special relevance to development of La/B-based reflective multilayer coatings for applications that require extreme accuracy at high heat loads over extended duration, such as optics for EUVL and free electron lasers.

References

[1] E. Louis, A.E. Yakshin, T. Tsarfati, F. Bijkerk, *Progress in Surf. Sci.* **86**, 255 (2011).

[2] O. Wood, C-S Koay, K. Petrillo, H. Mizuno, S. Raghunathan, J. Arnold, D. Horak, M. Burkhardt *et al, Proc. SPIE* **7636,** 76361M (2010).

[3] N. I. Chkhalo, S. Kunstner, V. N. Polkovnikov, N. N. Salashchenko, F. Schäfers, S. D. Starikov1, *Appl. Phys. Lett.* **102**, 011602 (2013).

[4] A. M. Hawryluk and N. M. Ceglio, *Appl. Opt.* **32**(34), 7062 (1993).

[5] I. A. Makhotkin, E. Zoethout, E. Louis, A. M. Yakunin, S. Müllender, F. Bijkerk, *Opt. Express* **20**(11), 11778 (2012).

[6] C. Michaelsen, J. Wiesmann, R. Bormann, C. Nowak, C. Dieker, S. Hollensteiner, W. Jaeger, *Proc. SPIE* **4501**, 135 (2001).

[7] D. Attwood, *Soft X-Rays and Extreme Ultraviolet Radiation, Principles and Applications* (Cambridge University, 1999).

[8] S. L. Nyabero, R. W. E. van de Kruijs, A. E. Yakshin, E. Zoethout, F. Bijkerk, *J. Appl. Phys.* **112**, 054317 (2012).

[9] S. L. Nyabero, R. W. E. van de Kruijs, A. E. Yakshin, E. Zoethout, G. van Blanckenhagen, J. Bosgra, R. A. Loch, F. Bijkerk, *J. Appl. Phys.* **113**, 144310 (2013).

[10] T. Tsarfati, R. W. E. van de Kruijs, E. Zoethout, E. Louis, F. Bijkerk, *Thin Solid Films* **518**(5), 1365 (2009).

[11] T. Tsarfati, R. W. E. van de Kruijs, E. Zoethout, E. Louis, F. Bijkerk, *Thin Solid Films* **518**(24), 7249 (2010).

[12] R. Resel, E. Tamas, B. Sonderegger, P. Hofbauer, and J. Keckes, *J. Appl. Crystallogr.* **36**, 80 (2003).

[13] S. Bruijn, R. W. E. van de Kruijs, A. E. Yakshin, F. Bijkerk, *Appl. Surf. Sci.* **257**(7), 2707 (2011).

[14] R. C. Weast, *Handbook of Chemistry and Physics*, 64th ed. (CRC, 1984).

[15] T. Lundström, B. Lönnberg, J. Bauer, *J. Alloys Compd.* **267**, 54 (1998)

[16] I. A. Makhotkin, *Structural and reflective characteristics of multilayers for 6.x nm wavelength* (Ipskamp Drukkers, 2013).

[17] I. Nedelcu, R. W. E. van de Kruijs, A. E. Yakshin, F. Bijkerk, Phys. Rev. B **76**, 245404 (2007).

[18] http://www.materialsdata.com/products.htm

[19] W. Gruber, S. Chakravarty, C. Baehtz, H. Schmidt, *Defect and Diffusion Forum* Vol. **323 – 325**, 149 (2012)

[20] S. Toyoda, J. Okabayashi, H. Takahashi, M. Oshima, D. Lee, S. Sun, S. Sun, P. A. Pianetta, T. Ando, S. Fukuda, *Appl. Phys. Lett.* **87**, 182908 (2005).

[21] R. M. Shelby, S. Raoux, *J. Appl. Phys.* **105**, 104902 (2009).

8. Valorization and outlook

Multilayered nanoscale structures are currently proving to be viable as reflective coatings in both current and next generation advanced optical applications, particularly in the short wavelength range. Synchrotron facilities, free electron lasers and astrophysics optics tools are examples of state-of-the-art analytical and imaging technologies in which multilayers are employed as reflective coatings. In the past two decades, multilayer coatings have also been attracting a lot of attention from the semiconductor industry as the next generation lithography process – which employs EUV radiation – is considered to be a cost effective method for continuing the miniaturization of semiconductor devices. The application of reflective multilayer coatings in EUVL to manufacture smaller, faster, more powerful and more efficient electronic devices means that, the coatings would have an impact on our societies as a whole. However, EUVL has very high demands (Section 1.3), requiring the high performance of multilayer coatings to be realized and maintained over several years. It is therefore crucial for the semiconductor industry to devote resources to understand the factors that affect the performance of multilayer coatings.

In the past years, Carl Zeiss SMT – the developer of the optical systems for photolithography tools produced by ASML – has been initiating R&D programs involving FOM as a partner in multilayer research. The programs aim to understand the fundamentals of layer growth, multilayer properties and design multilayer coatings with enhanced reflectance and thermal stability. The work described in this thesis is part of the research program ‘Controlling photon and plasma induced processes at EUV optical surfaces (CP3E)’, which is co-financed by Carl Zeiss SMT and ASML. The CP3E program was initiated to meet the need of continued research on multilayer lifetime aspects raised by a previous successful program, eXtreme UV Multilayer Optics (XMO).

Intense or prolonged exposures of photon fluxes provide thermal loading onto multilayer coatings, causing diffusion and subsequent compound formation at the multilayer interfaces. This changes the optical properties of the coatings and generally deteriorates multilayer performance, resulting in severe distortions in imaging. One of the common methods used to mitigate the effects of diffusion and compound formation at the interfaces – loss of reflectance and changes in multilayer periodicity – is addition of ultra-thin diffusion barriers into the multilayer structure. For example, ultra-thin B_4C barriers are introduced into Mo/Si multilayer coatings (designed for $\lambda = 13.5$ nm) [1]. Another common method to enhance thermal stability is to replace an entire layer with a thermodynamically more stable compound. This method is suggested for La/B-based multilayer coatings (designed for $\lambda = 6.7$ nm), where La layers are replaced with LaN [2, 3].

As discussed in this work, the two mitigation strategies do not completely stop the diffusion induced effects at elevated temperatures or during prolonged photon exposures. For Mo/Si-based multilayers, it was shown in Chapters 3 and 4 how B_4C reacts with both Mo and Si. The unraveling of respective interface chemical reactions and their effects can be used to predict what period change effect – expansion or compaction – occurs at a certain temperature and/or time. At low temperatures (< 225 °C) and/or initial stages of photon exposure, formation of low density silicon borides at Si-B_4C interfaces results in period expansion. At elevated temperatures (> 225 °C) and/or later stages of prolonged photon exposure, formation of dense molybdenum silicide becomes dominant and results in period compaction. Similarly, LaN/B multilayers were shown to have an enhanced reflectance compared to La/B. However, LaN layers were found to be not inert and diffusion was still taking place in LaN/B multilayers, resulting in period expansion.

The period change effects can be detrimental for EUVL. To avoid distortions in imaging, the projection optics systems of EUVL tools require the period thickness of multilayer coatings to be matched with the employed radiation wavelength within tens of picometers. This is a huge challenge, particularly at elevated temperatures, when using the two methods discussed above. An alternative, self-correcting multilayer design was proposed in Chapter 5. The self-correcting process is achieved by balancing the effects of diffusion at the interfaces of multilayers. The design is based on a reference multilayer that exhibits compaction upon thermal loading, and includes an additional sub-structure, which expands upon thermal loading to compensate for the basic compaction. Using Mo/Si-based multilayers as an example, the optimization of the ratio of the number of the expanding periods (in this case, Mo/B_4C) to that of compacting periods (Mo/B_4C/Si/B_4C) was successfully demonstrated. Both the average periodicity and the centroid wavelength of the composite multilayer were preserved during annealing at 250 °C for 60 hours.

In Chapter 4, the detailed studies on Mo/B_4C multilayers revealed how factors like the availability of diffusing species and/or concentration of layer materials could affect the growth of compound interlayers and their structures. Hence, it should be possible to design a multilayer structure, with an optimal Mo to B_4C thickness ratio, which does not exhibit period change at a target elevated temperature. This could be useful for applications that employ intense photon fluxes, such as soft x-ray free electron lasers and synchrotrons, where high near-normal incidence reflectance is not a crucial requirement.

To fully explain diffusion processes in multilayers, *in-situ* GIXR was used together with WAXRD and XPS or AES depth profiling, as described in Chapter 2. The *in-situ* reflectometry analysis proved to be useful when the density of the growing compound interlayers was different from the average density of the layer materials; WAXRD measurements revealed consumption of polycrystalline layers; and XPS or AES depth profiling could provide qualitative information about atom intermixing in multilayers with relatively thick period thickness ($\Lambda > 5$ nm). However, for La/B-based multilayers designed for $\lambda = 6.7$ nm (i.e. $\Lambda \approx 3.5$ nm), these methods do not provide enough information about the internal structural changes, as observed in Chapter 7. Firstly, the densities of the compound interlayers are comparable to those of layer materials. Secondly, La, LaN, and B layers are amorphous and LaB_6 crystallites (present at the interlayers) do not grow during annealing, making it is difficult to deduce information about material consumption from WAXRD. And lastly, the layers are too thin for XPS or AES depth profiling. Therefore, another approach for elementary diffusion studies is needed for La/B-based multilayers. The analysis methods for reconstructing complete multilayer structures from GIXR scans and EUV reflectance spectra are currently optimized for La/B-based multilayers. These methods could provide further insight into diffusion processes in La/B-based multilayers. The optimization of the analysis methods is part of another industrial partnership program ‘Multilayer Optics for Lithography Beyond the Extreme Ultraviolet Wavelength Range’, which is carried out with support from the Dutch Technology Foundation (STW), in collaboration with Carl Zeiss SMT and ASML

References

[1] A. E. Yakshin, R. W. E. van de Kruijs, I. Nedelcu, E. Zoethout, E. Louis, F. Bijkerk, H. Enkisch, S. Muellender, *Proceedings SPIE* **6517**, 65170I (2007).

[2] T. Tsarfati, R. W. E. van de Kruijs, E. Zoethout, E. Louis, F. Bijkerk, *Thin Solid Films* **518**(5), 1365 (2009).

[3] T. Tsarfati, R. W. E. van de Kruijs, E. Zoethout, E. Louis, F. Bijkerk, *Thin Solid Films* **518**(24), 7249 (2010).

9. Summary

Nanoscale multilayered structures are employed as reflective coatings for short wavelengths in a wide range of analytical and imaging technologies. Thermal stability is vital for their functionality. This thesis addresses the thermally induced internal structural changes in Mo/Si-based and La/B-based multilayers, designed for the extreme ultraviolet wavelength range. The focus of the work is to study the diffusion phenomena and the interactions between nanoscale layers, with particular emphasis on the formation of compound interlayers during thermal loading.

Thermally induced diffusion and compound formation at the interfaces of multilayers can have adverse effects on the performance of multilayers. Intermixing of atoms deteriorates the multilayer optical contrast, resulting in reflectance losses. Moreover, the multilayer periodicity may change (compact or expand) if the density of the compound interlayer is different from the density of the not compounded state of the layer materials. The change in periodicity leads to a change in angular/spectral response of the optics, ultimately leading to image distortions and reduced reflectance.

Ultra-thin B_4C layers can be introduced at the interfaces of Mo/Si multilayers to mitigate Mo and Si interdiffusion. However, B_4C is chemically reactive with both Mo and Si[1], leading to interface chemistry in the multilayers. The research described in this thesis shows that the process of interface formation is a

---

[1] V.I.T.A. de Rooij-Lohmann, L. W. Veldhuizen, E. Zoethout, A. E. Yakshin, R. W. E. van de Kruijs, B. J. Thijsse, M. Gorgoi, F. Schäfers, F. Bijkerk, *Journal of Applied Physics* **108**, 094314 (2010).

complex interplay between formation of various compounds. At low temperatures (< 225 °C), the B_4C barrier decomposes and formation of – in particular – Si_xB_y leads to period expansion. On the contrary, at higher temperatures (> 225 °C) the diffusion of Si through the compounded interlayer accelerates and subsequent formation of Mo_xSi_y leads to period compaction.

While the interaction between Si and B_4C layers generally yields a low density interface and always results in multilayer period expansion, the interaction between Mo and B_4C layers is more complex. Using *in-situ* X-ray reflectometry, atomic concentration depth profiling and X-ray diffraction analysis, it was shown how the formed interlayer depended on the initial amounts of Mo and B_4C, the annealing temperature and the annealing time. Mo enrichment of already formed MoB_xC_y interlayers leads to formation of dense interlayers and yields compaction, while B and C enrichment of the interlayers forms low density compounds and yields expansion.

In detailed investigations, it was revealed that under certain conditions (temperature range and Mo to B_4C thickness ratio), the period changes in $Mo/B_4C/Si/B_4C$ are exactly opposite to those in Mo/B_4C. Furthermore, the temporal behavior of the two systems was shown to be virtually identical. These two observations led to a novel, self-correcting multilayer design. The new design is based on a reference $Mo/B_4C/Si/B_4C$ multilayer that exhibits compaction upon thermal loading, and includes an additional Mo/B_4C sub-structure that expands upon thermal loading to compensate for the intrinsic compaction. First experimental results show the successful working principle of such a "self-correcting" design, where the multilayer period and reflectance remains unchanged during at least tens of hours at elevated temperatures.

For development of coatings for a lithography illumination wavelength of ~6.7 nm, structural changes in La/B multilayers upon thermal loading were investigated. Due to high reactivity of La with B, relatively thick boride interlayers are found to be formed during deposition, resulting in poor optical contrast. During thermal loading, further interdiffusion at the interfaces is observed, leading to further deterioration of optical contrast. To mitigate interdiffusion and boride formation during deposition and thermal loading, La layers can be replaced with thermodynamically more stable LaN layers[2]. The passivation of the La layer with nitrogen results in not only an improved optical contrast leading to a higher reflectance, but also improves the thermal stability of the multilayers through reduced interdiffusion at the interfaces. The latter is

---

[2] T. Tsarfati, R. W. E. van de Kruijs, E. Zoethout, E. Louis, F. Bijkerk, *Thin Solid Films* **518**(5), 1365 (2009).

shown to effectively limit the reflectance loss due to diffusion induced contrast deterioration at elevated temperatures.

The results presented in this thesis demonstrate how understanding of thermally induced physical and chemical processes that occur at the interfaces of nanoscale layers can be used to improve the functionality of multilayered structures. This is crucial for high heat-load applications that are extremely sensitive to small changes in the multilayered structures. The application of extreme ultraviolet lithography in particular requires radiation hardness of the optical components, and as such this thesis contributes to the understanding of thermal effects in and further improvement of Mo/Si-based and La/B-based multilayer optical coatings.

10. Samenvatting

Multilaagstructuren met individuele laagdiktes in het nanometergebied worden veelvuldig gebruikt als reflecterende elementen voor licht met korte golflengtes voor diverse analytische en afbeeldingstoepassingen. De thermische stabiliteit van deze structuren is vitaal voor de goede werking van de uiteindelijke toepassing. Dit proefschrift behandelt specifiek de thermisch geïnduceerde structuurveranderingen in Mo/Si en La/B gebaseerde multilagen, welke ontwikkeld worden voor toepassing in het extreem ultraviolet golflengtegebied. Het hier beschreven onderzoek heeft als focus de diffusiefenomenen en interacties tussen nanometer dunne lagen te bestuderen, met nadruk op de vorming van verbindingen aan de grenslagen tijdens thermische belasting.

Thermisch geïnduceerde interdiffusie en vorming van verbindingen aan grenslagen hebben over het algemeen een negatief effect op de optische eigenschappen van multilaag structuren. Door het mixen van atomen aan de interfaces tussen lagen verminderd het optisch contrast en daardoor de reflectiviteit. Daarnaast kan de periode van de multilagen veranderen doordat de dichtheid van een gevormde verbinding aan het interface anders kan zijn dan de gemiddelde dichtheid van de afzonderlijke elementen. Deze veranderde periode resulteert weer in een verandering van de hoekafhankelijkheid en/of golflengteafhankelijkheid van de reflectiviteit en leidt uiteindelijk tot beeldvervorming en verminderde prestaties van de optieken.

Zeer dunne B_4C lagen, geplaatst tussen Mo and Si, kunnen gebruikt worden om de interdiffusie van Mo en Si te reduceren. B_4C is echter chemisch reactief met zowel Mo als Si[1], waardoor er nieuwe verbindingen plaats kunnen vinden. Het onderzoek dat in dit proefschrift beschreven staat laat zien dat het proces van tussenlaagvorming een samenspel is van de vorming van diverse verbindingen. Bij lage temperaturen (lager dan 225 °C) vind er decompositie van B_4C plaats en de vorming van een lage dichtheid Si_xB_y verbinding leidt tot vergroting van de multilaag periode. Boven 225°C diffundeert Si door de gevormde tussenlaag en de vorming van een hoge dichtheid Mo_xSi_y verbinding leidt uiteindelijk tot periodeverkleining.

Terwijl de interactie tussen Si en B_4C in het algemeen een lage dichtheid tussenlaag geeft, resulterend in periodevergroting, is the interactie tussen Mo en B_4C meer complex. Met behulp van X-ray reflectometry, atomaire diepteprofilering en X-ray diffractie is aangetoond dat de tussenlaag afhangt van de initieel aanwezige hoeveelheden Mo en B_4C, de verhittingstemperatuur, en de tijdsduur van verhitting. Molybdeen verrijking van de al gevormde MoB_xC_y tussenlagen resulteert in de vorming van dichte tussenlagen en periodeverkleining terwijl boor en koolstof verrijking van de MoB_xC_y tussenlagen resulteert in lage dichtheid verbindingen en periodevergroting.

Uit gedetailleerd onderzoek is gebleken dat onder specifieke condities (temperatuur gebied en Mo en B_4C laagdiktes) de periodeveranderingen in $Mo/B_4C/Si/B_4C$ multilagen tegenovergesteld zijn aan die in Mo/B_4C multilagen. Specifiek blijkt het tijdsafhankelijke gedrag voor deze twee systemen precies tegenovergesteld te zijn. Deze ontdekking heeft geleid tot een nieuw, zelfcorrigerend, multilaag ontwerp. Dit nieuwe ontwerp is gebaseerd op een referentie $Mo/B_4C/Si/B_4C$ multilaag die periodeverkleining laat zien tijdens thermische belasting, waaraan extra Mo/B_4C periodes zijn toegevoegd die deze periodeverkleining moeten compenseren. De resultaten laten zien dat dit principe succesvol is en zowel de multilaag periode als de reflectie onveranderd blijven tijdens tientallen uren van verhitting.

Veranderingen in de structuur van La/B multilagen onder thermische belasting zijn bestudeerd om verdere ontwikkeling van multilaagcoatings voor 6.7 nm te ondersteunen. Door de hoge reactiviteit van La met B worden relatief dikke lanthaanboride tussenlagen gevormd tijdens multilaag depositie, wat resulteert in een relatief slecht optisch contrast. Tijdens thermische belasting groeien deze tussenlagen door verdere interdiffusie, wat leidt tot nog meer contrastverlies.

---

[1] V.I.T.A. de Rooij-Lohmann, L. W. Veldhuizen, E. Zoethout, A. E. Yakshin, R. W. E. van de Kruijs, B. J. Thijsse, M. Gorgoi, F. Schäfers, F. Bijkerk, *Journal of Applied Physics* **108**, 094314 (2010).

Om de tussenlaaggroei tijdens depositie en onder thermische belasting te verminderen kunnen de La lagen vervangen worden door thermodynamisch stabielere LaN lagen[2]. Passivatie van de La laag met behulp van stikstof resulteert niet alleen in een beter optisch contrast en daardoor een hogere reflectie, maar leidt ook tot een thermisch stabielere multilaag door verminderde interdiffusie aan de LaN/B interfaces. Dit laatste zorgt ervoor dat het reflectieverlies door contrastverlies op hoge temperaturen beperkt blijft.

De resultaten die in dit proefschrift worden getoond demonstreren hoe een gedetailleerd begrip van thermisch geïnduceerde fysische en chemische processen aan de interfaces tussen nanometer dunne lagen gebruikt kan worden om de functionaliteit van multilaagstructuren voor optische toepassingen te verbeteren. Dit begrip is cruciaal voor hoge temperatuurstoepassingen waar de optische prestaties van multilagen sterk kunnen veranderen door veranderingen in de multilaagstructuur. In het bijzonder de toepassing van multilagen als reflecterende optische elementen in extreem ultraviolet lithografie vereist extreme stabiliteit onder belichting en dit proefschrift draagt bij aan het begrip van thermisch geïnduceerde veranderingen in, en daardoor de verdere ontwikkeling van, zowel Mo/Si als La/B gebaseerde stabiele optische coatings.

---

[2] T. Tsarfati, R. W. E. van de Kruijs, E. Zoethout, E. Louis, F. Bijkerk, *Thin Solid Films* **518**(5), 1365 (2009).

Acknowledgements

Pursuing a PhD had never been on my plans. However, my mindset shifted after being encouraged by both Dick de Boer and Marcel Krijn, whom I worked with at Philips Research, in Eindhoven. I then found out that looking for a topic or project that I can focus on for four years was pretty difficult and time consuming. Eventually, I managed to find something interesting – called "nSI" – on the internet! To keep the long story short, after meeting Fred, Eric and Andrey in August 2009, I was confident that I could pursue a PhD at the Nanolayer Surfaces and Interfaces department of FOM DIFFER (in Nieuwegein). I still remember the lab tour by Erwin vividly. He was on top form, in terms of challenging one's "knowledge" as usual, but I did not get fazed by the occasion!

A couple of months later I joined the nSI department, which I referred to as my other home for the following four years. I believe I was fortunate to have Robbert as my daily supervisor. Coming into a rather new field, I experienced challenging times in the first year with no clear picture where the PhD was headed. But, with Robbert's guidance I found myself comfortable. More importantly, his love for science was infectious. Since most people at our department used to come to the office that I shared with Robbert for discussions, I could not help but listen to most of them. These, together with regular discussions on my experiments with him and Andrey, enabled me to learn a lot.

I would also like to express my gratitude for my colleagues' support, enthusiasm, friendliness and immense knowledge. (Personal elaborate acknowledgments will be added.) Here, I would like to thank Veronique and

Saskia who made me feel at home in the group, especially in the first six months. Occasionally, I would be glad when Jeroen, Rolf, Slava, Qiushi or Teodor would get bored of their work and pass by my desk for chats about our latest results, progress and any useful papers we had come across. The chats – although I have to say some of them were far too random – made me enjoy working at the institute. Thank you!

My PhD would have not been possible without the contributions of Gisela and Kerstin (of Carl Zeiss SMT), Erwin, Frenk, Santi, Bob, Machiel, Arend-Jan and Kees. Most of the time I felt like they went out of their way to help with the measurements and analysis, coatings or make sure the diffractometer was available and working well. Asanteni sana!

I am not sure I would ever find the right words to express my gratitude to my family and friends who have been very supportive throughout my journey – from Chang'ombe Primary School to now, ASML. My mom and my sister Nanzighe, I will always remember the sacrifices you made. I cannot thank you enough. Abraham, thank you for being there – supporting and advising. Jos, you have been an ideal catapult… I will always remember my first ever internship at HFML in Nijmegen, which certainly opened my eyes. Vinny and George, I always knew there would be another meet up to unwind. Lastly but not least, I am very grateful to have Letshani, who has been more than a partner to me. Ngiyabonga!

Curriculum Vitae

Steven Lawrence Nyabero was born on 29 July 1983 in Dar es Salaam, Tanzania. He attended Chang'ombe Primary School, Dar es Salaam, from 1991-1997. He then completed O-Level studies at Aga Khan Mzizima Secondary School, Dar es Salaam, in 2001. In 2002, he was awarded a scholarship by the International School of Tanganyika (IST), Dar es Salaam, to study the International Baccalaureate diploma. Afterwards he went to Germany where he pursued BSc. in Physics at Jacobs University Bremen, and MSc. in Applied Physics at Technische Universität München. While pursuing the above mentioned degrees, between 2004 and 2009, he got numerous opportunities for short- and long-term internships at several research groups in Germany and The Netherlands. Some of the internships were carried out at the High Field Magnet Laboratory of Radboud University Nijmegen (The Netherlands), Hamburger Synchrotronstrahlungslabor (HASYLAB) of Deutsches Electronen-Synchrotron (DESY) (Germany), Trium Analysis Online GmbH (Germany) and Philips Research (The Netherlands). He started his PhD research in November 2009 at the Nanolayer Surfaces and Interfaces department of the FOM Dutch Institute for Fundamental Energy Research, Nieuwegein, under the supervision of Prof. dr. Fred Bijkerk. A selection of the results of the research can be read in this thesis.